The Role of Prolyl 4-Hydroxylase in Pancreatic β-cell Insulin Secretion

by

Sarah Marie Janssen

A thesis

presented to the University of Waterloo

in fulfillment of the

thesis requirements for the degree of

Master of Science

in

Pharmacy

Waterloo, Ontario, Canada, 2017

Author's Declaration

I hereby declare that I am the sole author of this thesis. This is a true copy of my thesis, including any required final revisions, as accepted by my examiners.

I understand that my thesis may be made electronically available to the public.

Abstract

Type 2 diabetes mellitus (T2D) is characterized by chronic hyperglycemia and peripheral insulin resistance. In response to elevated blood glucose levels, pancreatic β-cells release insulin which occurs in a biphasic manner. First-phase insulin secretion occurs via the K_{ATP} channel-dependent pathway during the first 10 minutes after a glucose load. Second-phase insulin secretion, K_{ATP} channel-independent pathways, results in a slow and sustained release of insulin, which can last for several hours after a glucose load. The mechanisms underlying K_{ATP} channel-independent pathways remain incompletely understood. It is suggested that anaperlosis, increased production of tricarboxylic acid (TCA) cycle intermediates, regulates second-phase insulin secretion. Anaplerotic pathways involve the production of cytosolic α-ketoglutarate (αKG) that may enhance prolyl 4-hydroxlase (PHD) activity. PHDs are well-established regulators of the hypoxia response pathway. However, PHD may play a role in insulin secretion with both short- and long-term effects through prolyl hydroxylation of key proteins. Inhibition of PHD via dimethyloxalylglycine (DMOG) decreased oxygen consumption rate (OCR) in both INS-1 832/13 cells and primary mouse islets. DMOG treated primary mouse islets demonstrated enhanced second-phase insulin secretion when stimulated with high glucose (HG). Intraperitoneal glucose tolerance tests (ipGTTs) in male C57BL/6J mice treated with DMOG revealed improved glucose tolerance during second-phase insulin secretion and improved insulin sensitivity during first-phase insulin secretion. The results presented in this thesis reveal that PHD plays a role in both first- and second-phase insulin secretion and may be a potential target for the treatment of T2D.

Acknowledgements

First and foremost, I would like to thank my supervisor Dr. Jamie Joseph for the opportunity to be a part of his lab and for his immense support and guidance throughout my thesis project. Dr. Joseph consistently challenged us and helped us to grow as scientists. I would also like to thank my advisory committee, Dr. Paul Spagnuolo and Dr. Michael Beazely for their continual support. I would like to thank all of the graduate students at the School of Pharmacy for providing a welcoming atmosphere, endless support, and a listening ear. I would especially like to thank Monica. Thank you for your invaluable assistance and teaching me everything there was to know in the lab. My thesis project would not be what it is without your contributions. To Thomas, thank you for loving me and encouraging me to reach my full potential and achieve my goals. Last but not least, I would like to thank my parents, thank you for being my biggest supporters and for believing in me always.

Table of Contents

List of Abbreviations

Acronym	Name
A1C	Glycated hemoglobin
ADP	Adenosine diphosphate
ATP	Adenosine triphosphate
BCA	Bicinchoninic acid
CIC	Citrate isocitrate carrier
Cre	Cre recombinase
CYP	Cytochrome P450
DIC	Dicarboxylate carrier
DMαKG	Dimethyl α-ketoglutarate
DMM	Dimethyl maleate
DMOG	Dimethyloxalylglycine
DNP	2,4-Dinitrophenol
DPP-4	Dipeptidyl peptidase-4
EDHB	Ethyl-3,4-dihydroxybenzoate
ELISA	Enzyme-linked immunosorbent assay
ETC	Electron transport chain
GFP	Green fluorescent protein
GIP	Glucose-dependent insulinotropic peptide

GLP-1	Glucagon-like peptide 1
GLUT	Glucose transporter
GSIS	Glucose-stimulated insulin secretion
HFD	High fat diet
HG	High glucose
HIFα	Hypoxia inducible factor α
HRE	HIF response elements
ICDc	$NADP^+$-dependent isocitrate dehydrogenase
ERT2	Estrogen receptor fusion protein 2
ipGTT	Intraperitoneal glucose tolerance test
KRB	Krebs-Ringer bicarbonate buffer
KO	Knockout
LDHA	Lactate dehydrogenase
LG	Low glucose
MALDI-MS	Matrix assisted laser desorption/ionization mass spectrometry
NADPH	Nicotinamide adenine dinucleotide phosphate
NT	No treatment
OCR	Oxygen consumption rate
OGC	2-oxoglutarate carrier
PBS	Phosphate-buffered saline

PC	Pyruvate carboxylase
PCR	Polymerase chain reaction
PDH	Pyruvate dehydrogenase
PDK1	Pyruvate dehydrogenase kinase 1
PHD	Prolyl 4-hydroxylase
PKM2	Pyruvate kinase M2
PPAR-γ	Peroxisome proliferator-activated receptor γ
PVDF	Polyvinylfluoride
pVHL	Von Hippel Lindau protein
RFP	Red fluorescent protein
RIA	Radioimmunoassay
RIP	Rat insulin promoter
SGLT-2	Sodium-dependent glucose transporter 2
shGFP	Small hairpin greed fluorescent protein
siRNA	Small interfering RNA
SUR	Sulfonylurea receptor subunits
T1D	Type 1 diabetes
T2D	Type 2 diabetes
TBS	Tris-buffered saline
TCA	Tricarboxylic acid cycle

TOF	Time of flight
TZD	Thiazolidinedione
WT	Wildtype

List of Figures

List of Tables

Chapter 1: Introduction

1.1 Diabetes mellitus

1.1.1 Background

The incidence of diabetes is increasing worldwide. In 2014, 6.7% of Canadians 12 years of age or older reported to be diagnosed with diabetes, consisting of 7.5% for males and 5.8% for females.[1] According to the World Health Organization (WHO), 422 million adults are living with type 1 diabetes (T1D) or type 2 diabetes (T2D) with 1.5 million deaths in 2012 related to diabetes complications and 2.2 million deaths related to elevated blood glucose levels.[2] The incidence of diabetes cases has emphasized the need to develop effective treatment options and implement strategies to promote diabetes prevention through lifestyle changes.

T1D is less common compared to T2D and is an autoimmune disorder that is commonly diagnosed in younger individuals.[3] The immune system is unable to recognize autoantigens presented on β-cells, which include glutamic acid decarboxylase (GAD), insulin, insulinoma-associated antigen-2 (IA2), and zinc transporter 8.[3,4] B-lymphocytes produce autoantibodies directed against β-cell autoantigens.[3,4] T-cells and macrophages target autoantibodies inducing inflammation by increasing cytokine levels.[3] Increased levels of cytokines, such as tumor necrosis factor α (TNFα), interleukin-1β (IL-1β), and interferon γ (IFN-γ), suppress insulin secretion and result in β-cell dysfunction and apoptosis.[3] Serum levels of these autoantibodies is indicative of T1D development, with the presence of multiple autoantibodies resulting in approximately 70% risk of T2D development.[4]

In contrast to T1D, T2D has a slower progression and accounts for 90% of all diabetes cases.[5,6] T2D is associated with obesity resulting from nutrient overload from fat and refined carbohydrates, physical inactivity and a genetic predisposition.[3] Aside from obesity, major risk

factors for T2D include a body mass index (BMI) of ≥ 25 kg/m^2; ethnicity, with a higher incidence in Native Americans, African-Americans and Hispanic Americans; age of ≥ 45 years; hypertension of ≥ 140/90 mmHg; elevated cholesterol or triglyceride levels, and a family history of T2D.[3]

Glucose metabolism is the main stimulus for pancreatic β-cell insulin secretion where insulin demonstrates systemic effects in adipose tissue, skeletal muscle and liver. Approximately 98% of the pancreas mass consists of acinar tissue, which produces exocrine enzymes for digestion.[7] The remaining 2% of the pancreas mass is the endocrine portion and consists of the islets of Langerhans.[5,7] Pancreatic islets consist of α, β, δ, ε and γ cell types.[7] β-cells secrete insulin; α-cells secrete glucagon, which increases hepatic glucose production during hypoglycemic conditions to increase blood glucose levels; δ-cells secrete somatostatin, an inhibitor of both insulin and glucagon; ε-cells secrete ghrelin, a hormone that increases appetite; and γ-cells secrete pancreatic polypeptide, a regulator for gastrointestinal secretion.[7] Although islets consist of 2% of the pancreas, they are highly vascularized and receive 10-20% of the total blood flow.[5]

Obesity from chronic over-nutrition and physical inactivity results in peripheral insulin resistance.[3] Pancreatic β-cells respond to insulin resistance via insulin hypersecretion to maintain normal blood glucose levels, known as normoglycemia, which is between 4-6 mmol/L.[3,7,8] In this prediabetes state, pancreatic β-cells undergo compensation involving increased β-cell mass, insulin biosynthesis and nutrient-stimulated insulin secretion.[3,5,8] Susceptible β-cells begin to fatigue due to increased oxidative stress and endoplasmic reticulum (ER) stress from increased proinsulin, the precursor to insulin, production. β-cell fatigue results in increased blood glucose levels, known as hyperglycemia, and β-cells are no longer able to sustain compensation.[8]

Glucolipotoxicity, elevated blood glucose and lipid concentrations, peripheral and pancreatic inflammation and oxidative stress eventually leads to β-cell failure, β-cell apoptosis and T2D diagnosis.[5,7]

T2D is associated with chronic low-grade inflammation and is associated with increased pro-inflammatory cytokines, including TNFα, IL-1β, and IFN-γ in the periphery and in the pancreas, which are insulin secretion suppressors and lead to β-cell apoptosis.[3,5] Throughout the progression of T2D, islet inflammation, glucolipotoxicity and ER stress resulting from increased insulin secretion during compensation ultimately leads to β-cell apoptosis and subsequent hyperglycemia.[5] T2D is a complex disease, affecting peripheral tissues including the liver, skeletal muscle and adipose tissue that rely on insulin for anabolic pathways.[7] There are several anti-hyperglycemic medications that work to restore normoglycemia through various mechanisms within the peripheral tissues and the pancreas.

1.1.2 Treatment options

Glycated hemoglobin (A1C) is considered the gold standard for the diagnosis of T2D.[9] Glycated hemoglobin is the binding of glucose to the amino group of valine on the β chain of hemoglobin.[10] The binding of glucose to hemoglobin is correlated to blood glucose concentrations over 8 to 12 weeks.[10] T2D is diagnosed when a patient displays A1C levels ≥ 6.5%.[11] Despite A1C values to be the gold standard for T2D, there are limitations due to differences in glucose metabolism and hemoglobin glycation between individuals.[9] When A1C levels are ≥ 6.5%, lifestyle modifications through diet and exercise are initiated and anti-hyperglycemic agents are often prescribed to lower A1C levels. Metformin is the most

commonly prescribed anti-hyperglycemic agent and can be used alone or in combinational therapy if A1C levels are not obtained.[12]

Metformin, part of the biguanide drug class, is the first line of defense for the management of hyperglycemia. Metformin decreases hepatic glucose production and glucose absorption in the small intestine, as well as, increases glucose uptake and utilization to restore normoglycemia.[12,13] Metformin is involved in the phosphorylation and activation of AMP-activated protein kinase (AMPK), increasing glucose uptake in skeletal muscle and liver for glucose storage and utilization.[13] Double-blind placebo control clinical trials proved a significant effect for metformin on reducing blood glucose levels and after a three month period metformin was able to reduce A1C levels by approximately 1%.[14] Metformin has been shown to work in the small intestine, liver and kidney via the liver specific organic cation transporter (OCT) 1 and kidney-specific OCT2.[12,13]

Aside from metformin's effects on restoring blood glucose levels, metformin may have other beneficial effects including cardiovascular protective effects via anti-inflammatory properties.[15,16] Metformin has been shown to inhibit macrophage differentiation by AMPK activation, playing a beneficial role in the reduction of insulin resistance and atherosclerosis.[15]

Metformin is the first anti-hyperglycemic agent prescribed as it presents the least side effects, including hypoglycemic events and weightgain.[16] Metformin has also been shown to have beneficial effects on atherosclerosis, a complication that arises from chronic hyperglycemia.[16] Metformin was found to reduce atherosclerosis in mice fed a high fat diet (HFD) by inhibiting angiotensin II type 1 receptor via AMPK.[17]

Another class of anti-hyperglycemic agents includes the insulin secretogogue's sulfonylureas and meglitinides. These drug classes inhibit K_{ATP} channels on the β-cell

membrane, leading to depolarization and increased insulin secretion.[6] Both sulfonylureas and meglitinides bind to the sulfonylurea receptor (SUR) subunits, SUR1 and SUR2, on the K_{ATP} channels.[18] Sulfonylureas are glucose-independent, leading to continuous inhibition of K_{ATP} channels resulting in increased basal insulin secretion, which increases the risk for hypoglycemia.[18] Meglitinides however, are glucose-dependent, leading to increased insulin secretion postprandially.[6,18,19]

Sulfonylureas are metabolized by cytochrome P450 (CYP) 2C9, whereas meglitinides are primarily metabolized by CYP 3A4.[20,21] However, genetic variants of these liver enzymes lead to differences in efficacy and side effects.[20] Despite the side effects of sulfonylureas, they have been found to reduce A1C levels by approximately 1.0 to 1.25%.[14]

Other anti-hyperglycemic agents work to improve insulin sensitivity in adipose tissue. Thiazolidinediones (TZD) target peroxisome proliferator-activated receptor-gamma (PPAR-γ) to promote adipocyte differentiation to recover insulin sensitivity.[6,22-24] Aside from adipocyte differentiation, PPAR-γ also increases glucose transporter 4 (GLUT4) expression for glucose uptake in adipose tissue.[25] PPAR-γ regulates TNFα, adiponectin and leptin, which all play a role in insulin sensitivity.[24,25] Despite the beneficial effects of TZD's in improving insulin sensitivity and its ability to significantly decrease A1C levels by approximately 1.25%, there are side effects including fluid retention, weight gain and congestive heart failure.[14,25] Many TZDs have been removed from the market due to liver failure and only pioglitazone and rosiglitazone remain available.[24] More recently, rosiglitazone was linked with increased risk of myocardial infarction.[24]

Other anti-hyperglycemic agents work to decrease glucose absorption in the small intestine to maintain blood glucose levels. Acarbose is a competitive inhibitor of α-

glucosidase.[26] α-glucosidase is a small intestine brush border enzyme that breaks 1,4α-bonds, digesting starch and disaccharides to produce glucose.[26] Acarbose inhibits the breakdown of starch and disaccharides, decreasing blood glucose levels and insulin secretion postprandially.[26]

Insulinotropic hormones, glucose-dependent insulinotropic peptide (GIP) and glucagon-like peptide 1 (GLP-1), are gastrointestinal peptides secreted from small intestine endocrine cells.[24,27,28] GIP and GLP-1 are secreted to increase glucose-stimulated insulin secretion (GSIS).[27] GIP and GLP-1 have a short duration of action and are inactivated by the enzyme dipeptidyl peptidase-4 (DPP-4).[27] GLP-1 is a potent insulinotropic hormone and GLP-1 agonists aid in sustaining insulin secretion.[24] GLP-1 agonists significantly improve A1C levels, promote weight loss and have a low risk of hypoglycemia.[29] There are numerous side effects including nausea, vomiting, and indigestion and is not suggested for patients with gastrointestinal diseases.[24]

DPP-4 cleaves at proline or alanine residues on the N-terminus of GIP and GLP-1.[24] DPP-4 inhibitors prevent the degradation of GLP-1 by DPP-4, sustaining GSIS and delaying hyperglycemia in T2D patients.[24,27,28] DPP-4 inhibitors also work to increase cell proliferation and decrease cell apoptosis to maintain β-cell mass.[24,27,28] Clinical trials reveal that DPP-4 inhibitors show a moderate effect on A1C levels, decreasing A1C levels by approximately 0.75%.[14] DPP-4 inhibitors display a low risk for hypoglycemia and do not result in weight gain.[30] However, randomized control trials assessing the risk of saxagliptin, a DPP-4 inhibitor, for heart failure found that patients who had a family history of cardiovascular disease treated with saxagliptin were more likely to develop heart failure compared to placebo controls.[30] However, according to a recent meta-analysis, the association between saxagliptin and heart failure remains unknown.[30]

The newest class of anti-hyperglycemic agents, sodium-dependent glucose transporter 2 (SGLT-2) inhibitors, prevent glucose reabsorption from the kidneys and promote glucose excretion in the urine.[31-33] Approximately 180 grams of glucose is filtered by the kidneys and almost all is reabsorbed by the kidneys via SGLT-2.[33] Preventing glucose reabsorption decreases blood glucose levels, insulin levels and promotes weight loss.[32,33] SGLT-2 inhibitors were also found to improve risk factors for cardiovascular disease including blood pressure, arterial stiffness, and dyslipidemia.[31]

Although there are numerous beneficial effects of SGLT-2 inhibitors, there are several side effects and the long-term consequences of altered electrolyte balance that occurs with SGLT-2 inhibitors is unknown.[33] As well, clinical trials consisting of patients treated with the SGLT-2 inhibitor dapagliflozin, reported a small number of cases of breast and bladder cancer [33]

Apart from the oral anti-hyperglycemic agents described above, insulin therapy has been primarily used as a treatment option for T1D to replace the loss of β-cell insulin secretion.[34] Although anti-hyperglycemic agents are effective at reducing A1C levels, typically between 0.8% and 2.0%, more than half of T2D patients fail to maintain normoglycemia.[35] In order to decrease the risk of diabetic complications that arise from chronic hyperglycemia, insulin therapy is introduced as an add on to oral medications to stimulate basal insulin secretion.[35,36] Insulin therapy includes mixed insulins or insulin coformulations targeting blood glucose levels in a fed and fasted state.[35] If normoglycemia is not achieved then a combination of mixed insulins and rapid-acting insulin is introduced, which is injected before a meal targeting blood glucose levels in a fed state.[35] Personalized treatment plans are required when introducing insulin therapy in combination with other anti-hyperglycemic agents, as the risk of hypoglycemia is increased, particularly with sulfonylurea treatment.[36] Anti-hyperglycemic agents and insulin

therapy work to improve insulin sensitivity and attain normoglycemia as measured by A1C levels.

All treatment options work through different mechanisms of action, targeting the pancreas, skeletal muscle, liver and adipose tissue. T2D is a highly complex disease affecting multiple tissues with the pancreas as the central organ for regulating glucose homeostasis. Sulfonylureas and meglitinides target first-phase insulin secretion in the pancreas to stimulate GSIS. However, second-phase insulin secretion accounts for approximately 70% of total insulin secretion, emphasizing the need to investigate potential targets of second-phase insulin secretion for drug development.[37]

1.2 Glucose-stimulated insulin secretion pathway

1.2.1 K_{ATP} channel-dependent pathway

GSIS from pancreatic β-cells is biphasic. First-phase insulin secretion occurs within the first 10 minutes after a glucose load, whereas, second-phase insulin secretion displays a slow and sustained release of insulin for up to two to three hours after a glucose load.[38] The well-studied model of insulin secretion begins with increased blood glucose levels. Glucose is taken up by glucose transporter 2 (GLUT2) in the pancreas and is metabolized generating pyruvate, which feeds into the tricarboxylic acid (TCA) cycle.[38-41] Pyruvate can enter the TCA cycle via pyruvate dehydrogenase (PDH) or pyruvate carboxylase (PC).[38-41] This subsequently leads to an increase in the ATP/ADP ratio, which closes the ATP-sensitive K^+-channels causing membrane depolarization.[38-41] Membrane depolarization opens voltage-gated calcium channels and allows for an influx of calcium ions. Increased intracellular calcium ions causes insulin granule exocytosis.[38-41] Insulin granules that are in close proximity to the plasma membrane and are docked near voltage-gated calcium channels are known as the "readily releasable pool" (50 to

100 granules).[38,42] The release of this readily releasable pool of insulin granules is regulated by the K_{ATP} channel-dependent pathway or the "triggering pathway".[39,40] The K_{ATP} channel-dependent pathway is critical for first-phase insulin secreton.[38-40] Second-phase insulin secretion may either stimulate the production of new insulin granules, or exocytosis of a larger pool of insulin granules located further from the calcium channels.[42] It is suggested that the K_{ATP} channel-dependent pathway is not the only pathway for GSIS and a second pathway exists K_{ATP} channel-independent pathways.[43]

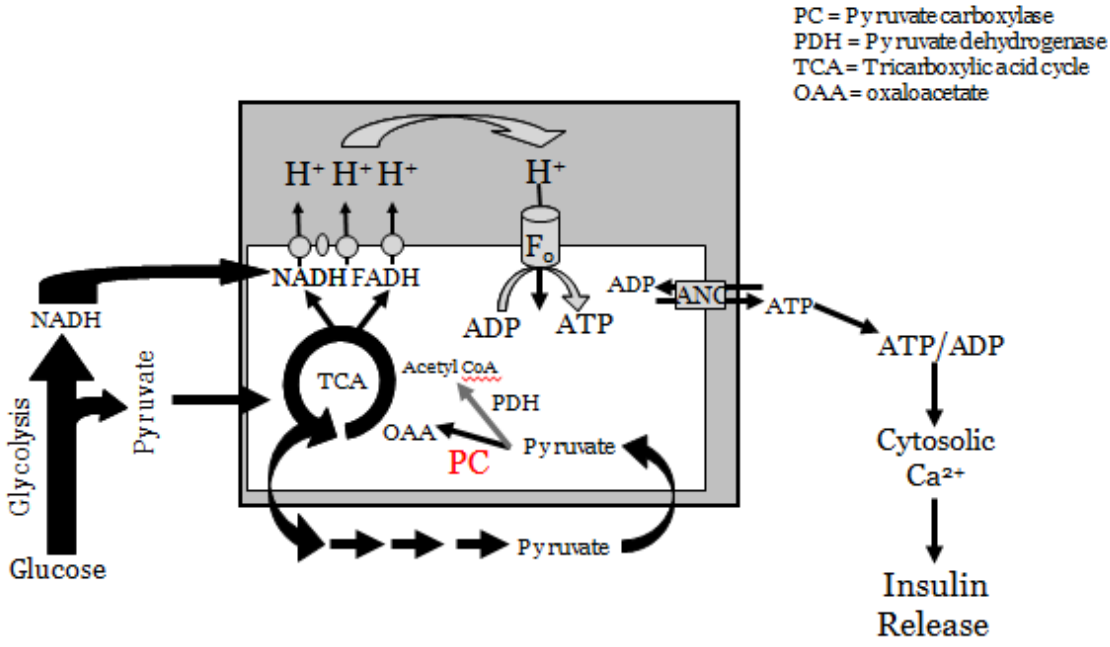

Figure 1.1: K_{ATP} channel-dependent pathway.

A schematic representation of the K_{ATP} channel-dependent pathway is shown above. Two pyruvate molecules are produced from one molecule of glucose via glycolysis in the cytosol. Pyruvate enters the mitochondrial matrix via mitochondrial pyruvate carrier (MPC) and enters the TCA cycle via PDH or PC. The TCA cycle generates cofactors that enter the electron transport chain (ETC) to pump protons into the intermembrane space forming the proton motive force. Protons enter the mitochondrial matrix via ATP synthase to generate ATP. Increased ATP/ADP leads to an influx of calcium ions and insulin granule exocytosis from the 'readily releasable pool'. *Illustration reproduced courtesy of Dr. Jamie Joseph.*

1.2.2 K_{ATP} channel-independent pathways

K_{ATP} channel-independent pathways, also called "amplifying pathways", are suggested to regulate second-phase insulin secretion.[43] Anaplerosis is the net production of TCA cycle

intermediates and is suggested to be important for second-phase insulin secretion.[43] Pyruvate produced via glycolysis in the cytosol can enter the TCA cycle by PDH to produce acetyl-CoA or PC to produce oxaloacetate, a substrate in the TCA cycle.[37,44] PDH and PC are expressed in the pancreas with 40-50% of the pyruvate generated during glycolysis entering the TCA cycle via PC.[44]

Oxaloacetate production by PC leads to the conversion of TCA cycle intermediates including citrate, isocitrate and malate.[37] These TCA cycle intermediates translocate to the cytosol with subsequent reconversion to pyruvate.[37] This "pyruvate cycling" produces by-products αKG and NADPH that may stimulate insulin secretion and involves three pyruvate cycling pathways.[37,45,46] The malate/pyruvate and the citrate/pyruvate pathways produce NADPH via malic enzyme, whereas, the isocitrate/pyruvate pathway produces NADPH and αKG via $NADP^+$-dependent isocitrate dehydrogenase (ICDc).[37] When these pathways are inhibited, there is a significant reduction in pyruvate cycling and GSIS.[46]

In the isocitrate/pyruvate pathway, oxaloacetate is converted to citrate via citrate synthase, which is then translocated to the cytosol by the citrate isocitrate carrier (CIC) and isomerized to isocitrate.[3745,46] Once in the cytosol, isocitrate produces αKG and NADPH via ICDc. αKG can then re-enter the mitochondrial matrix via the 2-oxoglutarate carrier (OGC) to stimulate production of TCA cycle intermediates.[37,45,46] Cytosolic αKG is a β-cell secretagogue but the mechanism remains inconclusive.[37] αKG is a co-substrate for the enzyme prolyl 4-hydroxylase (PHD), which may play a role in the regulation of insulin secretion via K_{ATP} channel-independent pathways.[47,48]

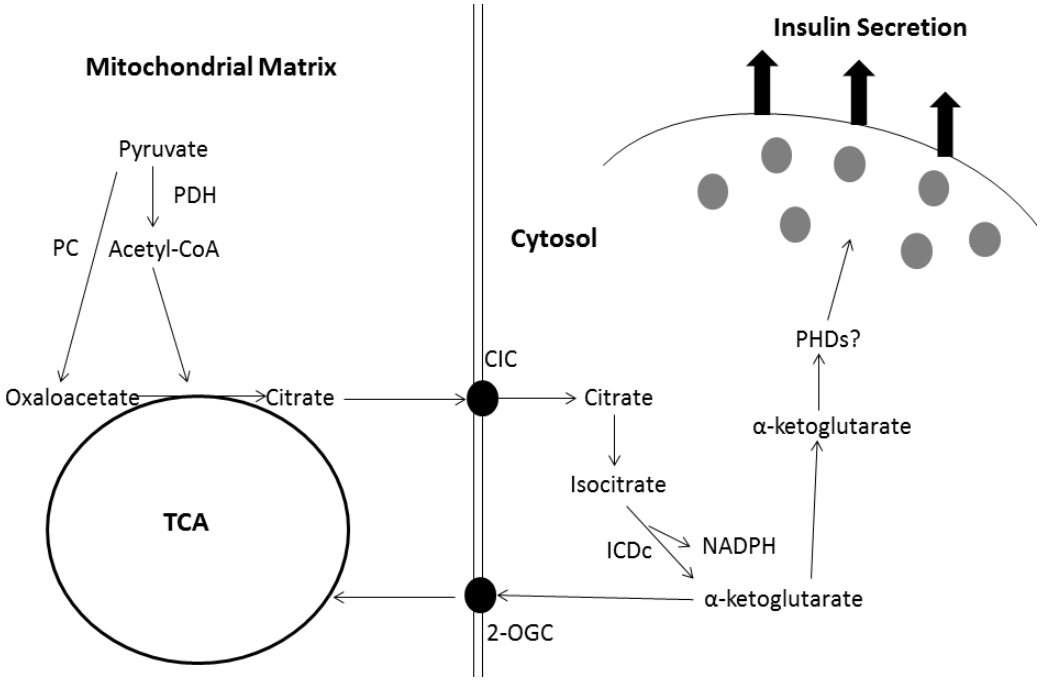

Figure 1.2: Pyruvate/isocitrate pathway.

A schematic representation of the pyruvate/isocitrate pathway is shown above. PC converts pyruvate to oxaloacetate which enters the TCA cycle. Oxaloacetate produces citrate via citrate synthase and citrate is translocated to the cytosol via CIC. In the cytosol, citrate is isomerized to isocitrate which produces NADPH and αKG via ICDc. αKG may re-enter the TCA cycle in the mitochondria via 2-OGC but may also act as a co-substrate for PHD to regulate GSIS.

1.3 Prolyl 4-hydroxylases

1.3.1 PHD isoenzymes

There are three isoforms of prolyl 4-hydroxylases (PHD): PHD1, PHD2 and PHD3. Other names for the PHD enzymes include Egl nine homolog (Egln), as well as, hypoxia inducible factor prolyl 4-hydroxylases (HIF-P4H).[49-53] Previously described PHDs are responsible for altering collagen for exocytosis .[54] Type I and type II collagen PHDs regulate collagen formation and are localized in the ER.[55] Bruick and colleagues (2001) hypothesized that a novel class of PHDs were responsible for regulating the hypoxia response pathway by

hydroxylating proline residues on hypoxia inducible factor α (HIFα). HIFα is localized in the cytosol and is, therefore, unlikely that type I and type II collagen PHDs proline hydroxylate HIFα.[55]

In humans, PHD1, PHD2 and PHD3 are composed of 407, 426 and 239 amino acids, respectively.[49,52] A transmembrane PHD (PHD-TM) has also been described that consists of a 502 polypeptide located in the ER with the catalytic domain within the lumen between residues 59 and 82.[49] At the amino acid level, PHD1, PHD2, and PHD3 are 42-59% identical to each other.[49] These isoenzymes contain the hydroxylase domain at the C-terminal end, with 55% identity.[52] However, the N-terminal ends of each isoenzyme vary where PHD3 has a shorter N-terminal sequence.[52]

A key difference between PHD1-3 includes different subcellular localizations. PHD1 was found to be exclusively expressed in the nucleus; PHD2 mainly expressed in the cytosol and PHD3 expressed in almost equal proportions in the cytosol and nucleus.[56] Another study determined all PHDs to be expressed mainly in the cytosol in a wide variety of human tissues, including both islets and acinar tissue of the pancreas with PHD3 also expressed in the nucleus.[57] PHD2 is expressed in many tissues and cell lines studied, whereas the highest mRNA levels of PHD1 and PHD3 were found in the placenta and heart, respectively.[49] PHD-TM mRNA levels were highest in the human brain and pancreas.[58]

PHDs are part of the 2-oxoglutarate dioxygenase superfamily and require molecular oxygen and αKG as co-substrates, and Fe^{2+} and ascorbate as cofactors.[49,51-53,59,60] The catalytic site for all dioxygenases is located in a double-stranded β-helix jelly-roll core.[49] Originally, it was determined that PHDs have a K_m value for oxygen between 230 and 250μM but is now suggested to be approximately 100μM.[51-53] This K_m value, which is the concentration of oxygen

required for the half-maximal catalytic rate, is significantly higher than required in tissues, making molecular oxygen necessary for PHD activity.[51-53] One oxygen atom contributes to the oxidative decarboxylation of αKG generating succinate and CO_2 and the second oxygen atom contributes to the hydroxylation of proline.[53] αKG is an electron donor that is oxidized to succinate. Succinate and fumarate, substrates in the TCA cycle, inhibit PHD activity via competitive inhibition.[53,59,60] Fumarate and succinate inhibit all PHD isoenzymes with fumarate having a K_i value, the concentration for half maximal inhibition, of 50-80μM and succinate having a K_i value of 350-460μM.[60] The use of iron chelators that competitively inhibit Fe^{2+} that were used to stabilize HIFα before the discovery of PHDs validate the requirement of Fe^{2+} for PHD activity.[54,61] The Fe^{2+} binding site is contained in residues H313, D315 and H374 in human PHD2.[49] In mice, the Fe^{2+} binding site is contained in residues H271 and D273 for PHD1, H290 and D292 for PHD2 and H135 and D137 for PHD3.[62] Ascorbate ensures maximal catalytic activity and has been reported to reduce Fe^{3+} from increased ROS production back to Fe^{2+}.[52,53] The canonical pathway for PHD is through the regulation of HIFα in the hypoxia response pathway.

1.3.2 Role of PHD in the hypoxia response pathway

PHD's ability to regulate HIFα in the hypoxia response pathway, an adaptive pathway for temporary cell survival when oxygen levels are insufficient, has been well documented.[49,63] Human HIFα consists of three isoforms, HIF1α, HIF2α and HIF3α.[49,53,64] HIF contains an unstable α subunit and a stable β subunit and is the main regulator for oxygen homeostasis.[51,53,59] PHD2 is the main regulator in the hypoxia response pathway, as conditional knockout (KO) of PHD2 in adult mice leads to excessive angiogenesis, a process that is upregulated with HIFα

stabilization.[49] PHD2 is preferential to HIF1α compared to HIF2α, whereas the opposite is true for PHD3.[49] PHDs hydroxylate proline residues at Pro-402 and Pro-564 in –Leu-X-X-Leu-Ala-Pro sequences located in the oxygen-dependent degradation domain (ODDD) of HIFα in normoxic environments, where there is sufficient oxygen availability.[49,51-53] Both proline residues in HIFα are located on the C-terminal end of the polypeptide.[51,52]

The hydroxylated proline residues are recognized by the von Hippel-Lindau protein (pVHL) E3 ubiquitin ligase complex and targeted for ubiquitination and proteasomal degradation.[51-53,59,63-65] However, under hypoxic conditions, PHD is inhibited and HIFα is stabilized HIFα localizes to the nucleus and forms a heterodimer with HIFβ.[49,51-53,59,63] The activated heterodimer binds to hypoxia-response elements (HREs) located in the regulatory regions of over 100 genes involved in decreasing oxygen consumption and increasing oxygen availability.[53] These genes include those involved with angiogenesis, such as VEGF; erythropoiesis, energy metabolism, apoptosis and cell proliferation.[53,59,63] In particular, HIFα upregulates genes that shunt glucose away from oxidative metabolism in the mitochondria and increase glycolysis.[66] Glucose transporter 1 (GLUT1), lactate dehydrogenase (LDHA) and pyruvate dehydrogenase kinase 1 (PDK1), which phosphorylates and inhibits pyruvate dehydrogenase and acetyl-CoA production, have all be shown to increase with HIFα stabilization.[66]

PHD2 KO mouse models lead to complications including polycythemia, increased ratio of red blood cell concentration to blood volume, and congestive heart failure.[64] Rishi and colleagues (2015) performed femoral artery ligations in PHD1 and PHD3 double KO mice. They determined that PHD1 and PHD3 double KO mice displayed increased VEGF levels and improved blood flow.[50] In contrast, Takeda and colleagues (2008) determined that not only did

PHD2 KO mice lead to overexpression of erythropoietin (EPO) resulting in polycythemia, but PHD1 and PHD3 double KO mice also led to polycythemia to a lesser extent. Hyperinsulinemia in T2D creates a hypoxic microenvironment, stabilizing HIFα to upregulate genes inducing oxidative stress and proinflammatory cytokines, resulting in insulin resistance.[68] There is evidence that the hypoxia response pathway plays a role in the pathogenesis of T2D.

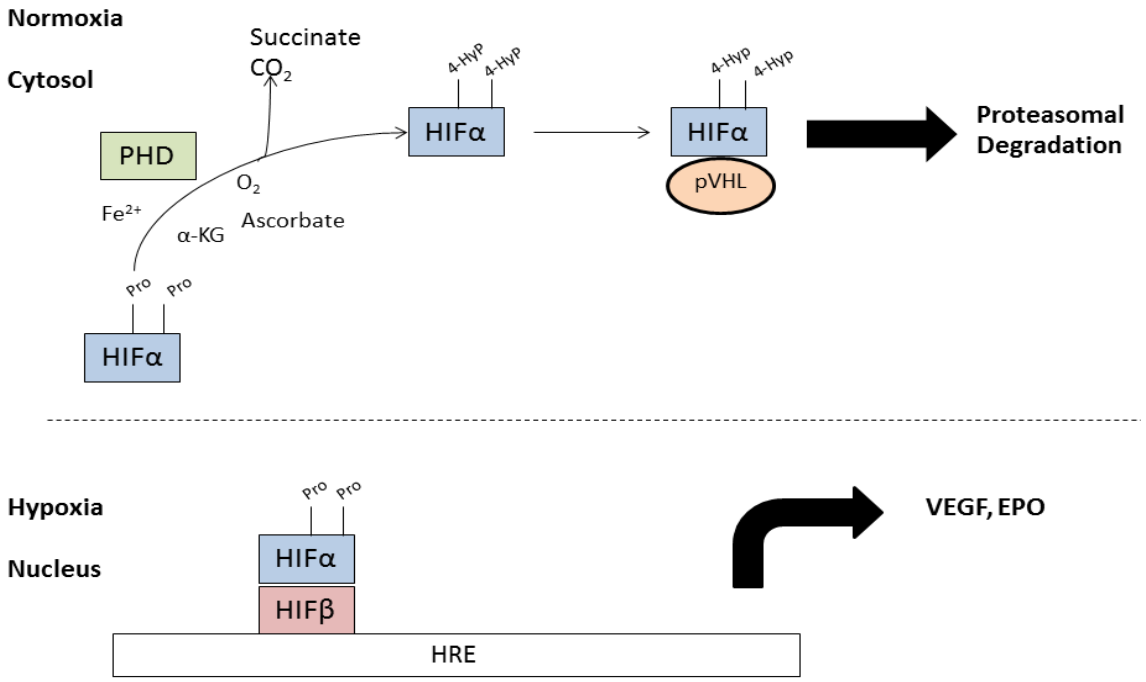

Figure 1.3: Hypoxia response pathway.

A schematic representation of the regulation of HIFα by PHD is shown above. PHDs hydroxylate proline residues on HIFα in normoxic conditions. Prolyl hydroxylated HIFα is recognized and targeted by pVHL for degradation. In hypoxic conditions, HIFα localizes to the nucleus and forms a heterodimer with transcription factor HIFβ. HIFα/HIFβ binds to HREs on DNA to upregulate genes involved in increasing oxygen availability and decreasing oxygen consumption including genes involved in angiogenesis and glycolytic enzymes.

1.3.3 Role of the hypoxia response pathway in T2D

There is conflicting evidence regarding the specific roles of the hypoxia response pathway in β-cell metabolism, function and development. Heinis and colleagues (2010) cultured rat embryonic β-cells to determine the role of oxygen tension in β-cell differentiation. When rat embryonic β-cells were exposed to hypoxia, HIF1α was stabilized and neurogenin 3 (Ngn3) was reduced.[69] Ngn3 is a transcription factor that is expressed in endocrine progenitor cells during embryogenesis and induces β-cell differentiation.[69] Embryonic β-cells exposed to hypoxia or treated with dimethyloxalylglycine (DMOG), a PHD inhibitor, increased HIF1α expression and decreased β-cell differentiation.[69] In a subsequent study, Heinis and colleagues (2012) demonstrated that Ngn3 and, therefore, β-cell development was decreased in pVHL depleted embryonic islets at E13.5. It was found that increased HIF1α resulted in decreased β-cell differentiation, potentially due to decreased ATP levels when HIF1α is upregulated.[70]

MIN6 cells, a mouse-derived β-cell line, and primary mouse islets display cellular hypoxia when stimulated with high glucose.[71] Glucose leads to a significant increase in oxygen consumption and consequent β-cell hypoxia.[71] Mild hypoxia during increased insulin secretion leads to HIF1α upregulation, causing a shift to anaerobic metabolism to alleviate the high oxygen demand.[71] Hypoxia, upregulated by increased oxygen consumption during GSIS, is exacerbated when oxygen availability is compromised.[71] Sato and colleagues (2011) determined oxygen availability to be impaired in both C57BL/6J mice on a HFD and leptin-deficient (ob/ob) mice. This was associated with defective microcirculation and blood supply that is seen in T2D.[71] Inducing HIF1α via hypoxia would perhaps reduce insulin secretion but also play a protective role during severe hypoxia.[72]

Similarly, INS-1 832/2 glucose unresponsive cells showed increased HIF1α and anaerobic metabolism compared to INS-1 832/13 glucose responsive cells.[73] Spegel and colleagues (2011) observed LDHA expression in glucose unresponsive cells, which was not expressed in 832/13 glucose responsive cells. Higher HIF1α protein levels were associated with impaired GSIS.[73] Another study demonstrated that hypoxia was correlated with a 23% decrease in insulin content and a 35% decrease in insulin biosynthesis in primary rat islets.[74] However, when primary islets were exposed to diazoxide, a K_{ATP} channel activator, prior to hypoxia the negative effects of hypoxia were counteracted and β-cell death was decreased.[74] Preconditioning with diazoxide opens K_{ATP} channels and inhibits Ca^{2+} influx, reducing basal glucose-stimulated mitochondrial metabolism.[72,74] Preconditioning altered basal mitochondrial metabolism and upregulated target genes of HIF1α prior to being exposed to hypoxia, possibly having protective effects.[74]

In contrast, a study using β-cell specific HIF1α KO mice determined that HIF1α is essential for β-cell function.[75] Cheng and colleagues (2010) observed that mitochondrial ATP production was significantly reduced in HIF1α KO mice. As well, this decrease in ATP production resulted in impaired glucose tolerance and β-cell dysfunction.[75] Iron chelators, deferoxamine (DFO) and deferasirox (DFS), were used to inhibit PHD, stabilizing HIFα and significantly improving glucose tolerance and insulin secretion in wild type (WT) mice on a HFD.[75] HIF1α displayed a dose-response relationship with β-cell function and an increase in glucose transporters was observed with iron chelators.[75] A modest increase in HIF1α appeared to have beneficial effects on β-cell function but overexpression seen in severe hypoxia resulted in toxicity.[75]

Chronic hyperglycemia in diabetic patients may in part, regulate the hypoxia response pathway via HIF1α. Sergiu-Bogdan and colleagues (2004) demonstrated that the protective effects of HIF1α are impaired by hyperglycemia using human primary dermal fibroblasts and endothelial cells. These observations were reproduced *in vivo* using biopsies of diabetic chronic foot ulcers displaying both hypoxia and hyperglycemia compared to chronic venous ulcers, which display a similar hypoxic environment.[76] HIF1α protein levels were lower in diabetic chronic foot ulcers compared to control chronic venous ulcers.[76] However, the data presented may be more relevant to treating the complications that arise from T2D, as the interaction between hyperglycemia and hypoxia may be a causal factor in other diabetic complications, including retinopathy, neuropathy and kidney disease.[76] These observations may not be pertinent, specifically in the regulation of insulin secretion but rather the global effects of hyperglycemia seen in diabetic patients.

Rodent models have been used to study the role of hypoxia in β-cell GSIS. PHD hypomorph mice, expressing reduced amounts of whole body PHD2 mRNA, were fed a chow or HFD.[77] PHD2 hypomorph mice on both diets had less adipose tissue, smaller adipocytes and decreased adipose tissue inflammation resulting in improved glucose tolerance and insulin sensitivity.[78] PHD2 hypomorph mice also displayed increased HIF1α stabilization and upregulation of HIF1α target genes, involving glucose transporters and glycolytic enzymes.[78] These results were replicated with oral administration of the PHD2 inhibitor FG-4497 in WT mice on both diets.[78]

Taniguchi and colleagues (2013) explored the effects of HIFα on insulin sensitivity using hepatic specific PHD3*fl/fl* mouse. PHD3*fl/fl* hepatocytes were infected with an adenovirus containing Cre recombinase, which targets the *loxP* sites within the PHD3 gene to generate a

knockdown.[79] Acute hepatic PHD3 knockdown resulted in HIF2α stabilization and improved glucose tolerance and insulin sensitivity.[79] The same results were shown in hepatic specific PHD3 KO mice.[79] This resulted in a 30% decrease in blood glucose levels, as well as a 50% decrease in plasma insulin levels.[79] HIF2α stimulated insulin receptor substrate 2 (IRS2), which is necessary for insulin sensitivity.[79] Interestingly, additional KO of other PHD isoforms led to a further increase in HIF2α which did not improve insulin sensitivity but rather led to toxicity and hepatic steatosis.[79]

There are several models used to demonstrate the role of the hypoxia response pathway in T2D and specifically β-cell function, including HIFα, pVHL and PHD KO animal models. However, in humans, T2D is associated with severe hypoxia, as excessive glucose from nutrient overload places a high demand on the mitochondria and oxidative phosphorylation, leading to decreased ATP production in the β-cell.[71] HIFα is also thought to be associated with glucose intolerance and insulin insensitivity in β-cells but may have beneficial effects with diabetic complications.[76] It is plausible that HIFα is beneficial at low levels but could lead to toxicity if overexpressed.[75] PHDs are the main regulators of HIFα , however, PHDs also regulate non-HIFα targets; with PHD3 having the widest range of targets.[80] PHD has been shown to prolyl hydroxylate other proteins that may be involved in regulating insulin secretion.

1.3.4 Other targets of PHDs

PHDs prolyl hydroxylate other proteins apart from HIFα. Particularly, PHD3 is thought to play a significant role in apoptosis and tumor development.[81] Growing tumors have poor vasculature leading to decreased oxygen availability, which triggers the hypoxia response pathway as a means of temporary cell survival.[81] PHD3 is downregulated in many types of

cancer such as pancreatic, colon and metastatic melanoma.[82] PHD3 regulates cell proliferation, differentiation, and migration and therefore, may play a role in metastatic cancers.[82,83]

Actin filaments are required for cell motility and dysregulation of actin is associated with cancer development and metastasis.[82] Luo and colleagues (2014) demonstrate that PHD3 is a negative regulator of F-actin, which inhibits metastasis via hydroxylation on proline residues -307 and -322. Inhibition of F-actin production led to decreased cell migration and, therefore, metastasis.[82] Paired box 2 (Pax2) is a transcription factor that regulates cell differentiation, proliferation, migration, and survival.[84] Pax2 is expressed in a variety of cancers including leukemia, breast, prostate, kidney, and bladder.[84] PHD3 was found to hydroxylate and target Pax2 for degradation post transcriptionally; however, the mechanism remains unclear.[84]

Sprouty homolog 2 (SPRY2) inhibits cell surface receptors tyrosine kinases, which regulate cell proliferation and migration.[83] Anderson and colleagues (2011) showed that PHD3 has a stronger interaction with SPRY2 proteins compared to PHD1 and PHD2 through immunoblot analysis in HeLa cells. PHDs interact with SPRY2, inhibiting proliferation and migration.[83] Receptor tyrosine kinase, c-kit plays a role in β-cell maturation and function and islet vascularization.[85] β-cell specific mutation of c-kit resulted in impaired vasculature and β-cell function whereas, overexpression in mice significantly improved islet vasculature and β-cell function.[85] PHD3 regulation of SPRY2 elucidate PHD3 as a potential target for the treatment of cancer but further research is warranted to investigate whether regulation of these proteins by PHD plays a role in β-cell function.

Activating transcription factor 4 (ATF4) is a regulator of the unfolded protein response, determining cell fate.[65] Koditz and colleagues (2007) showed that PHD3 interacts with the leucine zipper motif, or zipper II, of ATF4, negatively regulating ATF4. Inhibition of PHDs via

DMOG and incubation in 1% oxygen induced ATF4 activity in HeLa cells.[65] More recently, it was shown that ATF4 interacts with PHD1.[86] PHD1 positively regulated ATF4 in HeLa and HEK293T cells, contrary to PHD3.[86] Immunoprecipitation experiments, where proline residues were mutated to alanine, did not affect the interaction of PHD1 or PHD3 with ATF4, suggesting that PHD1 and PHD3 do not regulate ATF4 via prolyl hydroxylation.[85] ATF4 induced 4E-BP1 in MIN6 β-cells and primary mouse islets, promoting β-cell survival under ER stress.[87] 4E-BP1 KO mice displayed increased ER stress-induced β-cell apoptosis.[87] PHD interacts with ATF4 in cancer cell lines but PHD could potentially interact with ATF4 in β-cells to regulate ER stress induced-apoptosis.

β_2-adrenergic receptors (β_2AR) are G-protein coupled receptors that regulate receptor homeostasis and play a role in cardiovascular disease and pulmonary function.[88] Hypoxia present in patients with heart failure and asthma, stabilizes β_2AR and increases catecholamine release.[88] This adaptation works to increase cardiac output and peripheral vasodilation to increase oxygen availability.[88] Xie and colleagues (2009) found that siRNA inhibition of PHD3 increased β_2AR and PHD3 deficient mice displayed increased blood pressure and heart contractility via prolyl hydroxylation of β_2AR at proline residues -382 and -395. PHD targets proteins that are involved in a variety of cancers and cardiovascular disease, for which T2D is a major risk factor. PHD also targets glycolytic enzymes that alter glucose metabolism and could potentially play a role in insulin secretion.

1.3.5 The role of PHD in altering glucose metabolism

The hypoxia response pathway is an adaptation for temporary cell survival and works to increase oxygen availability and decrease oxygen consumption. Proteins that are prolyl

hydroxylated via PHD are recognized by pVHL ubiquitin E3 ligase complex and targeted for degradation. pVHL plays a role in oxygen sensing and energy homeostasis.[89] Vhlh gene KO, the gene encoding pVHL, in β-cells of adult mice using the Cre-lox system resulted in β-cell dysfunction, impaired glucose tolerance and reduced GSIS *in vivo*.[89] Interestingly, insulin secretion was normal compared to WT controls at basal conditions but when glucose stimulus was increased, insulin secretion was impaired *in vivo*.[89]

PDH catalyzes the conversion of pyruvate to acetyl-CoA, which enters the TCA cycle for ATP production.[90] PDH is composed of E1α, E1β, E2 and E3 subunits.[90] PDH activity is determined by phosphorylation and dephosphorylation via PDK1, where PDK1 is upregulated in hypoxic environments.[90] PDK1 inhibits PDH by phosphorylating the E1α subunit, decreasing acetyl-CoA production and oxidative metabolism.[90] Kikuchi and colleagues (2014) determined that PHD3 KO mouse embryonic fibroblasts (MEFs) and PHD3-depleted MCF7 breast cancer cells showed decreased PDH function via immunoprecipitation and western blot analysis PHD3 KO MEFs were resistant to cell death during prolonged hypoxia.[90] PHD3 was shown to interact with the E1β subunit of the PDH complex and positively regulate PDH to increase acetyl-CoA production.[90]

PHD3 has also been shown to interact with pyruvate kinase M2 (PKM2), which catalyzes the final reaction in glycolysis, producing pyruvate and ATP.[91] PHD3 acts as a coactivator by binding to PKM2 to enhance PKM2's interaction with HIFα, stabilizing HIFα and increasing GLUT1, lactate dehydrogenase A (LDHA) and PDK1.[91] These proteins enhance glucose uptake, lactate production, and inhibit oxidative metabolism, respectively, resulting in the Warburg effect.[91] The Warburg effect is a metabolic shift towards glycolysis to reduce oxygen utilization in many types of cancer cells.[91] PHD3 knockdown in HeLa, MEFs, RCC4, Hep3B and

HEK293T cells via retrovirus or lentivirus resulted in reduced glucose uptake and lactate production, and increased oxygen consumption.[91] It was determined using *in vitro* hydroxylation assays that PHD3 hydroxylates proline residues at positions -403 and -408 on PKM2.[91]

Some cancers, such as acute myeloid leukemia rely on fatty acid oxidation (FAO).[92] PHD3 was shown to inhibit FAO by hydroxylating proline residues at position -450 and activating acetyl-CoA carboxylase 2 (ACC2) in 293T cells.[92] ACC2 inhibits carnitine palmitoyl transferase 1 (CPT1), thereby reducing long-chain fatty acid translocation from the cytosol into the mitochondria for oxidative metabolism.[92] Repression of FAO by PHD3 resulted in increased apoptosis and PHD3 overexpression resulted in a 50% reduction of FAO in cells.[92]

Cell lines and animal models using siRNA inhibition and pharmacological inhibitors including broad and specific inhibitors have been used to study the role of PHD in a variety of pathways. A well-established PHD inhibitor used in the experiments that are presented in this thesis is the synthetic αKG analogue, DMOG, to investigate the role of PHD in GSIS.

1.4 Pharmacological inhibitors of PHDs

1.4.1 Dimethyloxalylglycine (DMOG)

DMOG is a competitive inhibitor of all PHD isoforms and other members of the 2-oxoglutarate dioxygenase superfamily.[93,94] DMOG is a synthetic amide analogue of αKG and is able to penetrate cell membranes where it is then converted to N-oxalylglycine (NOG) via carboxylesterases.[93,94] DMOG also increases the amount of substrate that binds to PHDs.[95]

Zhdanov and colleagues (2015) measured ATP production in HCT116 cancer cells treated with DMOG and deprived of glucose. There was a significant decrease in ATP concentration in cells deprived of glucose 30 minutes after DMOG treatment and ATP levels were almost depleted after four hours of DMOG treatment compared to control cells.[93] These

results reveal that DMOG is fast-acting and may alter metabolism faster than HIF-dependent mechanisms.[93]

DMOG has been used to study oxygen-induced retinopathy (OIR).[96,97] The first phase of OIR hyperoxia results from decreased VEGF due to destabilization of HIFα.[96,97] OIR rats were intraperitoneally injected with 200µg/g DMOG causing systemic reduction in PHD, stabilizing HIFα.[96,97] Intraperitoneal injection of 200µg/g was sufficient to upregulate HIFα and provide protective effects in hyperoxic OIR rats.[96,97] Before the discovery of PHD, iron chelators were used to induce HIFα expression. More recently, selective PHD inhibitors have been developed, some of which are in clinical trials for end stage renal disease.

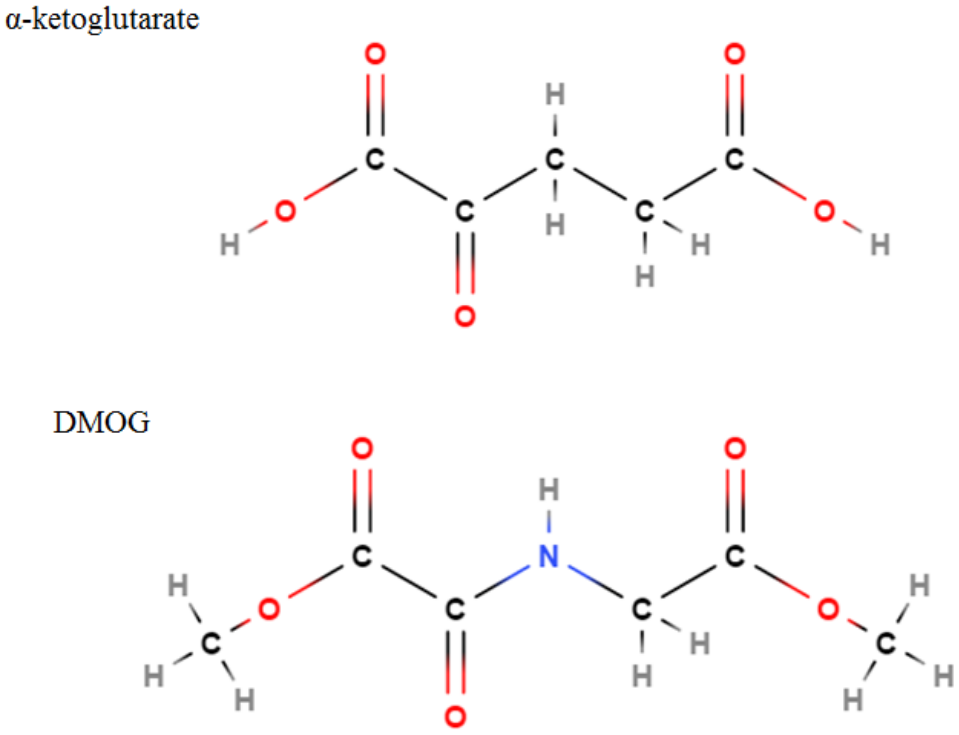

Figure 1.4: Comparing αKG and DMOG.

The chemical structures of the TCA cycle intermediate αKG and the PHD inhibitor DMOG. Images were designed using the open source web-based program MolView.

1.4.2 Other inhibitors of PHD

Other PHD inhibitors include iron chelators and selective PHD inhibitors.[47,94,98] The iron chelator ethyl-3,4-dihydroxybenzoate (EDHB) is a competitive inhibitor of PHD, creating an iron deficient environment resulting in decreased PHD activity.[98] EDHB also displays a strong inhibition towards αKG and ascorbate.[98] Huang and colleagues (2016) found EDHB reduced GSIS in 832/13 cells at 100 and 2000µmol/L but increased GSIS at 200 and 500µmol/L. EDHB reduced the ATP/ADP ratio and TCA cycle intermediates including pyruvate, citrate, fumarate, and malate in 832/13 cells, suggesting PHD plays a role in oxidative metabolism.[47] However, EDHB is not as specific as other PHD inhibitors and is suggested to play a negative role in iron metabolism.[98]

FG-4592, also known as Roxadustat, is a hypoxia mimetic and is currently in phase III clinical trials for the treatment of anemia and chronic kidney disease via upregulation of erythropoietin (EPO) through HIFα stabilization.[99,100] FG-4592 treated HEK293T cells displayed increased GLUT1, hexokinase 2, and LDHA, upregulating glycolysis by 25%.[99] FG-4592 shunts carbon away from aerobic metabolism and towards anaerobic metabolism in both a hypoxic and normoxic environment.[99] FG-4592 may also play a beneficial role in mitochondrial dysfunction and a potential treatment option for T2D.[99,100] Clinical trials using another hypoxia mimetic, GSK1278863, reported decreased serum cholesterol levels and improved HDL/LDL lipoprotein profiles as side effects.[101]

FG-2216 (IOX3) was used in a phase I clinical trial in 12 end-stage renal disease patients who were on dialysis.[102,103] Oral administration of 20mg/kg body weight FG-2216 increased endogenous EPO production. However, this study lasted 7 days and the long-term effects of FG-2216 is unknown.[102] Chronic HIFα stabilizers could potentially lead to polycythemia.[102] Chan

and colleagues (2016) assessed the regulation of hypoxia-regulated genes and found that FG-2216 resulted in a 35% increase in HIFα gene targets, compared to DMOG, which resulted in a 50% increase in HIFα gene targets.

IOX2 is a selective PHD2 inhibitor, where the thiazole ring displaces the side chain of αKG.[103] IOX2 has a 400-fold selectivity for PHD2, whereas IOX4 has an 857-fold selectivity for PHD2 but is also suggested to be a potent inhibitor of PHD1 and PHD3.[103] Mice were injected with IOX2, IOX4 and DMOG to assess potency.[103] IOX2 was shown to have the strongest induction of HIF1α and HIF2α with DMOG displaying the lowest induction.[103]However, Chan and colleagues (2016) concluded that DMOG better represented the hypoxic response compared to selective PHD inhibitors through *in vitro* hydroxylation assays in MCF-7 cells compared to cells incubated in 0.5% oxygen. HIF1α and HIF2α were significantly upregulated by both hypoxia and DMOG and upregulated to a lesser extent by FG-2216 and IOX2.[94] PHD inhibitors have been used in multiple cell lines, rodent models and human clinical trials to assess the role of PHD and HIFα in disease states. The experiments presented in this thesis focus on exploring the role of PHD using DMOG in primary mouse islets and male C57BL/6J mice, as well as, discussing future research exploring the role of PHD in a transgenic mouse model.

1.5 Animal models

1.5.1 Cre-lox System

Another approach to studying the role of specific genes in disease states is to use a transgenic mouse model, which can either overexpress or KO a gene of interest. The Cre-*lox* system is done by homologous recombination in embryonic stem cells and introduces nucleotide sequences, or *loxP* sites, on either side of an exon within a gene, flanking the gene to be

deleted.[104] These *loxP* sequences are recognized by the Cre-recombinase (Cre) enzyme, which recognizes the *loxP* sites to generate a KO.[104]

Mice that contain *loxP* sequences around a specific exon within a gene are crossed with mice that express Cre under a tissue-specific promotor to allow deletion of the gene in a particular tissue.[104] Previous models used Cre expressed on the rat Ins-2 gene, but Ins-2 is also expressed in the hypothalamus in both embryonic and adult mice.[104] Thorens and colleagues (2015) generated mice expressing Cre on the β-cell specific Ins-1 gene. Mice expressing Cre on the eostrogen receptor fusion protein (Cre^{ERT2}), in which Cre is activated via tamoxifen injections to induce a knockdown in a time-controlled manner.[104] Cre^{ERT2} may be beneficial when studying disease states with later onsets, such as T2D.

Thorens and colleagues (2015) demonstrated the selectivity of expressing Cre on the Ins-1 gene by crossing Ins-1^{Cre} and Ins-$1^{CreERT2}$ mice with Rosa26-eYFP mice to determine tissues containing *loxP* site recombination by immunofluorescence. Recombination was exclusively in β-cells for both Ins-1^{Cre} and Ins-$1^{CreERT2}$ mice.[104] It was concluded that four injections of tamoxifen over a two week period in 10 week old male mice resulted in a knockdown with 60-70% recombination.[104] Ins-1^{Cre} and Ins-$1^{CreERT2}$ mice can then be crossed with mouse models containing *loxP* sites around an exon within a particular gene, such as PHD, to generate PHD KO mice.

1.5.2 PHD transgenic mice

In the experiments presented in this thesis, transgenic PHD123*fl/fl* mice and PHD2*fl*/*fl* mice were used, with *loxP* sequences around exon 2 for PHD2 and PHD3, and *loxP* sequences

around exon 3 for PHD1.[62] All of the *loxP* sites are approximately 230 base pairs long and located in the intron sequences.[62]

When PHD123*fl/fl* and PHD2*fl/fl* mice are crossed with C57BL/6J mice expressing Cre recombinase exclusively in pancreatic β-cells, the result is offspring with exon 2 or exon 3deleted, generating PHD KO mice in β-cells.[62] These exons contain residues His-271 and Asp-273 in PHD1, His-290 and Asp-292 in PHD2, and His-135 and Asp-137 in PHD3.[62] These histidine and aspartate residues are required for Fe^{2+} binding, and therefore PHD activity.[62]

1.6 Rationale

The complexity of T2D poses a major issue in treatment and management, often leading to combinational therapy with adverse effects. Understanding the mechanisms of pancreatic β-cell insulin secretion, particularly involvement of K_{ATP} channel-independent pathways, is needed to develop more effective treatment strategies. Therefore, our lab studies the role of PHD in second-phase insulin secretion utilizing cytosolic αKG as a co-substrate to regulate insulin secretion. Previous studies elucidate the importance of pyruvate cycling through PC to generate metabolites, such as αKG, that results in increased GSIS.[105]

Pyruvate enters the mitochondria and undergoes oxidative metabolism to increase insulin secretion. Pancreatic β-cells express abundant PC and PDH and in approximately equal proportions.[105-107] In gluconeogenic tissues, the formation of glucose from non-glucose precursors such as the liver, PC plays a major role.[107] Gluconeogenic enzymes phosphoenolpyruvate and fructose-1,6-bisphosphotase are rate-limiting but are not expressed in pancreatic β-cells, signifying another role for PC in islets.[107] In particular, PC is reduced in β-cells of T2D rodent models.[105] siRNA inhibition of PC in 832/13 cells and dispersed rat islets demonstrated decreased insulin secretion, proliferation in 832/13 cells and TCA cycle

intermediate concentrations of oxaloacetate, malate, ATP and NADPH, suggesting that PC is required for anaplerosis.[105] Overexpression of PC led to increased insulin secretion and proliferation, whereas, inhibition of PDH in 832/13 cells did not significantly reduce insulin secretion.[105]

Pyruvate cycling plays a role in stimulating insulin secretion and depends on the transport of TCA cycle metabolites to the cytosol.[46] TCA cycle intermediates including NADPH and αKG may function as coupling factors linking glycolysis in the cytosol to cellular respiration in the mitochondria leading to increased GSIS.[46,108] There are three pathways involved in pyruvate cycling: the pyruvate/malate pathway, pyruvate/citrate pathway, and pyruvate/isocitrate pathway that generate NADPH and αKG, important signaling molecules that are involved in insulin secretion.[46] In the pyruvate/malate pathway, malate is transported to the cytosol by dicarboxylate carrier (DIC) and malic enzyme converts malate to pyruvate, producing NADPH.[46,108] Inhibition of DIC resulted in inhibition of the pyruvate/malate shuttle and reduced NADPH and GSIS in 832/13 cells and primary rat islets.[46]

The citrate isocitrate carrier (CIC) transports citrate and isocitrate from the mitochondria to the cytosol and is involved in the pyruvate/citrate and pyruvate/isocitrate shuttles.[46] Pharmacological inhibition of CIC resulted in decreased GSIS in 832/13 cells and primary rat islets in first- and second-phase insulin secretion.[109] As well, overexpression of CIC resulted in increased GSIS, demonstrating the importance of cytosolic citrate and isocitrate in insulin secretion.[109] NADP-dependent isocitrate dehydrogenase (ICDc) converts cytosolic isocitrate to αKG, producing NADPH as a by-product.[46,110] Ronnenbaum (2006) and colleagues found that siRNA inhibition of ICDc resulted in decreased GSIS in both 832/13 cells and primary rat islets, highlighting the importance of cytosolic αKG and NADPH in insulin secretion.

Using liquid chromatography/mass spectrometry, Lorenz and colleagues (2013) observed a transient decrease in αKG after a glucose stimulus but a 3- to 4- fold increase at later time points. The later increase supports the role of αKG in anaplerosis to augment second-phase insulin secretion via pyruvate cycling.[112] Huang and Joseph (2014) revealed that αKG levels did not increase until 10 minutes after a glucose load in 832/13 cells and continued to rise through the 60 minute period. These results suggest that αKG is a coupling factor in K_{ATP} channel-independent pathways.[40] Transportation of αKG from the mitochondria to the cytosol is facilitated by the 2-oxoglutarate carrier (OGC).[110] OGC siRNA knockdown in 832/13 cells and primary rat islets revealed significantly reduced GSIS.[110] Pharmacological inhibition of OGC via dimethyl-2OG also decreased GSIS.[110]

αKG plays a role in second-phase insulin secretion but the mechanism remains incompletely understood. Fallon and colleagues (2008) used EDHB in human and rat pancreatic islets. EDHB was found to inhibit PHD by approximately 50% and reduced insulin secretion by 90%.[48] It is suggested that αKG translocation to the cytosol is required for insulin secretion by serving as a co-substrate for PHDs.[48] EDHB also inhibited glucose utilization, ATP content and TCA cycle intermediates pyruvate, citrate, fumarate and malate.[47] siRNA inhibition of PHD1, PHD2, and PHD3 in 832/13 cells determined that PHD1 and PHD3 knockdown decreased GSIS whereas PHD2 did not affect GSIS.[47] Our lab chose to further explore the role of PHDs in pancreatic β-cell insulin secretion using the pharmacological inhibitor DMOG in both INS-1 832/13 cells and primary mouse islets to study acute effects of PHD inhibition. We have also generated PHD KO transgenic mice to explore both short- and long-term effects of PHD in insulin secretion.

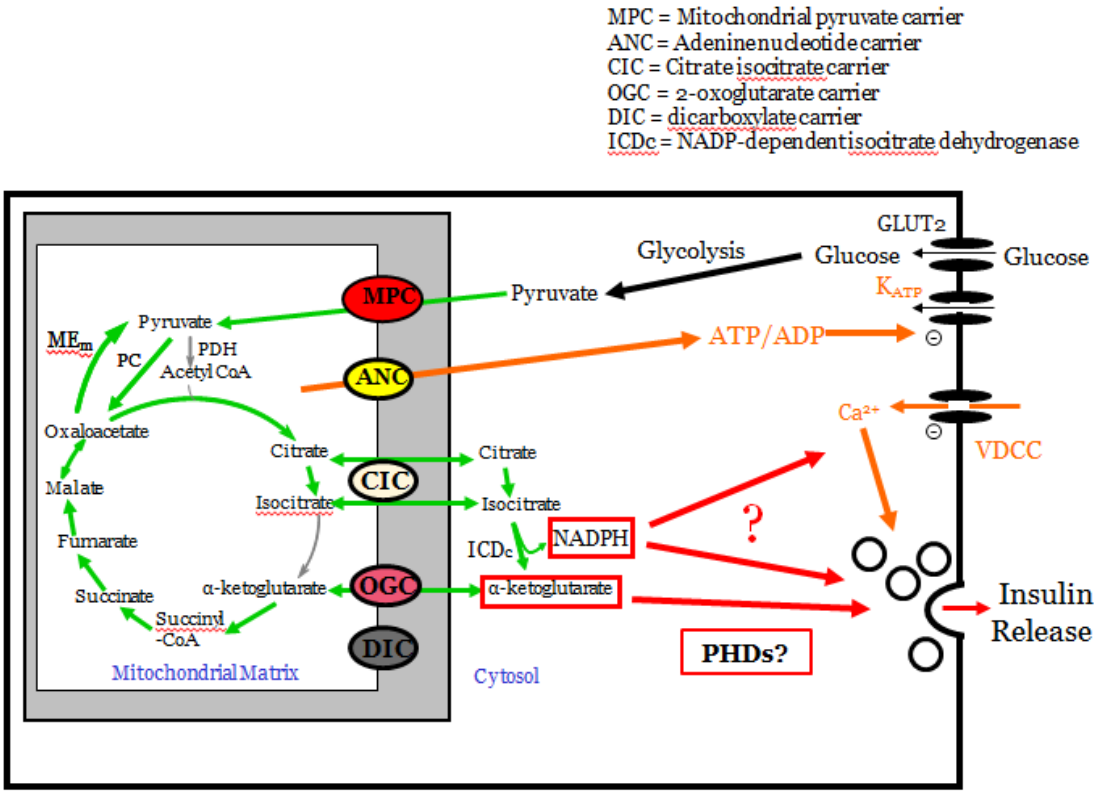

Figure 1.5: TCA cycle intermediate transport carriers.

CIC transports citrate and isocitrate from the mitochondria to the cytosol. ICDc converts isocitrate to αKG and produces NADPH. NADPH and αKG may be signaling molecules that stimulate insulin secretion. αKG also acts as a co-substrate for PHD, which may directly regulate insulin secretion. *Illustration reproduced courtesy of Dr. Jamie Joseph.*

Chapter 2: Objectives and Hypothesis

2.1 Hypothesis

Nutrient-stimulated anaplerosis increases cytosolic αKG, enhancing PHD activity resulting in short- and long-term effects on insulin secretion.

2.2 Objectives

1. Confirm expression and subcellular localization of PHD1, PHD2, and PHD3 in INS-1 832/13 cells and primary mouse islets by western blot analysis and immunofluorescence.
2. Assess the role of PHDs using DMOG *in vitro* by measuring oxygen consumption rate and both static and dynamic insulin secretion.
3. Assess the role of PHDs using DMOG *in vivo* by measuring blood glucose levels and plasma insulin levels in response to an exogenous glucose load.
4. Identify prolyl hydroxylated proteins by PHDs in INS-1 832/13 cells via MALDI mass spectrometry.

Chapter 3: Methods

3.1 PHD expression and subcellular localization

3.1.1 Western blot

Protein samples were collected from 832/13 cells and primary mouse islets after an insulin secretion assay. Protease inhibitor cocktail (Sigma, Oakville, ON) was diluted in a 1X lysis buffer (diluted in milliQ H_2O) (Cell Signaling, Danvers, MA, USA) (1:400) and was added to 832/13 cells or a 3X lysis buffer (diluted in milliQ H_2O) (Cell Signaling, Danvers, MA, USA) was added to isolated islets (120-150 islets/treatment) infected with shGFP, RIP Cre adenovirus (Vector Biolabs, Malvern, PA, USA) or no treatment (NT). 832/13 cells were treated with low glucose (LG) (2mM) and islets were treated with LG (2mM), high glucose (HG) (16.7mM), LG (2mM) + KCl (30mM) + diazoxide (200µM), HG (16.7mM) + KCl (30mM) + diazoxide (200µM) or HG (16.7mM) + dimethyl maleate (DMM) (10mM) + dimethyl α-ketoglutarate (DMαKG) (10mM). All treatments were diluted in cell Krebs-Ringer bicarbonate buffer (KRB) (KRB stock (4.32mM KCl, 1.20mM $MgSO_4$, 1.5mM KH_2PO_4), 129mM NaCl, 10mM HEPES, 5mM HCO_3, 3.11mM $CaCl_2$, 0.1% BSA, pH 7.4) or islet KRB (KRB stock (120mM NaCl, 4.8mM KCl, 2.5mM $CaCl_2$, 1.2mM $MgCl_2$), 5mM HEPES, 24mM HCO_3, 0.1% BSA, pH 7.4). 832/13 cells were scraped and centrifuged at 12,500 rpm for 30 minutes at 4˚C. Islets were incubated on ice for 15 minutes and centrifuged at 12,500 rpm for 30 minutes at 4˚C. Protein concentration for 832/13 cells was determined by a bicinchoninic acid (BCA) protein assay. NuPAGE LDS sample buffer (4X) (ThermoFisher Scientific, Carlsbad, CA), NuPAGE reducing agent (10X) (ThermoFisher Scientific, Carlsbad, CA) and deionized water were added to approximately 20µg of protein from 832/13 cells and total protein for islets (120-150 islets/treatment). Samples were heated at 70˚C for 10 minutes and run on a NuPAGE 10% Bis-

Tris SDS polyacrylamide Mini Gel (ThermoFisher Scientific, Carlsbad, CA) with 1X running buffer (Life Technologies, Carlsbad, CA) (supplemented with NuPAGE antioxidant (ThermoRisher Scientific, Carlsbad, CA)) for 50 minutes with a maximum voltage of 200V.

A 0.45 µM pore size Invitolon PVDF membrane (Life Technologies, Carlsbad, CA) was activated using methanol and protein samples were transferred to a PVDF membrane for 1.5 hours with a maximum voltage of 30V in 1X transfer buffer (ThermoFisher Scientific, Carlsbad, CA) (supplemented with NuPAGE antioxidant (ThermoFisher Scientific, Carlsbad, CA)). PVDF membranes were washed twice for five minutes with tris-buffered saline (TBS) (0.1% tween). PVDF membranes were incubated for 30 minutes with superblock blocking buffer (ThermoFisher Scientific, Carlsbad, CA). PVDF membranes were incubated for two hours for all primary antibodies and one hour for all secondary antibodies at room temperature with three five minute washes in between with TBS (0.1% tween). The following antibodies were used: rabbit Anti-PHD1/prolyl hydroxylase (1:1000) (Abcam, Toronto, ON), rabbit PHD2/Egln1 Rabbit mAb (1:1000) (Cell Signaling, Danvers, MA), rabbit Anti-PHD3 (1:1000) (Abcam, Toronto, ON), Anti Rabbit IgG (1:10000) (Sigma, Oakville, ON), Anti-Mouse IgG (1:10000) (Sigma, Oakville, ON) and mouse Monoclonal Anti-γ-Tubulin (1:10000) (Sigma, Oakville, ON). Images were detected using Kodak Image Station 4000 MM Pro using 1mL Luminata Crescendo Western HRP Substrate (Millipore, Billerica, MA). Western Blot images were analyzed using Imagej (https://imagej.nih.gov/ij/) (Bethesda, MD, USA).

3.1.2 Immunofluorescence

Male mouse pancreases were isolated and fixed in Z-fix solution (Anatech, LTD, MI, USA). Fixed pancreases were sent to the Animal Health Laboratory at the University of Guelph

to be mounted on formalin-fixed, paraffin-embedded slides. Slides were placed in three xylene baths for five minutes each. Slides were then placed in two 100% ethanol baths for five minutes each and then 70% ethanol once for five minutes. Slides were rinsed under running water for approximately 30 seconds. 400mL 1X antigen retrieval solution (Dako, Mississauga, ON) was microwaved on high for four minutes. Slides were then placed in the antigen retrieval solution and microwaved on high for an additional five minutes. Slides were cooled for one minute under running water. Slides were blocked with superblock solution (Thermo Scientific, Mississauga, ON) for 30 minutes.

Rabbit mAb PHD1 (1:100), Rabbit mAb PHD2 (1:50) or Rabbit pAb PHD3 (1:100) antibodies were diluted in superblock solution and 1mL of diluted antibody was placed on each slide and incubated overnight at 4˚C. The following morning, slides were washed three times for five minutes with PBS. Alexa Fluor® 647 anti-rabbit IgG secondary antibody (1:500) (Life Technologies, OR, USA) was diluted in superblock solution and 1mL of diluted antibody was placed on each slide and incubated for two hours at room temperature. Slides were washed three times for five minutes with PBS. Guinea pig anti-insulin antibody (1:600) (Dako, Mississauga, ON) was diluted in superblock and 1mL was added to each slide and incubated for two hours at room temperature. After incubation, slides were washed three times for five minutes with PBS. Anti-Guinea Alexa Fluor® 488 secondary antibody (1:500) (Jackson Immunoresearch, PA, USA) was diluted in superblock and 1mL was added to each slide and incubated for two hours at

room temperature. After incubation, slides were washed three times for five minutes with PBS and then rinsed for 30 seconds under running water. Slides were placed in 50%, 70% and 100% ethanol baths for one minute each. Slides were then placed in three xylene baths for five minutes each. One drop of Prolong Gold (Life Technologies, Mississauga, ON) was added to a cover slip and placed on each slide. Slides were set to dry overnight at room temperature. Immunofluorescence was analyzed using a Nikon Eclipse Ti microscope (Mississauga, ON, CA).

3.2 *In vitro* experiments

3.2.1 Oxygen consumption rate (OCR)

Oxygen consumption was measured using Seahorse Bioscience XF24 Respiration Assay (Lexington, MA, USA). 832/13 cells were plated at a concentration of 100,000 cells per well and islets were plated at a concentration of 45 islets per well. Cells were plated on a XF24 V7 culture microplate and grown for five days. Islets were plated on a V17 TC-treated XF24 islet capture microplate the following day after islet isolation. Each well of the utility plate in the XF24 extracellular flux assay kit was filled with 1mL of calibrant solution and hydrated overnight (37˚C, no CO_2). Cell media (RPMI-1640 supplemented with 50mL FBS, 11mL 50X INS (200mM glutamine, 100mM Na pyruvate, 35.2µL 2-mercaptoethanol) and 5mL P/S antibiotic) or islet growth media (RPMI-1640 supplemented with 0.5mL of HEPES (1M, pH 7.4), 5mL FBS, 0.1mL P/S/F (10000U/mL penicillin G sodium, 10000µg/mL of streptomycin sulfate, 25µg/mL of amphotericin B as fungizone) and 0.55mL 200mM glutamine) was replaced with LG (2mM) KRB for two one hour washes for 832/13 cells and two 30 minute washes for islets (37˚C, 5% CO_2). After two washes, wells were replaced with fresh LG (2mM) KRB. Port A row A in the sensor cartridge of the utility plated contained 16.7mM glucose. Port A in rows

B, C and D contained 200µM, 500µM, and 1000µM DMOG diluted in HG (16.7mM) KRB, respectively for 832/13 cells and 1mM, 5mM, and 10mM DMOG diluted in HG (16.7mM) KRB, respectively for islets. Port B in all rows contained 10µM oligomycin for 832/13 cells and 20µM oligomycin for islets, port C in all rows contained 50µM 2,4-dinitrophenol (DNP) + 20mM sodium pyruvate for 832/13 cells and 100µM DNP + 5mM DMM + 5mM DMαKG for islets, and port D in all rows contained 5µM of rotenone + 5µM myxothiazol for 832/13 cells and 10µM rotenone + 10µM myxothiazol for islets. 75µL of all drugs were added to each port in the cartridge sensor and all drugs were diluted in HG (16.7mM) KRB. The utility plate with the cartridge sensor was placed in the instrument tray and calibrated. The utility plate containing the calibrant solution was replaced with the cell or islet plate after calibration. The mix-wait-measure cycles were three minutes, two minutes, and three minutes, with at least three cycles for each injection.

Spare respiratory capacity was calculated by subtracting basal oxygen consumption rate (OCR) from pyruvate + DNP or DNP + DMM + DMαKG OCR values. Proton leak was calculated by subtracting rotenone + myxothiazol OCR values from oligomycin OCR values. ATP turnover was calculated by subtracting oligomycin OCR values from basal OCR values. Non mitochondrial oxygen consumption was calculated from rotenone + myxothiazol OCR values.

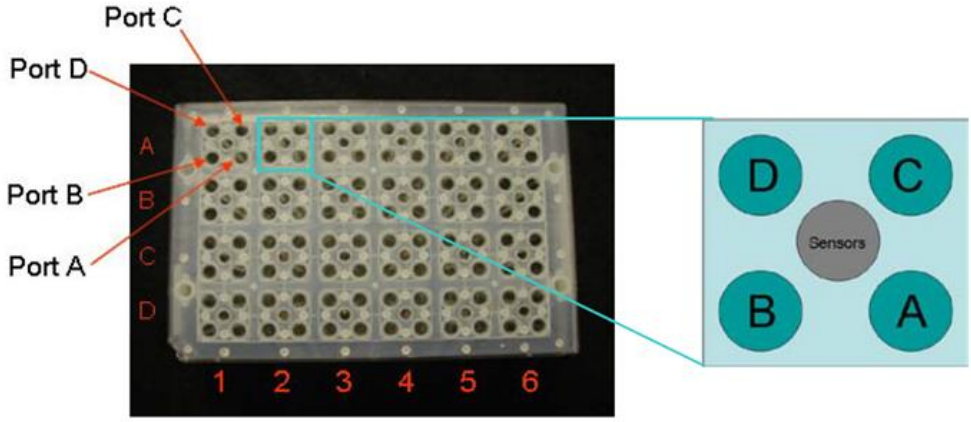

Figure 3.1: Seahorse Bioscience XF24 Respiration Assay sensor cartridge.

Drugs were loaded into respective ports in wells containing 832/13 cells or islets. Port A row A contained 75µL of HG (16.7mM) KRB, Port A rows B, C and D contained 75µL of 200µM, 500µM, and 1000µM DMOG diluted in HG (16.7mM) KRB, respectively for 832/13 cells and 1mM, 5mM, and 10mM diluted in HG (16.7mM) KRB, respectively for islets. Port B in all rows contained 75µL of oligomycin, port C in all rows contained 75µL of pyruvate + DNP for 832/13 cells and DNP + DMM + DMαKG for islets and port D in all rows contained 75µL of rotenone + myxothiazol. All ports in wells A1, B4, C3, and D5 contained 75µL of deionized water as blanks. *Illustration reproduced courtesy of Dr. Jamie Joseph.*

3.2.2 Islet isolation

Pancreatic islets were isolated from C57BL/6J male mice aged 10-14 weeks (Jackson Laboratories) or PHD123*fl/fl* male mice aged 10-14 weeks (University of Connecticut, USA). Mice were anesthetized with 100mg/kg body weight pentobarbital (54.7mg/mL solution, CEVA Sante Animale). Incisions were made in a T-shape form and the common bile duct was located. The bile duct was first sutured distally, where the bile duct meets the duodenum. A second suture was made proximally where the bile duct meets the liver. A small incision was made

approximately 1/3 below the proximal suture. A 27 ¾ G needle attached to a syringe containing digestion media (Hanks dissociation buffer supplemented with 10mM HEPES, 1.28µg/mL DNase I, and 0.4 wu units/mL of Liberase TL Research Grade (Roche)) was used to cannulate the common bile duct. The pancreas was perfused with approximately 2-3mL of digestion media. A blunt dissection was performed to remove surrounding tissue and to isolate the pancreas. After islets were digested in a water bath for 30 minutes at 37˚C, islets were washed three times to remove debris and prevent DNA contamination. Islets were placed in a petri dish and picked under a stereomicroscope and cultured in 3mL islet growth media (RPMI-1640 supplemented with 10mM HEPES, 10% FBS, 0.1mL P/S/F and 2.2mM glutamine) in a 6-well plate until the day of assay (37˚C, 5% CO_2).

Approximately 150 islets per treatment from PHD123*fl/fl* male mice were picked into a 6-well plate containing 2mL of islet growth media. Islets were infected with a shGFP control virus or a RIP Cre adenovirus at a concentration of 2µL/mL compared to NT. 20mM glucose was added to all treatments and incubated for 18 hours overnight. The following day, the islets were washed with PBS and fresh islet growth media was added to each treatment. GFP and RFP were analyzed using a Nikon Eclipse Ti microscope on day two and three. On day four, an insulin secretion assay was performed and insulin concentrations were measured by a radioimmunoassay (RIA) (Millipore, Toronto, ON).

3.2.3 Islet dispersion

Approximately 120-150 islets were collected into each 1.5mL Eppendorf tube. Islets settled to the bottom and the media was removed. Islets were washed with 1mL of PBS. Islets settled to the bottom and PBS was removed. 250µL of trypsin + 2µL of DNase were added to

each tube and islets were transferred to a 48-well plate. The 48-well plate was incubated (37˚C, 5% CO_2) for two minutes at a time and checked for disintegration under a stereomicroscope and pipetted up and down to mix. The plate was incubated for a total of 10 minutes.

Once 70% of islets were dispersed in each well, 500µL of ice cold islet growth media was added to each well. Each well containing dispersed islets was transferred to a 1.5mL tube and centrifuged at 3,000 rpm for two minutes at 4˚C. A pellet was formed and the supernatant was removed. Another 500µL of ice cold islet growth media was added and the pellet was re-suspended. Dispersed islets were centrifuged at 3,000 rpm for two minutes at 4˚C. The supernatant was removed and the pellet was re-suspended in 1mL ice cold islet growth media. 500µL of dispersed islets was added to each well in a 48-well plate. The media was changed every day until an insulin secretion assay was performed.

3.2.4 Glucose-stimulated insulin secretion (GSIS) assay

Approximately 48 hours after islet dispersion, wells were washed twice with 200µL LG (2mM) KRB. The plate was rocked back and forth and inverted to remove LG (2mM) KRB. Wells were incubated (37˚C, 5% CO_2) twice with LG (2mM) KRB for 30 minutes and washed with 200µL LG (2mM) KRB in between incubations.

After two washes, wells were treated with LG (2mM) KRB, HG (16.7mM) KRB, LG (2mM) KRB + DMOG (5mM) or HG (16.7mM) KRB + DMOG (5mM). Wells containing treatments were incubated (37˚C, 5% CO_2) for one hour. After one hour incubation, 150µL of dispersed islets were collected and transferred to a 96-well plate. Samples were stored at -20˚C until an RIA was performed.

Islets infected with shGFP, RIP Cre adenovirus or NT were washed twice with LG (2mM) KRB and incubated twice for 30 minutes (37˚C, 5% CO_2) with LG (2mM) KRB. After incubations, islets were washed once with LG (2mM) KRB and incubated for one hour in the following treatments: LG (2mM) KRB, HG (16.7mM) KRB, LG (2mM) KRB + KCl (30mM) + diazoxide (200µM), HG (16.7mM) KRB + KCl (30mM) + diazoxide (200µM) and HG (16.7mM) KRB + DMM (10mM) + DMαKG (10mM) with 30 islets per treatment.

3.2.5 Islet perifusion

Islet perifusion was performed the following day after islet isolation using the Biorep Perifusion System (Biorep Teachnologies, FL, USA). Islets were incubated (37˚C, 5% CO_2) overnight. The peristalic pump was set up, connecting the solutions to the main pump and the main pump to the chambers. The chambers were set up and a fiberglass filter was placed on the bottom of each chamber. Chambers were filled with approximately 275µL of LG (2mM) KRB. 25 islets were washed and picked into each chamber. The solutions were delivered by the main pump to the islets contained within the perifusion chambers. The Perifusion System was primed to prevent air bubbles from forming within the tubes. The Perifusion System was then heated to 37˚C.

All treatments were perfused at a flow rate of 300µL/minute. Islets within all chambers were stimulated with LG (2mM) KRB for 70 minutes total, baseline measurements of insulin secretion were obtained in the first 60 minutes and samples were collected for the latter 10 minutes. Islets within the chambers were then stimulated with HG (16.7mM) KRB or HG (16.7mM) KRB + DMOG (5mM) for 40 minutes. Islets within all chambers were stimulated with HG (16.7mM) KRB + KCl (30mM) for the last 15 minutes.

Insulin samples (300µL) were collected in a 96-well plate and stored at -20˚C. The fiberglass filter containing islets in each chamber was collected in a 1.5mL tube. 100µL of acid ethanol (150 ethanol:47 H_2O:3 HCl) was added to each tube and samples were stored overnight at 4˚C and then stored at -20˚C until the day of assay. All insulin samples were measured by an RIA.

3.2.6 Radioimmunoassay (RIA)

Insulin samples from islet insulin secretion and islet perifusion assays were measured using a Sensitive Rat Insulin Radioimmunoassay Kit (RIA) (Millipore, Toronto, ON). The RIA kit was able to cross react with insulin samples secreted from mouse islets. ^{125}I-insulin sensitive tracer, a radioactive tracer, and a rat insulin antibody were added to each sample in equal amounts. The ^{125}I-insulin tracer and the unlabeled insulin samples compete for binding sites on the rat insulin antibody. Samples containing the rat insulin antibody and ^{125}I-insulin tracer were centrifuged at 3,000 g for 20 minutes at 4˚C and decanted. The bound ^{125}I-insulin tracer to unlabeled antigen ratio in the supernatant was measured using a gamma counter (PerkinElmer, Waltham, MA, USA). The less ^{125}I-insulin tracer present in the supernatant, the more insulin was present in the sample.

3.3 *In vivo* experiments

3.3.1 Intraperitoneal glucose tolerance tests (ipGTT)

C57BL/6J male mice aged 10-14 weeks were fasted for 16-17 hours prior to a glucose challenge. Mice were injected with 200µg/g DMOG or PBS control intraperitoneally 30 minutes prior to a glucose challenge. All mice were injected with 1.5g glucose/kg body weight intraperitoneally. Tail clips were performed and blood from the tail vein was measured with a

glucometer (Contour® Next, Bayer, Mississauga, ON, CA) at baseline, 10, 20, 30, 60, 90 and 120 minutes after an exogenous glucose load. Blood samples were collected at baseline, 10 and 30 minutes. Samples were centrifuged at 8,000 g for 10 minutes. Plasma was isolated and stored at -20˚C until day of assay. Plasma insulin was measured using an enzyme-linked immunosorbent assay (ELISA).

3.3.2 Enzyme-linked immunosorbent assay (ELISA)

Plasma insulin levels from ipGTTs were measured using a Rat/Mouse Insulin ELISA Kit (Millipore, Toronto, ON). Plasma insulin levels were added to a microtiter plate coated with mouse monoclonal anti-rat insulin antibodies. A rat/mouse insulin detection antibody (pre-titered biotinylated anti-insulin antibody) was added to the unknown samples to immobilize plasma insulin. To develop the plate, enzyme substrate 3,3',5,5'-tetramethylbenzidine was added to the samples. A stop solution (0.3M HCl) was added to terminate the colour development and the colour change was measured spectrophotometrically at an absorbance of 450 nm.

3.3.3 Genotyping and development of a KO mouse model

Transgenic mouse lines PHD123*fl/fl* and PHD2*fl/fl* were purchased from Dr. Guo-Hua Fong from the Center of Vascular Biology from the University of Connecticut (Farmington, CT, USA). Ins-1^{Cre}, Ins-1^{CreERT2}, and male C57BL/6J mice were purchased from Jackson Laboratories at four weeks of age (Bar Harbor, ME, USA). PHD and Ins-1^{Cre}/Ins-1^{CreERT2} mouse models were previously described.[62,105] DNA was collected from ear clippings and a DNA extraction was performed using a GeneJET Genomic DNA Purification kit (Thermo Scientific,

Mississauga, ON). DNA was amplified by polymerase chain reaction (PCR) using 2x Phusion Master Mix with GC or HF buffer (Thermo Scientific, Mississauga, ON), 1µM of each primer and corrected to a final volume of 20µL. The following primers were used: PHD1 forward: 5'-TGA GAC CAG GCA GAG GGA GTT-3', PHD1 reverse: 5'-GGA GCT GGA GTT CTA GGT CAG GTT-3', PHD2 forward: 5'-GTG TAC CTC AAC CTC CGC TC-3', PHD2 reverse: 5'-AGG GGA TTT GTA GTT GGC CG-3', PHD3 forward: 5'-GCT CGG AGA ACT TGA CAC GA-3', PHD3 reverse: 5'-TGA CCT CGT AGG GCT CAG AT-3', Ins-1 Cre common: 5'-GGA AGC AGA ATT CCA GAT ACT TG-3', Ins-1 Cre WT: 5'-GTC AAA CAG CAT CTT TGT GGT C-3', Ins-1 Cre mutant: 5'-GCT GGA AGA TGG CGA TTA CG-3'. Primers were obtained from Integrated DNA Technologies (Coralville, IA, USA) or Jackson Laboratories (Bar Harbor, ME, USA). The PCR products were separated by gel electrophoresis on a 1.2% agarose gel. The following band lengths were determined: WT PHD1: 500 base pairs (bp), floxedPHD1: 600 bp, WT PHD2: 1440 bp, floxedPHD2: 1900 bp, WT PHD3: 1070 bp, floxedPHD3: 1550 bp, WT Cre: 488 bp, and mutant Cre: 675 bp.

3.4 Protein identification

3.4.1 Protein isolation

Cells were plated in a 12-well plate at a concentration of 750,000 cells per well and grown to 100% confluency for five days. Wells were incubated (37˚C, 5% CO_2) twice with LG (2mM) KRB for one hour. After incubations, wells were treated with 500µL of cell media, LG (2mM) KRB, HG (16.7mM) KRB, 500µM DMOG, 10mM DMαKG, 0.1mM palmitate or 10mM glutamine + 10mM leucine and incubated for two hours (37˚C, 5% CO_2). After incubation, media containing treatments was removed and 200µL of cell extraction buffer (supplemented with 1mM PMSF and protease inhibitor cocktail (1:100)) (Invitrogen, Mississauga, ON) was

added. Wells were scraped and wells containing the same treatment were combined and transferred to a 1.5mL tube and stored at -20˚C.

Protein samples were thawed and centrifuged at 12,500 rpm for 20 minutes at 4˚C. The supernatant was transferred to a 1.5mL tube. Protein concentration was measured using a BCA assay. Protein samples were stored at -20˚C until co-immunoprecipitation was performed.

3.4.2 Co-immunoprecipitation

Co-immunoprecipitation was performed using Dynabeads® Protein G co-immunoprecipitation kit (Novex by Life Technologies, Mississauga, ON). Dynabeads® were re-suspended by vortexing for 30 seconds and 50µL was transferred to a 1.5mL tube for each treatment. The tubes were placed on a DynaMag™ magnet (Life Technologies, Mississauga, ON) and the supernatant was removed. Anti-hydroxyproline antibody (Abcam, Toronto, ON) was diluted in antibody binding and washing solution (Novex by Life Technologies, Mississauga, ON) and 200µL was added to each tube containing Dynabeads®. Dynabeads®-Ab complex was incubated for 10 minutes using the HulaMixer® Sample Mixer (Life Technologies, Mississauga, ON). The supernatant was removed and the Dynabeads®-Ab complex was washed with antibody binding and washing solution.

Dynabeads®-Ab complex was crosslinked using 5mM crosslinking reagent bis(sulfosuccinimidyl)suberate (BS3) (100mM BS3 stock diluted in PBS) (Thermo Scientific, Mississauga, ON) to prevent co-elution of the anti-hydroxyproline antibody. 200µL of 5mM BS3 solution was added to each tube and incubated at room temperature for 30 minutes using the sample mixer. 12.5µL of Quenching Buffer (Thermo Scientific, Mississauga, ON) was added to each tube and incubated for 15 minutes using the sample mixer. Tubes were washed once with

200µL of antibody binding and washing solution and the supernatant was removed using the magnet. 175µL of protein sample containing approximately 1mg of protein was added to each tube and incubated for 10 minutes using the sample mixer. After incubation, the tubes were placed on the magnet and the supernatant was removed and transferred to a new 1.5mL and stored at -20˚C.

The Dynabeads®-Ab-antigen complex was washed three times with 200µL of washing buffer (Novex by Life Technologies, Mississauga, ON). The tubes were placed on the magnet and the supernatant was re-suspended with 100µL of washing buffer. The bead suspension was transferred to a new 1.5mL tube. The tubes were placed on the magnet and the supernatant was removed. 20µL of Elution Buffer and 10µL of premixed NuPAGE® LDS Sample Buffer and NuPAGE Sample Reducing Agent (Life Technologies, Mississauga, ON) were added to each tube containing the Dynabeads®-Ab-antigen complex. The tubes were re-suspended by inverting and samples were heated for 10 minutes at 70˚C. The tubes were placed on the magnet and the supernatant containing 1mg of antigen was loaded onto a NuPage® 10% Bis-Tris SDS Polyacrylamide Mini Gel (Thermo Scientific, CA, USA) for 50 minutes. The gel was placed in 10% methanol, 10% glacial acetic acid overnight at 4˚C.

3.4.3 Silver staining

The gel containing prolyl hydroxylated protein was removed from 10% methanol, 10% glacial acetic acid solution and washed twice with deionized water and then washed three times for 10 minutes in deionized water on a shaker. The gel was incubated in sodium thiosulfate (0.04g in 5 mL milliQ water) for 90 seconds. The gel was washed three times with deionized water and silver nitrate was added (0.09g in 50mL milliQ water) and incubated for 10 minutes on

a shaker, staining the gel. The gel was washed three times with deionized water. Developer solution (1g potassium carbonate, 2mL diluted sodium sulfate, 23.1µL of 37% formaldehyde) was added and incubated until protein bands appeared. Developer solution was removed and the reaction was stopped with destain solution (10% methanol, 10% glacial acetic acid) for less than five minutes. Destain solution was removed and the gel was placed in milliQ water and stored at 4˚C until protein bands were excised.

Protein bands were excised using a blade washed with 70% ethanol between each cut to avoid contamination. Bands were cut 1-1.5mm wide and placed in 250µL of 5% acetic acid. Samples were stored at 4˚C until delivered to the MALDI-MS facility in the department of biochemistry at Western University for protein identification by MALDI-MS.

3.4.4 Matrix assisted laser desorption/ionization mass spectrometry (MALDI-MS)

Excised protein bands were delivered to the MALDI MS facility at Western University where an in-gel digestion was performed using a MassPREP automated digester station (PerkinElmer, Waltham, MA, USA). Protein bands were reduced using 10mM dithiotreitol (DTT) followed by alkylation using 55mM iodoacetamide (IAA) and digested using trypsin (prepared in 50mM ammonium bicarbonate, pH 8). Samples containing trypsin were incubated overnight at 20˚C to allow for trypsin absorption. The samples were incubated at 40˚C for seven hours. Peptides were extracted from the gel using 1% formic acid, 2% acetonitrile. Peptides were lyophilized and stored at -20˚C. Prior to MALDI TOF/TOF, peptides were reconstituted in 10% acetonitrile, 0.1% trifluoroacetic acid (TFA).

MALDI TOF/TOF MS was performed using AB Sciex 5800 TOF/TOF System (Framingham, MA, USA). The samples containing unknown peptides were mixed with the

MALDI matrix α-cyano-4-hydroxycinnamic acid (CHCA) (prepared as 5mg/mL in 6mM ammonium phosphate monobasic, 50% acetonitrile, 0.1% trifluoracetic acid) at a 1:1 ratio. The matrix-peptide solution was spotted on a MALDI plate and vaporized, which allowed the matrix and unknown peptides to co-crystallize. A 349 nm Nd:YLF OptiBeam On-Axis laser was aimed at the crystals to desorb and ionize the matrix crystals. The laser pulse rate was 400 Hz. The unknown peptide crystals were protonated via the ionized matrix. The same amount of kinetic energy was applied to all ions produced, allowing the ions to accelerate towards the reflectron detector. The reflectron mode was externally calibrated at 50 ppm mass tolerance and internally at 10 ppm. Each mass spectrum was collected as a sum of 500 shots. Using $KE=1/2mv^2$, the mass of each ion was determined, as the ions reached the detector at different times.

The instrument performed partial peptide sequencing and identification of post-translational modifications of selected ions. Sequence databases were searched using MASCOT. SwissProt, NCBIprot and EMBLE EST division databases were used for peptide mass fingerprinting and protein identification. Contaminants and CRAP databases were used to search for common contaminants present in the unknown peptide samples.

3.5 Statistical analysis

All results are expressed as mean ± SEM. Statistical significance was measured using Student's t-test or one-way or two-way ANOVA followed by multiple comparisons with a Holm-Sidak correction.

Chapter 4: Results

4.1 Confirmation of PHD expression in 832/13 cells by western blot analysis

PHD1, PHD2, and PHD3 expression was confirmed in 832/13 cells by western blot analysis. Approximately 20µg of isolated protein sample from 832/13 cells were incubated with LG (2mM) KRB for one hour (37˚C, 5% CO_2) to stimulate basal insulin secretion. Primary antibodies for PHD1, PHD2, PHD3, and tubulin were used to determine protein expression semi-quantitatively using Imagej (fig.4.1). Background noise was subtracted and relative density was calculated. All three PHD isoenzymes are expressed in 832/13 cells (fig.4.2).

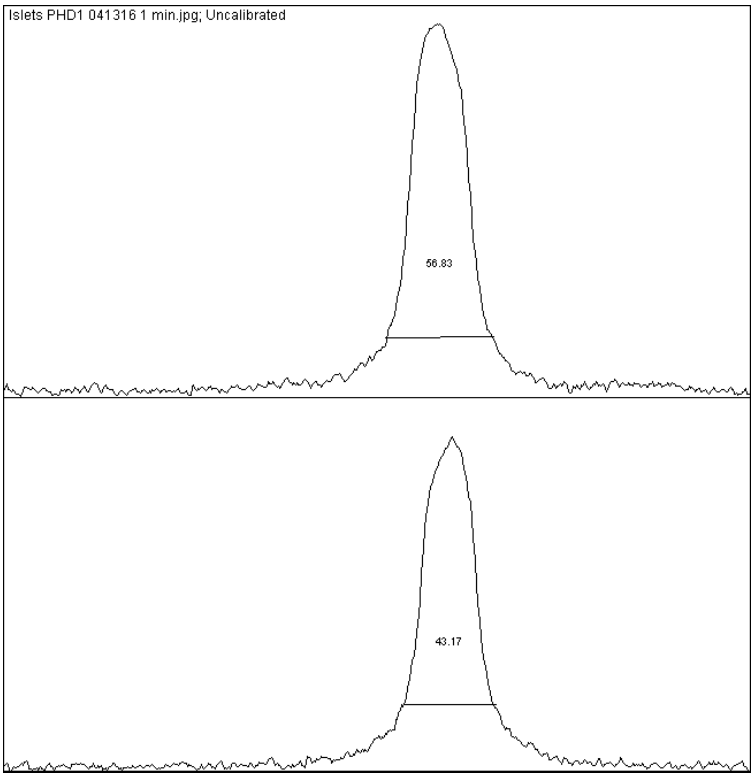

Figure 4.1: Western blot analysis using Imagej.

PHD1 peaks in 832/13 cells stimulated with LG (2mM) KRB are shown in the profile plot above. Relative density for each protein band was measured and background noise was subtracted. The percentage of the total size of the peak was measured using Imagej and corrected using tubulin. The average corrected value was calculated using two protein samples treated with LG (2mM) KRB and the relative density was calculated by dividing the corrected values by the average. Relative density calculations for PHD1, PHD2, and PHD3 are summarized in table 4.1.

Table 4.1: Imagej calculations for PHD1, PHD2 and PHD3 in 832/13 cells.

	Band Size (kDa)	Treatment	Area (Under peak)	Percentage (% of total size of all peaks)	Corrected	Average	Relative Density (% expressed)
PHD1	44	LG1	13975.05	56.832	1.142214	1.000691	1.141426
		LG2	10615.15	43.168	0.859167		0.858574
PHD2	50	LG1	1200.59	24.138	0.485127	0.499928	0.970395
		LG2	12857.54	25.862	0.514728		1.029605
PHD3	47	LG1	7283.426	49.787	1.000623	1.000003	1.00062
		LG2	7345.841	50.213	0.999383		0.99938
Tubulin	50	LG1	10616.45	49.756			
		LG2	10720.45	50.244			

Area under the peak and percentage of the total size of the peak were calculated using imageJ. The percentage of the size of the peak was corrected using tubulin and the corrected values were averaged for each isoenzyme. Two samples for each isoenzyme were used to calculate protein expression (LG1 and LG2). The relative density of the protein bands were calculated by dividing the corrected value by the average.

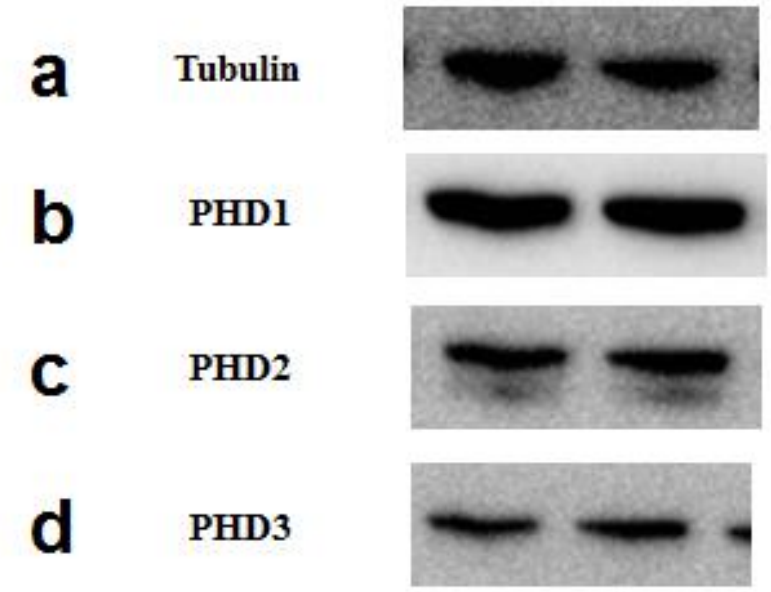

Figure 4.2: PHD expression in 832/13 cells by western blot analysis.

Approximately 20µg of total protein was isolated from 832/13 cells and protein concentration was determined by a BCA protein assay. Protein samples were analyzed by western blot for expression of all three PHD isoenzymes. Tubulin was used as a control. Results shown are from two samples treated with LG (2mM) KRB and protein intensity was measured by Imagej. PHD1 was determined to be approximately 44 kDa, PHD2 50 kDa, PHD3 47 kDa and tubulin 50 kDa.

4.2 Confirmation of PHD expression in mouse pancreases by immunofluorescence

Expression and subcellular localization of PHD1, PHD2, and PHD3 was confirmed by immunofluorescence in mouse pancreases. Primary antibodies for PHD1, PHD2, PHD3, and insulin; and Alex Fluor® 488 and Alexa Fluor® 647 secondary antibodies were used. It was determined that all three isoenzymes are expressed in the mouse pancreas with distinct subcellular localizations. Insulin is exclusively expressed in the cytosol within β-cells of islets (fig.4.3 A). PHD1 was found to be expressed in the cytosol of both islets and acinar tissue (fig.4.3 B). PHD2 was found to be expressed mainly in the cytosol of both islets and acinar tissue with a weak nuclear stain (fig.4.3 C), whereas PHD3 was found to be expressed mainly in the nucleus of both islets and acinar tissue with a weak cytosolic stain (fig.4.3 D). All PHD isoenzymes were expressed in islets and overlapped with insulin, suggesting that all three isoenzymes are present in β-cells.

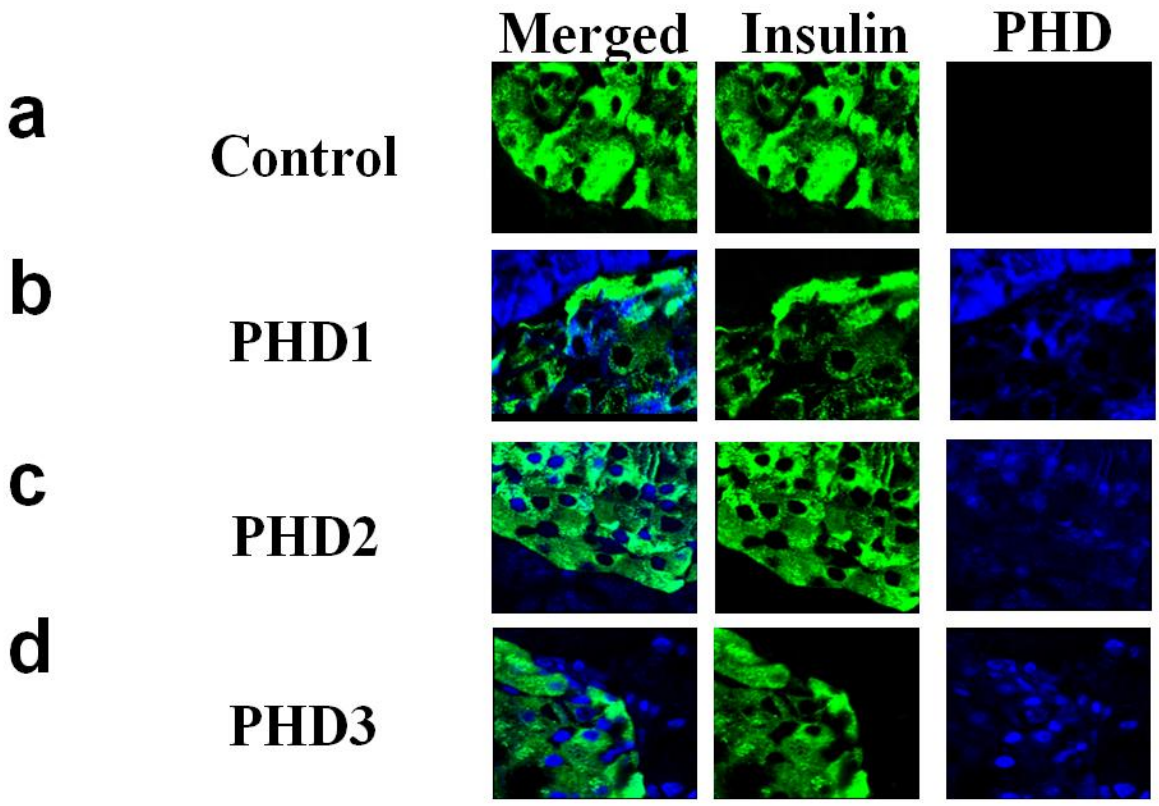

Figure 4.3: PHD expression in mouse pancreases.

Immunofluorescence staining of mouse pancreases aged 10-14 weeks. Formalin-fixed paraffin-embedded tissue slides were stained using primary antibodies for PHD1, PHD2, PHD3, and insulin. Alexa Fluor® 488 and Alexa Fluor® 647 secondary antibodies were used for insulin and PHD primary antibodies, respectively. Insulin alone was used as a control. **(a)** Staining with insulin antibody alone showed a strong stain for insulin exclusively in the cytosol of β-cells. **(b)** Staining with insulin and PHD1 antibodies showed a strong cytosolic stain for PHD1 in acinar tissue and islets. **(c)** Staining with insulin and PHD2 antibodies showed a strong cytosolic stain for PHD2 in both acinar tissue and islets and a weak nuclear stain. **(d)** Staining with insulin and PHD3 antibodies showed a strong nuclear stain for PHD3 in acinar tissue and islets with a weak cytosolic stain.

4.3 OCR is decreased in 832/13 cells and primary mouse islets treated with DMOG using Seahorse Bioscience XF24 Respiration Assay

OCR was measured in 832/13 cells and primary mouse islets to determine if oxygen consumption, and therefore, mitochondrial respiration was affected in cells and islets treated with the pharmacological inhibitor, DMOG. Oxygen consumption was measured in 832/13 cells treated with 200µM, 500µM, and 1000µM DMOG compared to NT containing HG (16.7mM) KRB (fig.4.4 A) and mouse islets treated with 1mM, 5mM, and 10mM DMOG compared to NT containing HG (16.7mM) KRB (fig.4.5 A). OCR was significantly reduced in 832/13 cells at 200µM, 500µM and 1000µM DMOG compared to NT when stimulated with HG and pyruvate + DNP. Area under the curve (AUC) was calculated from (fig.4.5 A). Islets treated with 5mM DMOG displayed significantly reduced OCR values compared to NT when islets were stimulated with HG ($p<0.05$) and DNP + DMM + DMαKG ($p<0.05$) (fig.4.5 B)

Oligomycin treatment resulted in decreased oxygen consumption in both 832/13 cells (fig.4.4 A) and primary islets (fig.4.5 A), representing the ATP that would be produced via mitochondrial respiration. Oligomycin OCR values were used to calculate ATP turnover and proton leak. Proton leak was not statistically different in DMOG treated cells compared to NT (fig. 4.4 B). However, there was a reduced trend in proton leak in 832/13 cells treated with DMOG at all concentrations, suggesting more H^+ are contributing to ATP production via ATP synthase. There was a statistically significant reduction in ATP turnover in 832/13 cells at 200µM ($p<0.01$), 500µM ($p<0.001$) and 1000µM ($p<0.001$) DMOG (fig.4.4 C) and at 1mM ($p<0.05$) and 5mM ($p<0.05$) DMOG in primary islets (fig. 4.5 D). ATP turnover represents ATP produced from mitochondrial respiration. Inhibition of PHD via DMOG results in reduced oxygen consumption leading to reduced ATP production from mitochondrial metabolism. These

results suggest that PHD plays a role in oxidative metabolism, decreasing the ATP/ADP ratio required for the K_{ATP} channel-dependent pathway.

Pyruvate, DMM, and DMαKG are TCA cycle intermediates that stimulate oxidative metabolism. DNP, a proton ionophore, dissipates the H^+ gradient and collapses the proton motive force allowing electron flow through the ETC to be uninhibited. These drugs were used to stimulate maximal respiration and to measure spare respiratory capacity. Spare respiratory capacity measures the ability of the cell to respond to an increase in energy demand, an indicator of cell fitness. Spare respiratory capacity was significantly reduced at 1000μM DMOG ($p<0.05$) in 832/13 cells (fig. 4.4 D).

Rotenone and myxothiazol, inhibitors of complex I and complex III in the ETC, respectively, were used to measure non mitochondrial oxygen consumption. Rotenone and myxothiazol treatment measures oxygen consumption that continues when oxidative metabolism is inhibited due to enzymes that consume oxygen, such as PHD. Non mitochondrial oxygen consumption was significantly reduced at 1000μM DMOG ($p<0.001$) in 832/13 cells (fig. 4.4 E). There was a reduced trend in non-mitochondrial oxygen in primary islets treated with 5mM and 10mM DMOG (fig. 4.5 C).

Respiration assays in 832/13 cells and primary mouse islets show that inhibition of PHD via DMOG results in decreased oxygen consumption and alters parameters of mitochondrial function. Decreased OCR when PHD is inhibited may indicate improved mitochondrial efficiency.

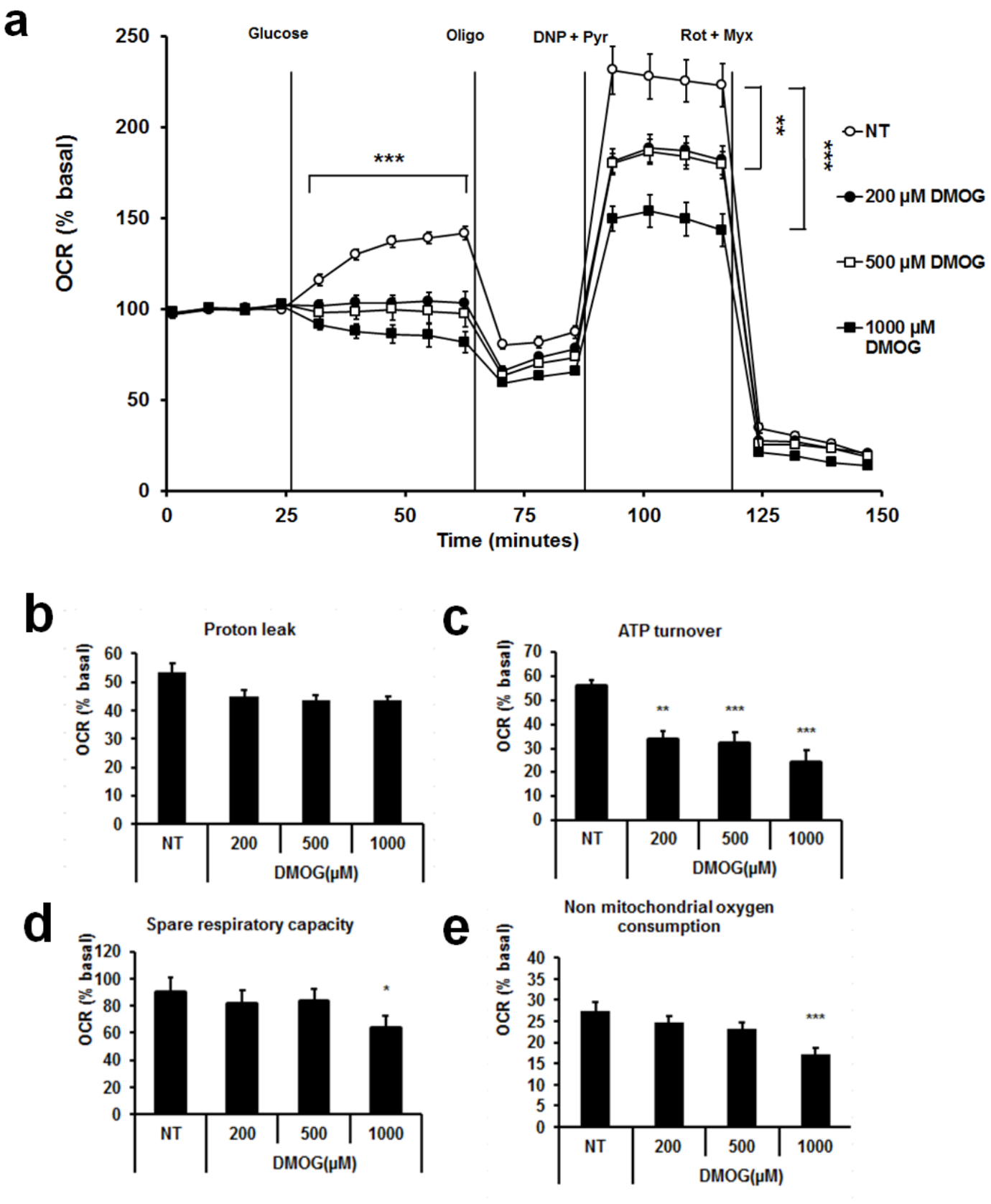
a
Glucose
Oligo
DNP + Pyr
Rot + Myx
OCR (% basal)
Time (minutes)
NT
200 µM DMOG
500 µM DMOG
1000 µM DMOG
b
Proton leak
c
ATP turnover
d
Spare respiratory capacity
e
Non mitochondrial oxygen consumption
DMOG(µM)

Figure 4.4: OCR in 832/13 cells.

Mitochondrial respiration summary in 832/13 cells is shown above. OCR was measured over 150 minutes using Seahorse XF24 Respiration Assay. (n=5). Assay was repeated 4 times. Data are mean ± SEM. **(a)** OCR was measured in the presence of HG (16.7mM) KRB for 40 minutes, oligomycin (10µM) for 25 minutes, DNP (50µM) + pyruvate (20mM) for 30 minutes, and rotenone (5µM) + myxothiazol (5µM) for 30 minutes. 832/13 cells were treated with 200µM, 500µM, and 1000µM DMOG compared to NT. ***$p<0.001$ at 200µM, 500µM, and 1000µM DMOG, **$p<0.01$ at 200µM and 500µM DMOG, ***$p<0.001$ at 1000µM DMOG by a paired t-test. **(b)** Proton leak was calculated by subtracting rotenone + myxothiazol OCR values from oligomycin OCR values. **(c)** ATP turnover was calculated by subtracting oligomycin OCR values from HG (16.7mM) OCR values. **$p<0.01$, ***$p<0.001$, ***$p<0.001$ by a paired t-test. **(d)** Spare respiratory capacity was calculated by subtracting basal OCR values from DNP + pyruvate OCR values. *<0.05 by a paired t-test. **(e)** Non mitochondrial oxygen consumption was determined by rotenone + myxothiazol OCR values. ***$p<0.001$ by a paired t-test.

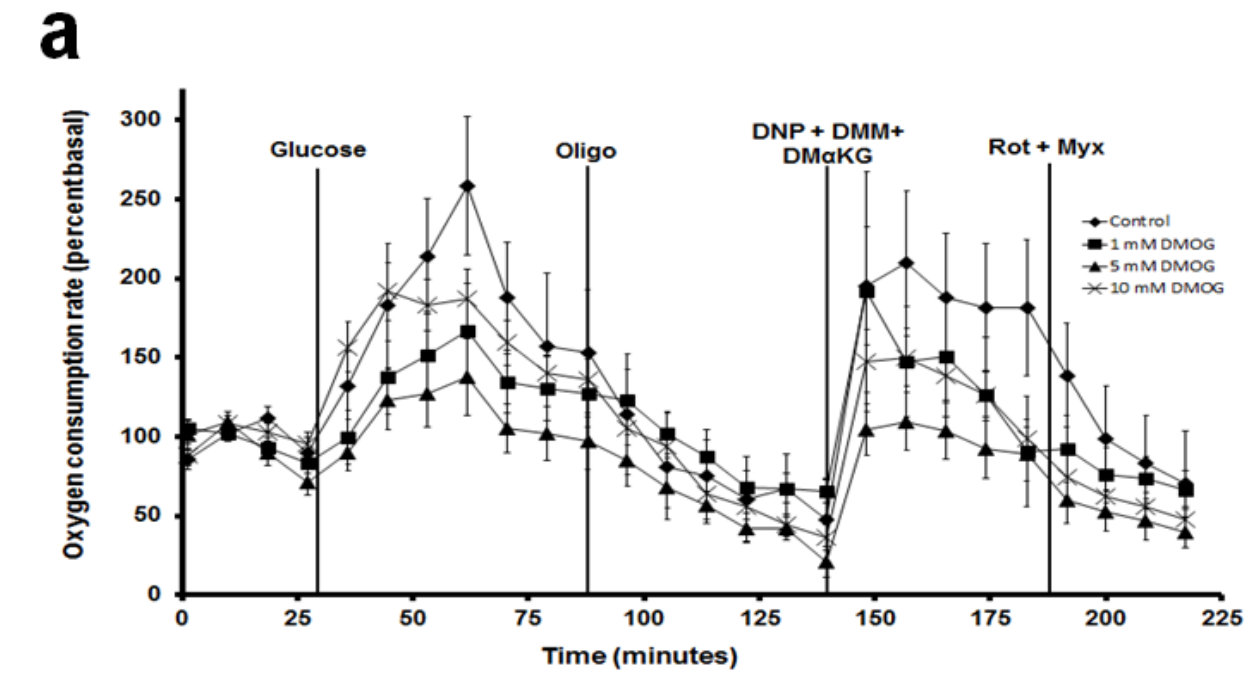
a
Glucose
Oligo
DNP + DMM+
DMαKG
Rot + Myx
Control
1 mM DMOG
5 mM DMOG
10 mM DMOG
Oxygen consumption rate (percent basal)
Time (minutes)
0
50
100
150
200
250
300
0
25
50
75
100
125
150
175
200
225

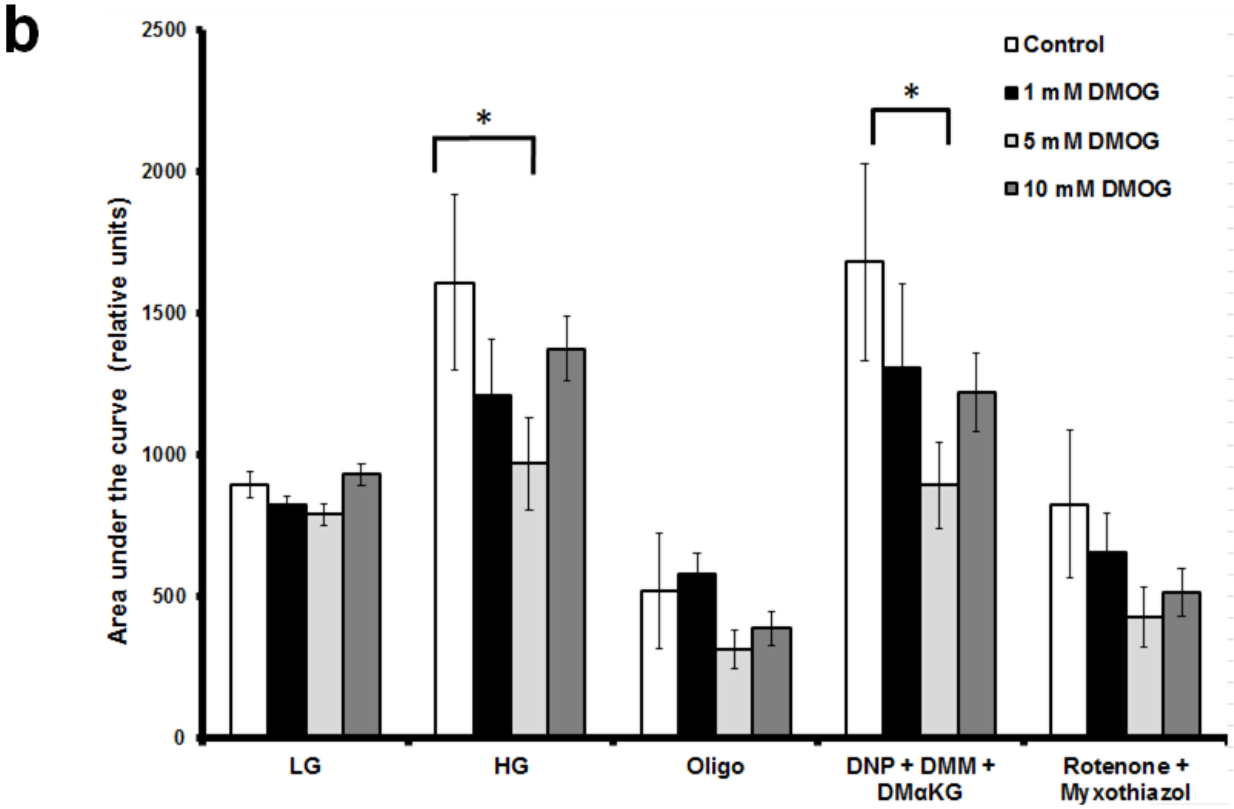
b
Control
1 mM DMOG
5 mM DMOG
10 mM DMOG
Area under the curve (relative units)
*
*
0
500
1000
1500
2000
2500
LG
HG
Oligo
DNP + DMM +
DMαKG
Rotenone +
Myxothiazol

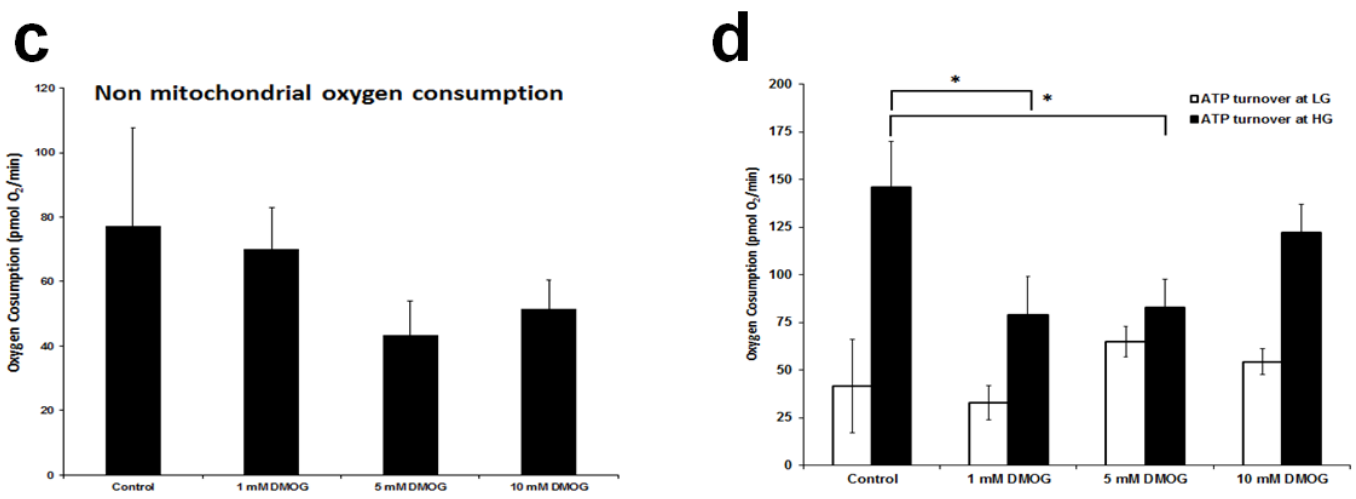

Figure 4.5: OCR in primary mouse islets.

Mitochondrial respiration summary in primary mouse islets from male C57BL/6J mice aged 10 weeks. OCR was measured over 220 minutes using Seahorse XF24 Respiration Assay. (n=5). Assay was repeated twice. Data are mean ± SEM. **(a)** OCR for primary mouse islets treated with 1mM, 5mM, and 10mM DMOG injected with HG (16.7mM) KRB for 60 minutes, 20µM oligomycin for 50 minutes, 100µM DNP + 10mM DMM + 10mM DMαKG for 45 minutes, and 10µM rotenone + 10µM myxothiazol for 40 minutes. **(b)** AUC of A. *p<0.05, *p<0.05 by a paired t-test. **(c)** Non mitochondrial oxygen consumption was determined by rotenone + myxothiazol OCR values. **(d)** ATP turnover was calculated by subtracting oligomycin OCR values from basal OCR values. *p<0.05, *p<0.05 by a paired t-test.

4.4 PHD inhibition using DMOG may enhance pancreatic β-cell insulin secretion

A GSIS was performed to assess whether PHD plays a role in pancreatic β-cell insulin secretion. Islets were isolated from male C57BL/6J mice and incubated overnight (37˚C, 5% CO_2). The following day, islets were dispersed and a GSIS was performed on day 3. Dispersed islets were treated with LG (2mM) KRB, HG (16.7mM) KRB, LG (2mM) KRB + 5mM DMOG, or HG (16.7mM) + 5mM DMOG for one hour (fig. 4.6). Insulin secretion remained

unaltered in dispersed islets treated with 5mM DMOG compared to NT when stimulated with LG (2mM) KRB. There was an increased trend in insulin secretion in dispersed islets treated with 5mM DMOG compared to NT when stimulated with HG (16.7mM) KRB. Acute inhibition of PHD via DMOG may play a role in GSIS.

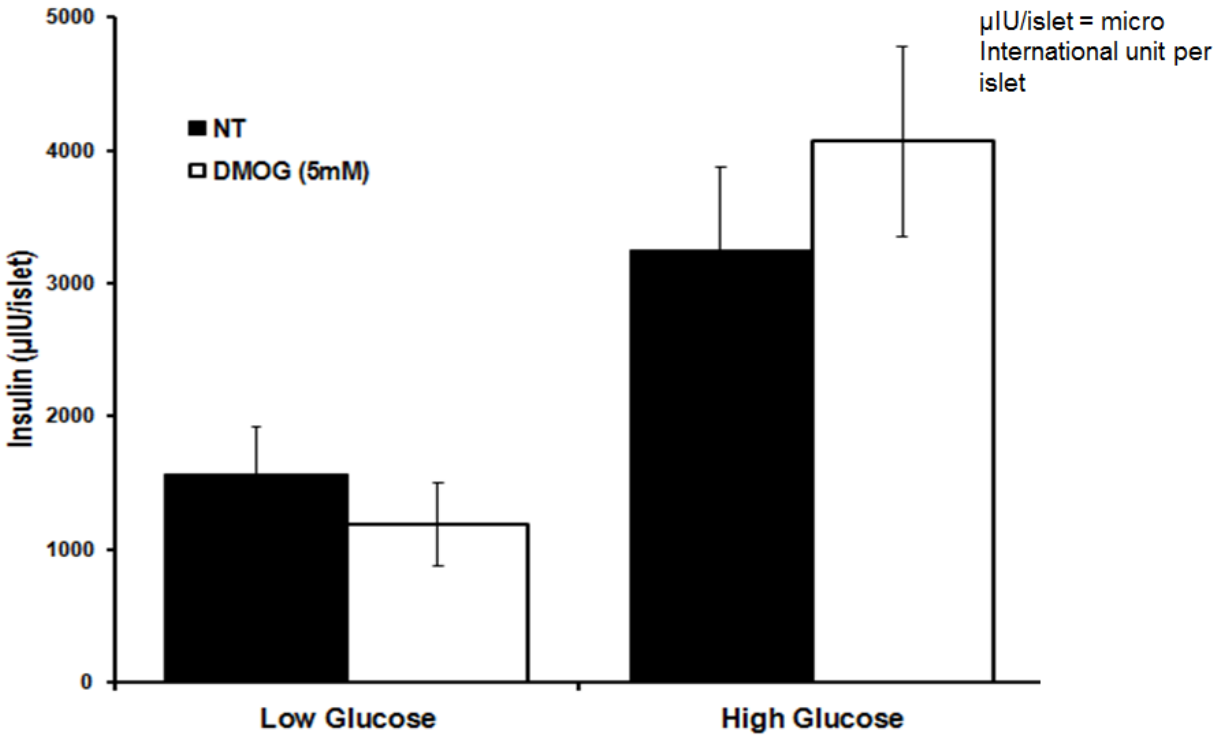

Figure 4.6: GSIS in primary mouse islets treated with 5mM DMOG.

Insulin secretion from C57BL/6J male mice aged 10-14 weeks. Dispersed islets were treated with 5mM DMOG compared to NT. Insulin secretion was measured in response to either LG (2mM) or HG (16.7mM) KRB. Insulin secretion was determined by RIA. Assay repeated three times in triplets. Data are mean ± SEM.

4.5 Inhibition of PHD using DMOG increases second phase insulin secretion

The role of PHD in second-phase insulin secretion was investigated by performing a perifusion assay. Dynamic insulin secretion was measured to determine whether there is a difference between first- and second-phase insulin secretion in primary mouse islets using 5mM

DMOG. Islets were stimulated with LG (2mM) KRB for the first 10 minutes to measure basal insulin secretion, HG (16.7mM) KRB or HG (16.7mM) KRB + 5mM DMOG for 40 minutes, and HG (16.7mM) KRB + KCl (30mM) for 15 minutes. Insulin secretion was significantly increased at 45 minutes ($p<0.05$) and 48 minutes ($p<0.05$) when treated with HG (16.7mM) KRB + 5mM DMOG compared to HG (16.7mM) KRB (fig.4.7 A). AUC revealed a statistically significant increase in GSIS in islets treated with HG (16.7mM) KRB + 5mM DMOG in the latter 30 minutes compared to NT ($p<0.01$) (fig.4.7 B). These results demonstrate that inhibition of PHD via DMOG enhances second-phase GSIS when stimulated with HG.

Total insulin content was measured in each chamber containing islets with the addition of extraction buffer. Total insulin content remained unchanged in DMOG treated islets compared to NT (fig.4.7 C).

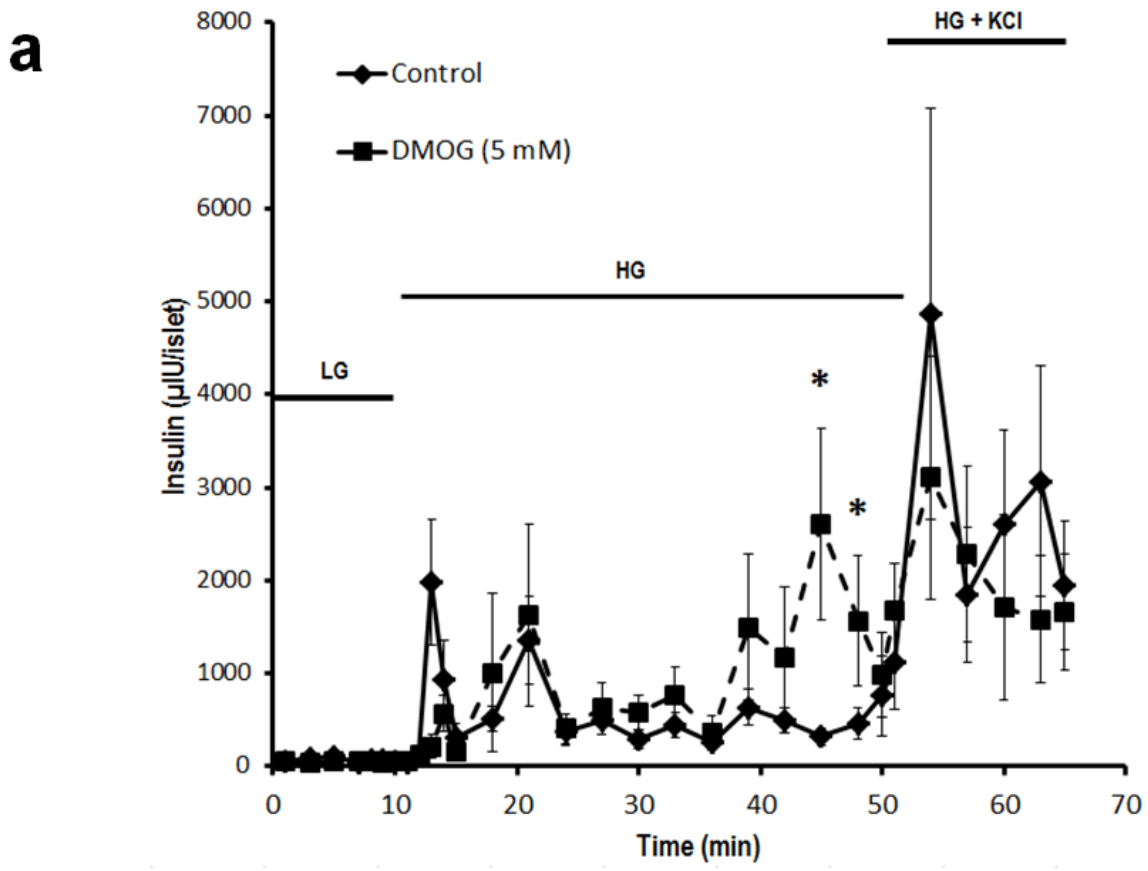

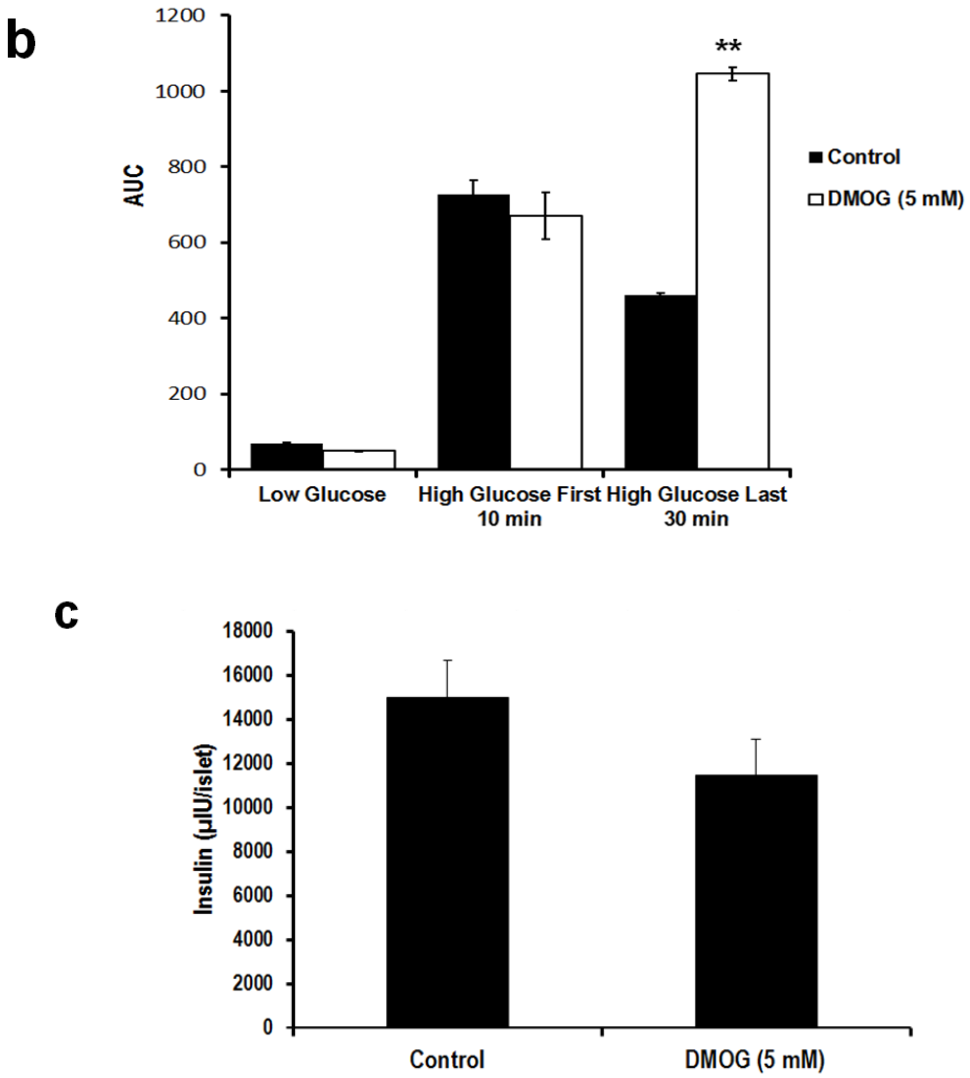

Figure 4.7: Perifusion in primary mouse islets treated with 5mM DMOG.

Islet perifusion measuring dynamic insulin secretion from C57BL/6J male mice aged 10-14 weeks over 65 minutes. Insulin secretion was determined by RIA. Assay repeated three times in triplets. Data are mean ± SEM. **(a)** Islets were stimulated with LG (2mM) KRB for 10 minutes, HG (16.7mM) KRB or HG (16.7mM) KRB + 5mM DMOG for 40 minutes and HG (16.7mM) KRB + KCl (30mM) for 15 minutes. *p<0.05, *p<0.05 by a one-way ANOVA. **(b)** AUC of A. **p<0.01 by a one-way ANOVA. **(c)** Total insulin content in primary mouse islets compared to NT.

4.6 Inhibition of PHD using DMOG improves glucose tolerance in C57BL/6J male mice

Inhibition of PHD via 5mM DMOG resulted in enhanced second-phase insulin secretion *in vitro*. The role of PHD in glucose homeostasis was next assessed *in vivo* using C57BL/6J male mice aged 10-14 weeks was assessed. Mice were injected intraperitoneally with 200µg/g body weight DMOG or PBS 30 minutes prior to an exogenous glucose load. All mice were injected intraperitoneally with 1.5g/kg body weight glucose and blood glucose levels were measured over a two hour period. Blood glucose levels remained unchanged during the first 30 minutes after a glucose challenge. Mice injected with 200µg/g body weight DMOG demonstrated improved glucose tolerance compared to PBS control mice at 90 minutes ($p<0.05$) and 120 minutes, although not statistically significant, after a glucose challenge (fig.4.8 A). These results further support the role of PHD in second-phase insulin secretion. Blood samples from the tail vein were collected at baseline, 10 and 30 minutes after a glucose injection and plasma insulin was measured by ELISA. Despite unchanged blood glucose levels during the first 30 minutes, mice injected with 200µg/g body weight DMOG demonstrated significantly reduced plasma insulin levels at 10 minutes ($p<0.01$) after glucose injection (fig.4.8 B). These findings suggest inhibition of PHD via 200µg/g body weight DMOG results in improved insulin sensitivity compared to PBS control mice. Inhibition of PHD via DMOG results in improved glucose tolerance during second-phase insulin secretion but may also play a role in first-phase insulin secretion, as revealed by ELISA.

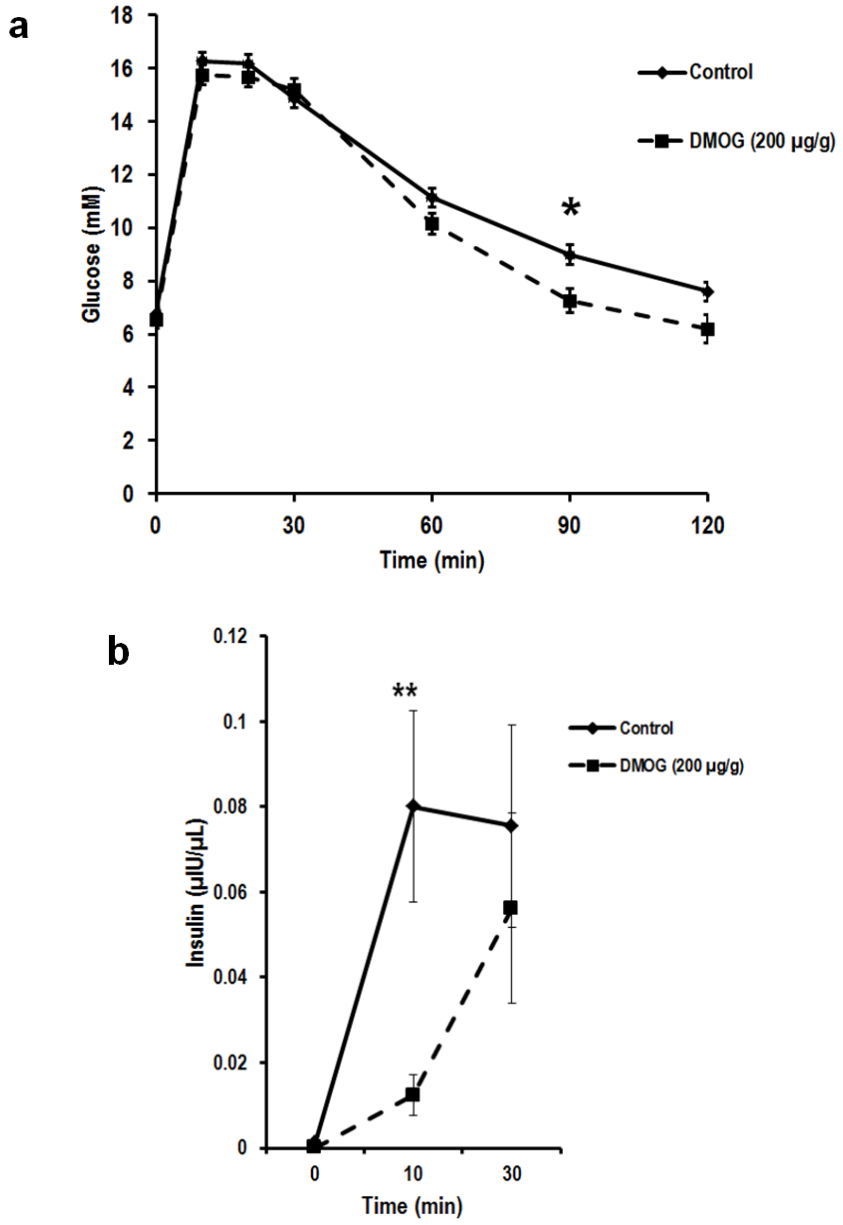

Figure 4.8: *In vivo* glucose homeostasis in C57BL/6J mice treated with DMOG.

Effects of DMOG (200µg/g body weight) on *in vivo* glucose homeostasis in C57BL/6J male mice aged 10-14 weeks. (n=12). Data are mean ± SEM. **(a)** Blood glucose levels during an ipGTT over a two hour period. *$p < 0.05$ at 90 minutes by a one-way ANOVA. **(b)** Plasma insulin levels measured by an ELISA at baseline, 10 minutes and 30 minutes. **$p<0.01$ at 10 minutes by a one-way ANOVA.

4.7 Development of a β-cell specific KO model

Two transgenic mouse lines with floxed exons (exon 3 for PHD1 and exon 2 for PHD2 and PHD3), PHD123*fl/fl* and PHD2*fl/fl*, were bred with C57BL/6J mice for three backcrosses and genotyped monthly (fig.4.9). The PHD123*fl/fl* line was isolated, generating PHD1+*/fl* (fig.4.10 A) and PHD3+*/fl* (fig.4.10 C) and these mice were bred with Ins-1^{Cre} mice (fig.4.10 D). Heterozygous mice for PHD1 and PHD3 with Cre recombinase inserted into the β-cell specific Ins-1 gene to target *loxP* sites on either side of exon 3 or exon 2 for PHD1 and PHD3, respectively were generated (PHD1+*/fl/Cre*, PHD3+*/fl/Cre*). After back crossing with C57BL/6J mice for three generations PHD2+*/fl* (fig.4.10 B) mice were isolated from the PHD2*fl/fl* mouse line. PHD2+*/fl* mice were bred with Ins-1^{Cre} and heterozygous mice for PHD2 with β-cell specific Cre recombinase were generated (PHD2+*/fl/Cre*).

PHD1+*/fl/Cre*, PHD2+*/fl/Cre* and PHD3+*/fl/Cre* mice were bred together (not from the same litter) to generate WT (PHD+/+*/Cre*), heterozygous (PHD+*/fl/Cre*) and KO (PHD*fl/fl/Cre*) mice for each PHD isoenzyme. The objective of developing three independent transgenic mouse lines is to conduct *in vitro* and *in vivo* experiments, assessing the long term effects of PHD in regulating pancreatic β-cell insulin secretion in a KO animal model. These results suggest pharmacological inhibition of PHD via DMOG augments second-phase insulin secretion *in vitro* and improves glucose tolerance *in vivo*, demonstrating the role of PHDs in short term regulation of insulin secretion. Future work involving β-cell specific PHD KO mice from the time of birth will investigate the long term effects of PHD in regulating insulin secretion and will explore which isoenzymes contribute to insulin secretion both *in vitro* and *in vivo.*

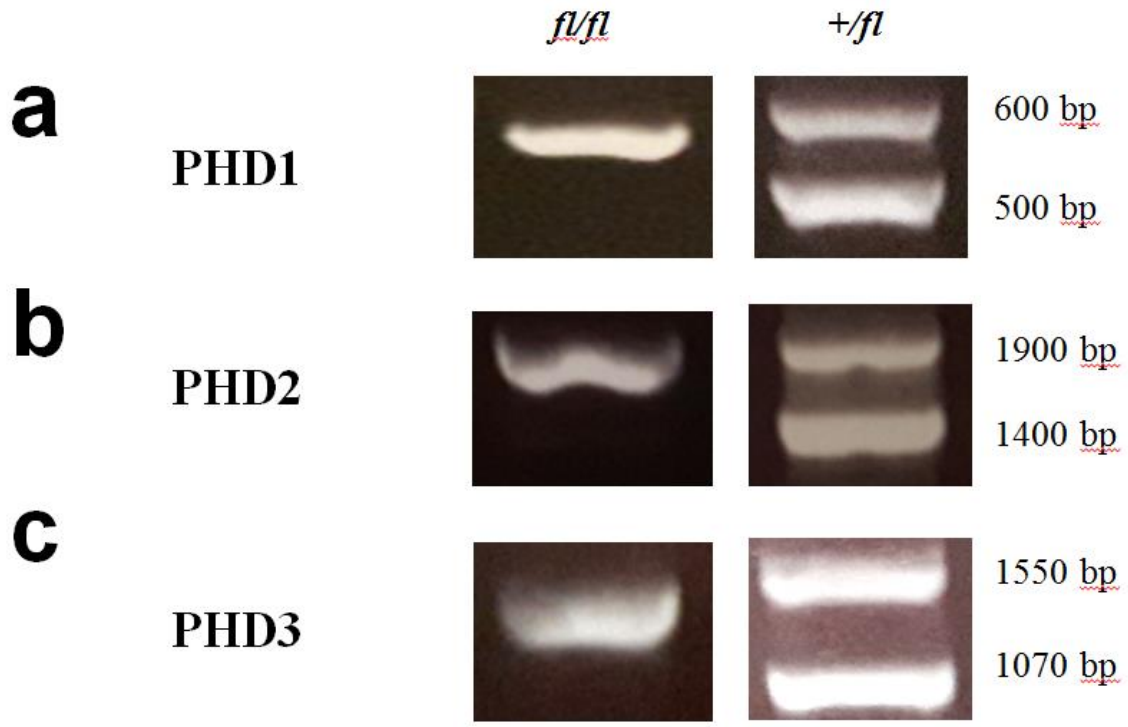

Figure 4.9: Genotyping of PHD123*fl/fl* and PHD123+/*fl* F1 generation mice by PCR analysis.

The PHD123*fl/fl* mouse line was purchased from Dr. Guo-Hua Fong from the University of Connecticut (Farmington, CT, USA). C57BL/6J mice were used for back crossing and were purchased from Jackson Laboratories (Bar Harbor, ME, USA). Primers were obtained from Integrated DNA Technologies (Coralville, IA, USA). **(a)** Genotyping for PHD1*fl/fl* and PHD1+/*fl* mice. WT protein band was 500 bp and floxed protein band was 600 bp. **(b)** Genotyping for PHD2*fl/fl* and PHD2+/*fl* mice. WT protein band was 1400 bp and floxed protein band was 1900 bp. **(c)** Genotyping for PHD3*fl/fl* and PHD3+/*fl* mice. WT protein band was 1070 bp and floxed protein band was 1550 bp.

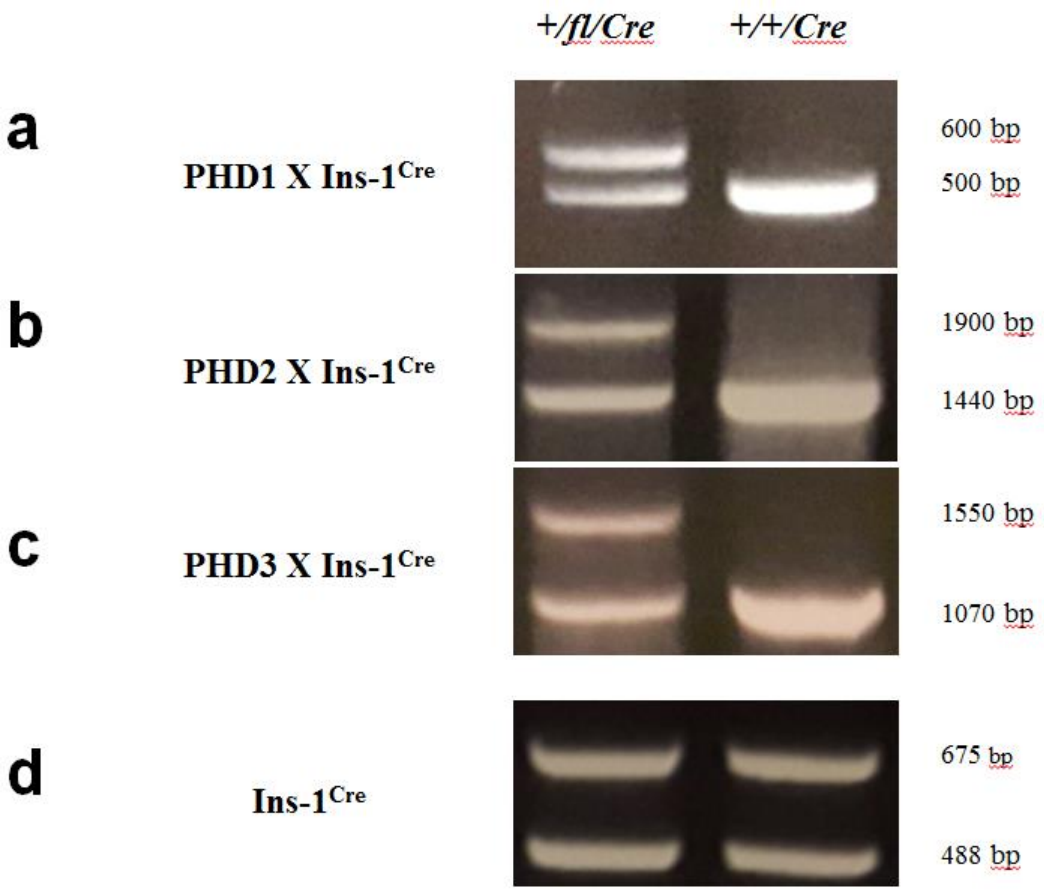

Figure 4.10: Genotyping of PHD+/*fl*/*Cre*, PHD+/+/*Cre*, and Ins-1^{Cre} mice by PCR analysis. PHD*fl*/*fl* mice were back crossed three generations with C57BL/6J mice. PHD+/*fl* were crossed with Ins-1^{Cre} to generate PHD+/*fl*/*Cre* and PHD+/+/*Cre* F1 mice. Ins-1^{Cre} mice were obtained from Jackson Laboratories (Bar Harbor, ME, USA). Primers were obtained from Jackson Laboratories (Bar Harbor, ME, USA) or Integrated DNA Technologies (Coralville, IA, USA). **(a)** Genotyping for PHD1+/*fl* X Ins-1^{Cre} mice. WT protein band was 500 bp and floxed protein band was 600 bp. **(b)** Genotyping for PHD2+/*fl* X Ins-1^{Cre} mice. WT protein band was 1400 bp and floxed protein band was 1900 bp. **(c)** Genotyping for PHD3+/*fl* X Ins-1^{Cre} mice. WT protein band was 1070 bp and floxed protein band was 1550 bp. **(d)** Genotyping of Ins-1^{Cre} mice. Common (WT) protein band was 488 bp and mutant (Cre expressing) protein band was 675 bp.

4.8 Identifying prolyl hydroxylated proteins by PHD

Short term inhibition of PHD via DMOG plays a role in GSIS *in vitro* and improves glucose tolerance *in vivo*. Since PHDs regulate proteins via prolyl hydroxylation, the next objective was to identify proteins with proline hydroxylation to explore whether PHD prolyl hydroxylated proteins have short term effects on insulin secretion. Co-immunoprecipitation using whole cell lysates from 832/13 cells was performed. An anti-hydroxyproline antibody was used to bind proteins with hydroxylated proline residues from protein samples treated with NT (cell growth media), LG (2mM) KRB, HG (16.7mM) KRB, glutamine (Glu) (10mM) + leucine (Leu) (10mM) and palmitate (Pal) (0.1mM) to investigate whether nutrient stimuli alters protein. Protein samples containing 1mg of protein were also treated with DMαKG (10mM) and DMOG (500μM) as positive and negative controls for PHD, respectively. After co-immunoprecipitation, gel electrophoresis was performed followed by silver staining of the polyacrylamide gel (fig. 4.11).

Protein bands from LG (2mM) KRB (38 kDa and 41 kDa), NT (20 kDa, 30 kDa, 38 kDa, 40 kDa, 60 kDa and 140 kDa), palmitate (0.1mM) (20 kDa, 38 kDa and 140 kDa) and DMαKG (10mM) (40kDa) were excised using a razor blade and delivered to Western University for protein identification (Table 4.1).

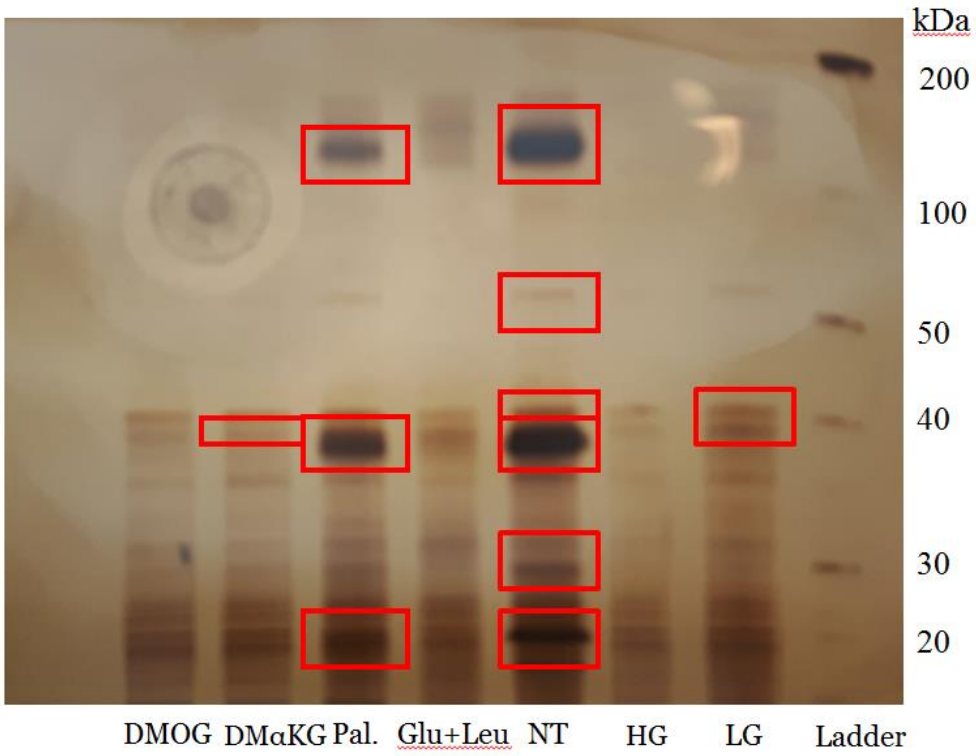

Figure 4.11: Silver stained gel containing prolyl hydroxylated protein from 832/13 cells. Protein bands were excised from a silver stained polyacrylamide gel containing prolyl hydroxylated protein from 832/13 cells. 38 kDa and 41 kDa protein bands were excised from LG (2mM) KRB; 20 kDa, 30 kDa, 38 kDa, 40 kDa, 60 kDa and 140 kDa protein bands were excised from NT (cell media); 20 kDa, 38 kDa and 140 kDa protein bands were excised from palmitate (0.1mM) treatment; and a 40 kDa protein band was excised from DMαKG (10mM) treatment. Protein band lengths are approximate.

Glucose (LG, HG), amino acids (glutamine + leucine) and saturated fatty acids (palmitate) were used to investigate whether prolyl hydroxylated protein expression was affected by nutrient stimuli. 20 kDa and 38 kDa protein bands were observed to be downregulated when treated with LG (2mM) KRB, palmitate (0.1mM), and glutamine (10mM) + leucine (10mM) compared to NT. As well, 140 kDa protein bands appeared to be downregulated when treated

with palmitate and glutamine + leucine and unobserved in the LG treatment compared to NT; however, we were unable to excise protein bands from glutamine + leucine treatment. These observations suggest that nutrient stimuli regulate prolyl hydroxylated proteins. It is hypothesized that the unidentified proteins are proline hydroxylated via PHD and are regulated by nutrient stimuli. Previous experiments suggest that short term inhibition of PHD results in enhanced second-phase insulin secretion. It can be suggested that inhibition of PHD results in upregulation of unidentified proteins to enhance insulin secretion.

Protein bands were excised using a razor blade. Excised protein bands were stored in 5% acetic acid and delivered to the MALDI-MS Facility at Western University (London, ON, CA) for protein identification by MALDI-MS. Peaks Software using the hydroxyl modification of proline was used; however, prolyl hydroxylated proteins in the samples were unable to be identified. Table 4.2 shows a list of the protein samples with the approximate band lengths.

Table 4.2: Protein identification by MALDI-MS data

Sample	Size (kDa)
LG (2mM)	41
LG (2mM)	38
NT	140
NT	60
NT	40
NT	38
NT	30
NT	20
Palmitate (0.1mM)	140
Palmitate (0.1mM)	38
Palmitate (0.1mM)	20
DMαKG (10mM)	40

12 Protein bands were excised from a silver stained polyacrylamide gel treated with LG (2mM), NT, Palmitate and DMαKG. Protein bands of approximate size were excised across treatments for comparison.

Chapter 5: Discussion

5.1 Summary

The data presented in chapter four reveal the acute effects of PHD in oxidative mitochondrial metabolism and GSIS using the pharmacological inhibitor DMOG. PHD inhibition via DMOG resulted in a significant reduction in ATP turnover, spare respiratory capacity and non-mitochondrial oxygen consumption in 832/13 cells. Similarly, inhibition of PHD via DMOG resulted in decreased ATP turnover in primary mouse islets. The role of PHD in GSIS and glucose homeostasis was also assessed. Inhibition of PHD via 5mM DMOG resulted in enhanced second-phase insulin secretion *in vitro*, suggesting PHD plays a role in K_{ATP} channel-independent pathways. PHD inhibition in C57BL/6J male mice led to improved glucose tolerance at 90 and 120 minutes after an exogenous glucose load *in vivo*, further supporting PHD's involvement in second-phase insulin secretion. ELISA revealed inhibition of PHD results in decreased plasma insulin levels 10 minutes after a glucose challenge despite unchanged blood glucose levels. Improved insulin sensitivity at 10 minutes *in vivo* and decreased ATP turnover *in vitro* suggests that PHD may also play a role in the K_{ATP} channel-dependent pathway.

5.2 Expression of PHD isoenzymes in 832/13 cells and primary mouse islets

Western blot analysis using specific PHD primary antibodies, determined that PHD1, PHD2, and PHD3 are expressed in 832/13 cells. As well, all PHD isoenzymes are expressed with unique subcellular localizations in mouse pancreases, which was determined by immunofluorescence. PHD1 is expressed exclusively in the cytosol within acinar tissue and islets, PHD2 is expressed mainly in the cytosol within acinar tissue and islets with a weak

nuclear stain, and PHD3 is expressed mainly in the nucleus within the acinar tissue and islets with a weak cytosolic stain.

However, PHD expression differs between the mouse and human pancreas. In the human pancreas, PHD1 and PHD2 are expressed in the cytosol within islets, acinar tissue and pancreatic ducts, whereas PHD3 is expressed in the cytosol and nucleus within islets, acinar tissue and pancreatic ducts.[57] Differences in PHD expression between mice and human pancreases may be associated with differences in islet composition and organization.

Several rodent models have been developed to study pancreas physiology in T2D.[113] It is important to consider the differences between human and mice pancreases since findings from rodent models are generalized to humans.[113] Anatomically, the human pancreas is definite, with a distinct head, body, and tail, whereas the mouse pancreas is divided into 3 less-defined lobes.[113] The endocrine portion of the pancreas consists of 50-70% and 60-80% β-cells within the islet for humans and mice, respectively.[113,114] In rodents, β-cells comprise the core of the islet surrounded α-cells.[114] In humans, islets form a trilaminar plate consisting of a layer of β-cells surrounded by two layers of α-cells, which forms a U or O-shaped islet.[113] Human β-cells respond to lower blood glucose concentrations compared to mice.[113,115] Despite differences in endocrine cell distribution between mice and humans, islet size remains relatively the same in both species.[115]

Rodents and humans also display differences in oxidative metabolism and β-cell insulin secretion. PC is involved in pyruvate cycling, producing NADPH and αKG via the pyruvate/isocitrate pathway. It is hypothesized that cytosolic αKG acts as a co-substrate for PHD to regulate insulin secretion. However, PC was found to be reduced by 80-90% in human islets compared to mouse islets and 832/13 cells.[43] Similarly, pyruvate entering the TCA cycle in

human islets through PC was 20 to 30%, whereas pyruvate entering the TCA cycle through PC is approximately 50% in rodent models.[43,44]

5.3 OCR in 832/13 cells and primary mouse islets

5.3.1 In vitro findings of OCR in 832/13 cells

Oxidative metabolism was significantly decreased in 832/13 cells treated with DMOG. Proton leak, H^+ that is not coupled to ATP production, can be an indication of mitochondrial damage or a means of regulating ATP production. Proton leak was not significantly altered in DMOG treated cells but a reduced trend was observed. ATP turnover was decreased at all concentrations of DMOG, and spare respiratory capacity and non-mitochondrial oxygen consumption was significantly decreased at 1000μM DMOG.

5.3.2 In vitro findings of OCR in primary mouse islets

Oxidative metabolism was reduced in primary mouse islets treated with DMOG. OCR was decreased in islets treated with 5mM DMOG compared to NT when stimulated with HG (16.7mM) KRB and HG (16.7mM) KRB + DMM (10mM) + DMαKG (10mM) . There was a decreased trend for non-mitochondrial oxygen consumption, which is due to pathways other than oxidative respiration, with the greatest decrease at 5mM DMOG. ATP turnover was significantly reduced at 1mM and 5mM DMOG. Respiration assays demonstrate the role of PHD in mitochondrial metabolism. Inhibition of PHD via DMOG decreased OCR and parameters of mitochondrial function, which may affect GSIS.

5.3.3 OCR levels are decreased with PHD inhibition in 832/13 cells and primary mouse islets

OCR experiments reveal insights into metabolic activity by measuring parameters of mitochondrial metabolism in real time. These results show a significant decrease in oxygen consumption when 832/13 cells and primary mouse islets were treated with DMOG at HG (16.7mM) KRB. β-cells demonstrate increased rates of oxidative metabolism, requiring large quantities of oxygen for survival.[116] Islets are exposed to a higher partial pressure of oxygen compared to acinar tissue and are highly vascularized, demonstrating the metabolic demand of β-cells.[116] OCR is a parameter of β-cell function and represents the amount of energy released during oxidative metabolism.[116] Komatsu and colleagues (2016) incubated human islets in either a hypoxic, normoxic or hyperoxic environment and measured OCR. OCR levels were increased in islets incubated in a hyperoxic environment. DMOG is an effective hypoxia mimetic and inhibition of PHD via DMOG resulted in reduced OCR levels in 832/13 cells and islets. Leung and colleagues (2017) investigated the role of HIF1α in oxidative metabolism and HIF1α knockdown in ME180 and FaDu cells resulted in decreased lactate production and significantly increased OCR levels when exposed to a hypoxic environment, possibly resulting in increased hypoxia.[117] Inhibition of PHD via DMOG may lead to HIF1α stabilization at higher concentrations, and the findings presented in chapter four indicate that inhibition of PHD in both 832/13 cells and primary mouse islets results in decreased OCR compared to NT. The potential role of HIFα in decreasing OCR levels cannot be eliminated however; these results demonstrate the acute effects of PHD, which may be involved in non-HIFα-dependent pathways.

Glucose metabolism via mitochondrial respiration is linked to insulin secretion.[118] First-phase insulin secretion relies on increased ATP production from mitochondrial metabolism and impairments in first-phase insulin secretion is indicative of both T1D and T2D, more

specifically, impairments with mitochondrial membrane potential.[118] A decreased response of membrane potential to a glucose stimulus decreases OCR levels and negatively affects mitochondrial bioenergetics.[118]

Inhibition of PHD via DMOG was shown to alter parameters that represent mitochondrial function in both cells and islets. There was a reduced trend in proton leak in 832/13 cells treated with DMOG at all concentrations. Proton leak is the amount of H^+ that does not contribute to ATP production and is dissipated as heat. Increased proton leak could be a sign of mitochondrial damage or a means to regulate ATP production. Decreased proton leak suggests more H^+ ions are contributing to ATP production by ATP synthase. Uncoupling protein-2 (UCP-2) is an inner mitochondrial membrane protein that dissipates the proton motive force when glucose and fatty acids are abundant.[8,119] UCP-2 is induced in chronic glucose and fatty acid overload to aid in ROS reduction.[8] However, UCP-2 results in reduced ATP production and is associated with β-cell dysfunction and the development of T2D.[8,119] Hu and colleagues (2017) showed that palmitate treatment in 832/13 cells triggers UCP-2 activity resulting in impaired GSIS. ATP turnover was significantly reduced in both 832/13 cells and primary mouse islets. Reduced ATP synthesis via mitochondrial metabolism eventually leads to impaired GSIS and the onset of T2D.[119] Despite observing reduced ATP turnover in 832/13 cells and primary mouse islets, insulin secretion was increased in GSIS assays in primary mouse islets treated with DMOG *in vitro*. Gerenscer (2017) and colleagues determined that proton leak and ATP turnover regulate steady state membrane potential at LG (2mM) but not at HG (10mM) via determination of membrane potential values by fluorescence microscopy.

Spare respiratory capacity was decreased at 1000μM DMOG in 832/13 cells and is the cell's ability to respond to an increase in energy demand, such as glucose surplus. These

findings suggest that perhaps at high concentrations of DMOG in 832/13 cells, the β-cell is unable to effectively respond to an increase in energy demand but may also be due to off target effects. Decreased ATP production and spare respiratory capacity are correlated to T2D and indicate mitochondrial dysfunction.[120] Inhibition of PHD via DMOG reduces ATP production and spare respiratory capacity and in part, may regulate the K_{ATP} channel-dependent pathway by decreasing the ATP/ADP ratio at high concentrations of DMOG.

Non mitochondrial oxygen consumption is the amount of oxygen consumption that continues due to other metabolic pathways or enzymes. Non mitochondrial oxygen consumption was significantly reduced at 1000μM DMOG in 832/13 cells and reduced at 5mM and 10mM DMOG in primary mouse islets. PHD requires molecular oxygen as a co-substrate; therefore, inhibition of PHD via DMOG represents less oxygen being consumed by PHD for activity.

ATP production and oxygen consumption by mitochondrial respiration is linked to GSIS and appears to reach saturation at 16mM glucose in the pancreas.[121] Chronically elevated glucose levels that are characteristic of T2D leads to β-cell compensation and an increase in oxidative metabolism with a subsequent increase in OCR levels.[7] Therefore, decreased OCR levels with DMOG treatment suggests that 832/13 cells and primary mouse islets display more efficient GSIS compared to NT. As well, TCA cycle intermediates, notably citrate and isocitrate, increase in response to a glucose stimulus and lead to enhanced GSIS.[121] It is hypothesized that increased TCA cycle intermediates in response to glucose are involved in futile pyruvate cycling, generating cytosolic αKG. Cytosolic αKG acts as a co-substrate for PHD and may be involved in regulating GSIS. However, chronic hyperglycemia, a hallmark of T2D, impairs oxidative metabolism subsequently leading to reduced ATP production and GSIS.[120] Alarcon and colleagues (2016) measured OCR levels in diabetic mice (db/db) and isolated protein to measure

proinsulin concentration. Proinsulin biosynthesis in the ER, the precursor to insulin, was found to be increased with HG, linking oxidative metabolism to GSIS.[122]

PHD inhibition reduced oxidative metabolism in both 832/13 cells and primary mouse islets when stimulated with HG (16.7mM) KRB, altering parameters that indicate mitochondrial function and viability. *In vitro* and *in vivo* experiments assessing GSIS resulted in increases insulin secretion when PHD is inhibited in rodent models. Therefore, reduced OCR levels when PHD is inhibited suggest better mitochondrial efficiency. Further research is needed to determine if these results hold true for human islets and to determine the mechanisms by which PHD affects GSIS.

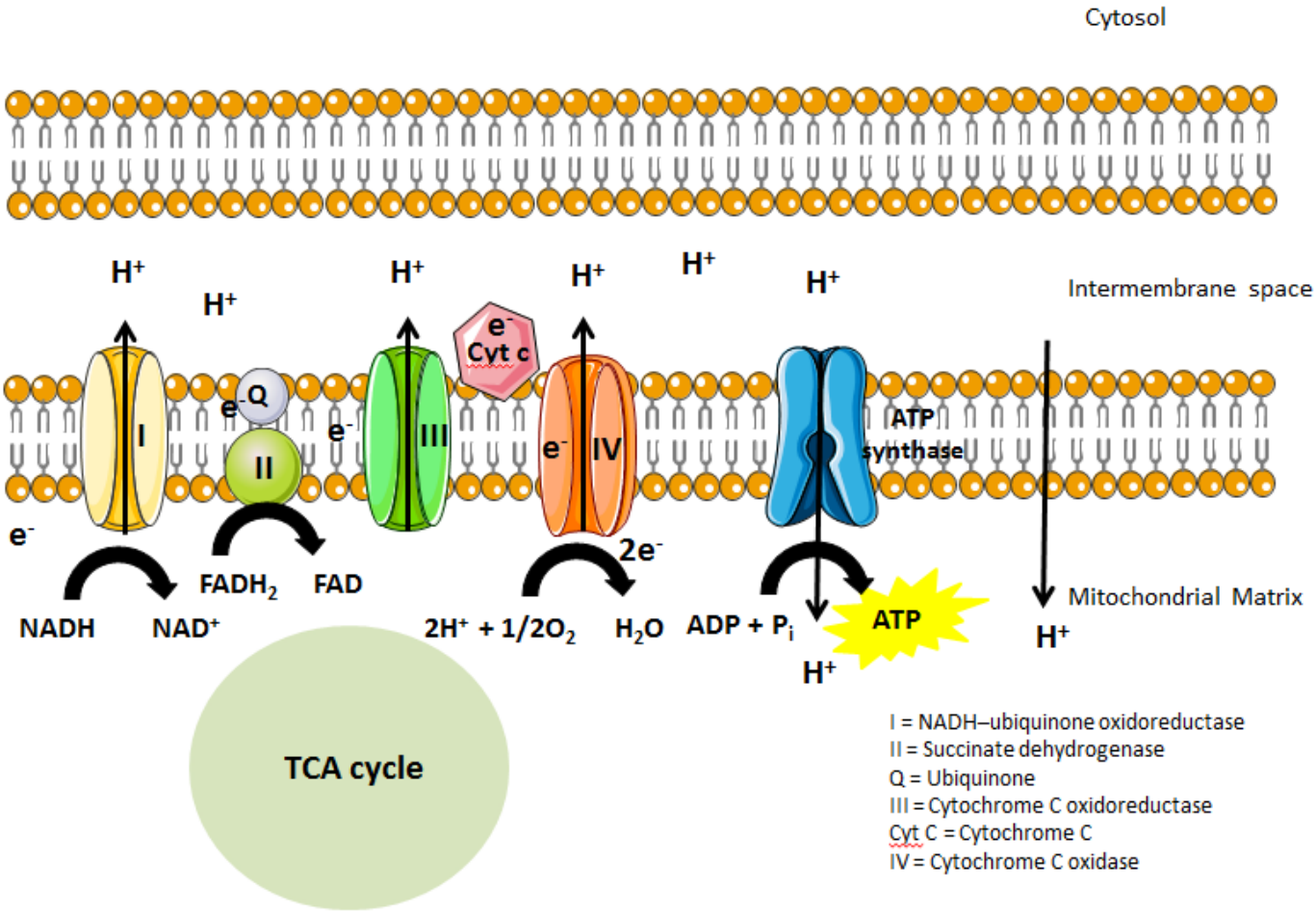

Figure 5.1: ATP production by oxidative metabolism.

Reducing equivalents from the TCA cycle enter the ETC via complex I and complex II. Electron flow pumps H^+ ions into the intermembrane space, generating the proton motive force. H^+ ions produce ATP in the mitochondrial matrix via ATP synthase. H^+ may also be dissipated as heat and does not contribute to ATP production. Image was reproduced from Servier Medical Art by Servier, licensed under CC BY 3.0.

5.4 Insulin secretion in male C57BL/6J primary mouse islets

5.4.1 In vitro findings from GSIS assays in primary mouse islets

Inhibition of PHD via 5mM DMOG led to alterations in glucose-stimulated mitochondrial respiration, including reduced ATP production and spare respiratory capacity.

This suggests that PHD inhibition decreases the K_{ATP} channel-dependent pathway by decreasing the ATP/ADP ratio. OCR levels were measured in real time and were reduced throughout the entire time period, suggesting that PHD is involved in K_{ATP} channel-independent pathways. These findings may lead to changes in insulin secretion. The acute effects of DMOG treated islets in static GSIS were next assessed. Primary islets were treated with 5mM DMOG for one hour stimulated with LG (2mM) KRB or HG (16.7mM) KRB compared to NT. There was an increased trend in increased insulin secretion with 5mM DMOG stimulated with HG (16.7mM) KRB.

5.4.2 In vitro findings from perifusion assays in primary mouse islets

Inhibition of PHD via DMOG alters mitochondrial metabolism by decreasing OCR levels alluding to alterations in K_{ATP} channel-independent pathways in both 832/13 cells and primary mouse islets. 5mM DMOG increased static insulin secretion in primary mouse islets via an insulin secretion assay when islets were stimulated with HG (16.7mM) KRB. A perifusion assay was performed in islets treated with 5mM DMOG to distinguish between first- and second-phase GSIS. There was a reduced trend in insulin secretion when DMOG treatment was initiated in primary islets with HG (16.7mM) KRB. These findings, along with reduced ATP turnover, suggest that inhibition of PHD via DMOG leads to reduced insulin secretion via the K_{ATP} channel-dependent pathway. It cannot be eliminated that PHD may alter first-phase insulin secretion, which occurs within the first 10 minutes after glucose stimulation. However, PHD may play a greater role in K_{ATP} channel-independent pathways through anaplerosis. There was a statistically significant increase in insulin secretion in islets treated with DMOG in the latter 30 minutes when stimulated with HG (16.7mM) KRB.

5.4.3 In vivo findings from ipGTTs in primary mouse islets

Acute systemic effects of PHDs were assessed by ipGTTs. Blood glucose levels were measured over a two hour period in C57BL/6J male mice aged 10-14 weeks injected with 200µg/g body weight DMOG compared to PBS controls. *In vitro* experiments using primary mouse islets treated with DMOG resulted in increased GSIS. It was hypothesized that C57BL/6J male mice injected with DMOG would display similar findings *in vivo*. Inhibition of PHD via DMOG resulted in decreased blood glucose levels at 90 and 120 minutes after an exogenous glucose load. Blood glucose levels remained unchanged in the first 30 minutes after a glucose challenge. Plasma insulin samples were collected at baseline, 10 and 30 minutes after glucose injection and an ELISA was performed to measure plasma insulin levels. Plasma insulin levels were significantly reduced in mice injected with DMOG at 10 minutes despite unchanged blood glucose levels.

The results discussed in chapter four suggest that PHD plays a role in both first- and second-phase GSIS. Mice injected with 200µg/g BW DMOG showed improved glucose tolerance at 90 and 120 minutes and improved insulin sensitivity at 10 minutes.

5.4.4 PHD inhibition via DMOG alters first- and second-phase insulin secretion

In vitro insulin secretion assays and *in vivo* ipGTTs demonstrate that acute inhibition of PHD leads to alterations in insulin secretion; however the exact mechanism remains inconclusive. There are three pyruvate cycling pathways producing NADPH and αKG that may be involved in the regulation of GSIS.[123] There is evidence that increased cytosolic αKG leads to sustained second-phase insulin release.[123] C57BL/6N mice fed a HFD showed reduced serum TCA cycle intermediates including pyruvate, citrate and αKG, suggesting impaired anaplerosis

in a T2D rodent model.[124] CIC, which transports citrate and isocitrate to the cytosol, and ICDc, which catalyzes the conversion of isocitrate to αKG and producing NADPH, are involved in GSIS.[109,123] Inhibition of CIC in 832/13 cells and primary rat islets using the pharmacological inhibitor 1,2,3-benzenetricarboxylate (BTC) significantly inhibited first- and second-phase insulin secretion.[109] siRNA knockdown of ICDc in 832/13 cells and primary rat islets also led to a significant reduction in GSIS.[111] However, Guay et al. (2013) found that ICDc negatively regulated GSIS in 832/13 cells and primary rat islets. RNAi knockdown of ICDc in 832/13 cells and primary rat islets resulted in enhanced GSIS with unaltered glucose metabolism.[125] Inhibition of ICDc increased mitochondrial isocitrate, acetyl-CoA and ATP and it is suggested that increased mitochondrial TCA cycle intermediates is coupled with increased GSIS.[125]

Currently, there is no specific role of cytosolic αKG in the pyruvate/isocitrate pathway.[48,123] αKG is a known co-substrate for PHD and it is suggested that PHD plays a role in GSIS. It is hypothesized that PHD may be one mechanism by which αKG regulates GSIS. 832/13 cells and primary rat islets were treated with the PHD inhibitor EDHB, which resulted in reduced GSIS.[47,48] siRNA knockdown for each PHD isoenzyme determined that PHD3 led to a greater reduction in GSIS compared to PHD1, and PHD2 did not reduce GSIS in 832/13 cells.[47]

Together, *in vitro* and *in vivo* experiments presented in this thesis assessing the role of PHD in GSIS via DMOG determined the opposite to be true. These differences could be due to variations in drug mechanisms and concentrations. Fallon and colleagues (2008) observed decreased GSIS with 1mM EDHB, an iron chelator, in primary rat islets and Huang and colleagues (2016) observed increased GSIS with 50µmol/L EDHB whereas 500µmol/L and 1000µmol/L EDHB significantly reduced GSIS. Respiration assays determined that 5mM DMOG displays alterations in oxidative metabolism compared to 1mM and 10mM DMOG.

5mM DMOG was continued for insulin secretion assays and there was an increased trend in insulin secretion. It is hypothesized that acute inhibition of PHD leads to enhanced insulin secretion, possibly through compensatory mechanisms affecting both first- and second-phase insulin secretion. Mice fed a HFD displayed impaired anaplerosis and reduced αKG levels, suggesting that TCA cycle intermediates are reduced in a diet-induced obesity rodent model, inhibiting PHD activity and leading to impaired GSIS.[124] Further research is warranted to investigate whether and how long term inhibition of PHD affects GSIS.

5.5 Protein Identification

5.5.1 Proline hydroxylation in 832/13 cells

Protein was isolated from 832/13 cells treated with LG, HG, leucine + glutamine, palmitate, DMOG, DMαKG and NT. Co-immunoprecipitation was performed using an anti-hydroxyproline antibody to isolate protein containing hydroxylated proline residues from whole cell lysate samples. Protein samples with hydroxylated proline residues were run on a polyacrylamide gel, which was then silver stained to identify band lengths for each treatment. Protein bands were excised and delivered to the MALDI-MS Facility at Western University for protein identification by MALD-MS. However, Proteins containing proline hydroxylation were unable to be identified by MALDI-MS. Silver staining may be more sensitive than MALDI-MS and therefore, the protein concentration was too low to be detected. Coomassie Brilliant Blue staining is less sensitive and may be a better method for gel staining for detection by MALD-MS.

5.5.2 Protein identification by MALDI-MS findings

Glucose, amino acids and fatty acids were observed to be downregulated compared to NT, suggesting that nutrient stimuli regulate prolyl hydroxylated protein expression. In the presence of PHD, prolyl hydroxylated protein appeared to be downregulated upon nutrient stimuli. Previous experiments demonstrated short term inhibition of PHD via DMOG results in enhanced second-phase insulin secretion. It is hypothesized that acute inhibition of PHD will result in upregulation of unidentified proteins to increase insulin secretion.

PHD, particularly PHD3, hydroxylates and regulates other proteins involved in altering glucose metabolism. However, it is currently unknown how these metabolic changes affect pancreatic β-cell insulin secretion. PHD3 interacts with the E1β subunit of PDH, the enzyme that catalyzes the conversion of pyruvate to acetyl-CoA, which feeds into the TCA cycle, coupling glycolysis with mitochondrial respiration.[90] PHD3 positively regulates PDH, however not through proline hydroxylation.[90] PHD3 also regulates pyruvate kinase M2, which catalyzes the last step of glycolysis, converting phosphoenolpyruvate and ADP to pyruvate and ATP.[91] PHD3 is suggested to act as a co-activator via hydroxylation of PKM2 to enhance PKM2's interaction with HIF1α.[91] Upregulation of HIF1α results in alterations in glucose metabolism by upregulating genes that reduce oxygen consumption and increase oxygen availability.[91] PHD3 plays a role in tumor proliferation and apoptosis that are independent of HIF1α.[81] Cancer cells treated with αKG showed increased cell apoptosis and decreased cell proliferation, which occurred independently of HIF1α but required PHD3.[81]

PHD3 is involved in the regulation of proteins that may be involved in altering glucose metabolism and potentially influence insulin secretion. From these experiments, it can be conferred that cytosolic αKG is required for PHD activity. PHD hydroxylates and regulates

currently unidentified proteins that may alter insulin secretion. Experiments discussed in chapter four reveal a novel role for PHDs that could be a potential target for drug development in the treatment of T2D. However, further research is needed to explore the mechanisms by which PHD regulates insulin secretion and determine which proteins are involved. The experiments discussed investigate the role of PHD in 832/13 cells and primary mouse islets but future work is needed to determine if these results translate to human islets.

5.6 Limitations and future work

One limitation of the experiments presented in this thesis is that all experiments apart from ipGTTs are performed *in vitro*. Isolated islets are removed from their natural environment and lack vasculature. Isolated islets are incubated (37˚C, 5% CO_2) for 18-72 hours prior to the day of assay. During this time, the islet core begins to die, particularly in larger islets, due to lack of oxygen diffusion.[126] Islets become less responsive to glucose stimuli, which causes impairments in metabolic activity.[126] However, we were able to perform *in vivo* ipGTTs to assess glucose tolerance in C57BL/6J male mice injected with DMOG and these observations showed similar trends to our *in vitro* experiments. Plasma insulin levels revealed improved insulin sensitivity upon DMOG injection. Future work should investigate the role of PHDs in insulin sensitivity by performing insulin tolerance tests (ITTs) in mice injected with DMOG. This will measure the effects of PHD inhibition on insulin sensitivity over a two hour period, allowing us to distinguish between first- and second-phase insulin secretion.

Another limitation of the experiments performed is that all experiments involved PHD inhibition using a pharmacological inhibitor. DMOG inhibits all three isoenzymes of PHD; therefore we cannot be certain if a specific isoenzyme plays a greater role in the regulation of insulin secretion. Further work investigating the role of PHD in pancreatic β-cell insulin

secretion involves the development of a transgenic mouse model using the Cre-lox system. Our lab is currently generating β-cell specific PHD1, PHD2, and PHD3 KO mouse models using Cre recombinase. Future work will involve performing *in vitro* and *in vivo* experiments using PHD KO mice, allowing us to address the long term effects of PHD in regulating insulin secretion.

We were able to conduct experiments using 832/13 cells and primary mouse islets. However, differences in islet architecture and metabolic activity between human and rodent islets have been addressed. Our results show strong evidence that PHD plays a role in oxidative metabolism and both first- and second-phase insulin secretion. Moving forward, studies using human islets should be performed to investigate if our findings translate to human islets.

Prolyl hydroxylated protein was isolated from 832/13 cells and silver staining for MALD-MS protein identification was performed. However, we were unable to identify prolyl hydroxylated protein within our samples. Future work will continue co-immunoprecipitation experiments followed by MALDI-MS to identify proteins that may be regulating insulin secretion. Coomassie Brilliant Blue staining is less sensitive and may be more compatible with MALD-MS. Identification of prolyl hydroxylated proteins in 832/13 cells would allow us to perform hydroxylation assays to determine which isoenzyme is involved in the hydroxylation of these proteins. Protein identification would provide insight into the mechanisms by which PHD regulates insulin secretion and future experiments investigating the role of these proteins in GSIS are needed.

5.7 Significance of the work

PHDs have been well-studied for their role in the hypoxia response pathway, where HIFα upregulates genes including EPO and VEGF that improve blood flow and oxygen availability in chronic kidney disease, cardiovascular disease, and cancer.[50,99] T2D is also associated with a

hypoxic environment, where HIFα becomes stabilized and forms a heterodimer with HIFβ to upregulate genes that promote angiogenesis and alter glucose metabolism including glycolytic enzymes and LDHA.[66]

K_{ATP} channel-independent pathways involve anaplerosis, where increased production of TCA cycle intermediates such as αKG are associated with second-phase insulin secretion.[39,111] αKG is produced in the pyruvate/isocitrate pathway which is positively correlated with increased GSIS. However, a defined pathway has not been identified for αKG. Our results reveal a novel pathway for PHD in the regulation of insulin secretion, whereby cytosolic αKG acts as a co-substrate for PHD, regulating insulin secretion.

However, there is conflicting evidence regarding the role of PHD in insulin secretion. Pharmacological inhibition of PHD was found to inhibit GSIS in both cells and primary rat islets.[47,48] Our results reveal that short term inhibition of PHD increased GSIS and affects both first- and second-phase insulin secretion. Further research is warranted in defining the mechanisms by which PHD affects insulin secretion both acutely and chronically. Nonetheless, PHDs are involved in pathways that are independent of HIFα and are a potential target for the treatment of T2D.

T2D is now considered a global epidemic and is associated with the development of other diseases, including CVD and stroke.[119,127,128] Currently, there are several approved anti-hyperglycemic agents that are used to treat and manage T2D that are effective at maintaining blood glucose levels.[127] Anti-hyperglycemic agents target one mechanism of a highly complex disease, resulting in patients often being prescribed a combination of agents. As well, emerging evidence reveals that these approved agents may be correlated with serious adverse effects and the long term use of these agents remains unclear.[127] The pancreas is the central organ for

glucose homeostasis and current anti-hyperglycemic agents targeting the pancreas include sulfonylureas and meglitinides, which target the K_{ATP} channel-dependent pathway. There are currently no anti-hyperglycemic agents that target K_{ATP} channel-independent pathways, which contributes 70% of total insulin secretion.[37] Understanding the mechanisms involved in K_{ATP} channel-independent pathways is of importance to development effective treatment options for T2D. With the findings presented in this thesis, PHD may be a potential target for drug development for the treatment and management of T2D.

References

1. Diabetes, 2014. Statistics Canada website http://www.statcan.gc.ca/pub/82-625x/2015001. Updated November 27, 2015. Accessed April 4, 2017.
2. Diabetes. World Health Organization website http://www.who.int/diabetes/en/. Updated November, 2016. Accessed April 4, 2017.
3. Newsholme P, Cruzat VF, Keanne KN, Carlessi R, Homem de Bittencourt PI. Molecular mechanisms of ROS production and oxidative stress in diabetes. *Biochem J.* 2016;473(24):4527-4550.
4. Knip M, Siljander H, Ilonen J, Simell O, Veijola R. Role of humoral beta-cell autoimmunity in type 1 diabetes. *Pediatr Diabetes.* 2016;17(22):17-24.
5. King BC, Blom AM. Non-traditional roles of complement in type 2 diabetes: metabolism, insulin secretion and glucose homeostasis. *Mol Immunol.* 2017;84:34-42.
6. Tran L, Zielinski A, Roach AH, et al. Pharmacologic treatment of type 2 diabetes: oral medication. *Ann Pharmacother.* 2015;49(5):540-556.
7. Jouvet N, Estall JL. The pancreas: bandmaster of glucose homeostasis. *Exp Cell Res.* 2017;pii: S0014-4827(17)30180-5.
8. Prentki M, Nolan CJ. Islet β-cell failure in type 2 diabetes. *J Clin Invest.* 2006;116(7):1802-1812.
9. Ahn CH, Min SH, Lee DW, Oh TJ, Kim KM, Moon JH, Choi SH, Park KS, Jang HC, Ha J, Sherman A, Lim S. Hemoglobin glycation index is associated with cardiovascular diseases in people with impaired glucose metabolism. *J Clin Endocrinol Metab.* 2017; doi: 10.1210/jc.2017-00191.
10. Sacks DB. Hemoglobin A_{1c} in diabetes: panacea or pointless? *Diabetes.* 2013;62:41-43.
11. Sobrin L. Longitudinal validation of hemoglobin A_{1c} criteria for diabetes diagnosis: risk of retinopathy.
12. Gong L, Goswamic S, Giacominic KM, Altmana RB, Kleina TE. Metformin pathways: pharmacokinetics and pharmacodynamics. *Pharmacogenet Genomics.* 2012;22(11):820-827.
13. Shu Y, Sheardown SA, Brown C, Owen RP, Zhang S, Castro RA, Ianculescu AG, Yue L, Lo JC, Burchard EG, Brett CM, Giacomini KM. Effect of genetic variation in the prganic cation transporter 1 (OCT1) on metformin action. *J Clin Invest.* 2007;117(5):1422-1431.
14. Sherifali D, Nerenberg K, Pullenayegum E, Cheng JE, Gerstein HC. The effect of oral antidiabetic agents on A1C levels: a systemic review and meta-analysis. *Diabetes Care.* 2010;33(8):1859-1864.
15. Hattori Y, Hattori K, Hayashi T. Pleiotropic benefits of metformin: macrophage targeting its anti-inflammatory mechanisms. *Diabetes.* 2015;64:1907-1909.
16. Boussageon R, Supper I, Bejan-Angoulvant T, Kellou N, Cucherat M, Boissel JP, Kassai B, Moreau A, Gueyffier F, Cornu C. Reappraisal of metformin efficacy in the treatment of type 2 diabetes: a meta-analysis of randomized controlled trials. *PLoS Med.* 2012;9(4):e1001204.
17. Forouzandeh F, Salazar G, Patrushev N, Xiong S, Hilenski L, Fei B, Alexander RW. Metformin beyond diabetes: pleiotropic benefits of metformin in attenuation of atherosclerosis. *J Am Heart Assoc.* 2014;3:e001202.

18. Elmi A, Idahl L, Sehlin J. Relationships between the Na^+/K^+ pump and ATP and ADP content in mouse pancreatic islets: effects of meglitinide and glibenclamide. *Br J Pharmacol.* 2000;131:1700-1706.
19. Hu S, Wang S, Fanelli B, et al. Pancreatic β-cell K_{ATP} channel activity and membrane-binding sites with nateglinide: a comparison with sulfonylureas and repaglinide. *J Pharmacol Exp Ther.* 2000;293(2):444-452.
20. Holstein A, Beil W, Kovacs P. CYP2C metabolism of oral antidiabetic drugs—impact on pharmacokinetics, drug interactions and pharmacogenetics aspects. *Expert Opin Drug Metab Toxicol.* 2012;8(12):1549-1563.
21. Scheen AJ. Drug-drug and food-drug pharmacokinetic interactions with new insulinotropic agents repaglinide and nateglinide. *Clin Pharmacokinet.* 2007;46(2):93-108.
22. Fürnsinn C, Waldhäusl W. Thiazolidinediones: metabolic actions *in vitro. Diabetologia.* 2002;45:1211-1223.
23. Hammarstedt A, Smith U. Thiazolidinediones (PPARγ ligands) increase IRS-1, UCP-2 and C/EBPα expression, but not transdifferentiation, in L6 muscle cells. *Diabetologia.* 2003;46:48-52.
24. Ruscic M, Baldessin L, Boccia D, Racagni G, Mitro N. Non-insulin anti-diabetic drugs: An update on pharmacological inhibitors. *Pharmacol Res.* 2017;115:14-24.
25. Ahmadian M, Suh JM, Hah N, Liddle C, Atkins AR, Downes M, Evans RM. PPARγ signaling and metabolism: the good, the bad and the future. *Nat Med.* 2013;19(5):557-566.
26. Marchand-Brustel YL, Rochet N, Grémeaux T, Marot I, Van Obberghen E. Effect of an α-glucosidase inhibitor on experimentally-induced obesity in mice. *Diabetologia.* 1990;33:24-30.
27. Takeda Y, Fujita Y, Honjo J, et al. Reduction of both beta cell death and alpha cell proliferation by dipeptidyl peptidase-4 inhibition in a streptozotocin-induced model of diabetes in mice. *Diabetologia.* 2012;55:404-412.
28. Zander M, Madsbad S, Deacon CF, Holst JJ. The metabolite generated by dipeptidyl-peptidase 4 metabolism of glucagon-like peptide-1 has no influence on plasma glucose levels in patients with type 2 diabetes. *Diabetologia.* 2006;49:360-374.
29. Htike Z, Zaccardi F, Papamargaritis D, Wedd DR, Khunti K, Davies MJ. Efficacy and safety of glucagon-like peptide-1 receptor agonists in type 2 diabetes: a systemic review and mixed-treatment comparison analysis. *Diabetes Obes Metab.* 2017;19:524-536.
30. Verma S, Goldenberg RM, Bhatt DL, Farkouh ME, Quan A, Teoh H, Connelly KA, Leiter LA, Friedrich JO. Dipeptidyl peptidase-4 inhibitors and the risk of heart failure: a systematic review and meta-analysis. *CMAJ.* 2017;5(1):e155-e177.
31. Imprialos K, Faselis C, Boutari C, Stavropoulis K, Athyros V, KaragiannisA, Doumas M. SGLT-2 inhibitors and cardiovascular risk in diabetes mellitus: a comprehensive and critical review of the literature. *Curr Pharm Des.* 2017;23(46):
32. Peters AL, Buschur EO, Buse JB, Cohan P, Diner JC, Hirsch IB. Euglycemic diabetic ketoacidosis: a potential complication of treatment with sodium-glucose cotransporter 2 inhibition. *Diabetes Care.* 2015;38:1687-1693.
33. Vallianou NG, Geladari E, Kazazis CE. SGLT-2 inhibitors: their pleiotropic properties. *Diabetes Metab Syndr.* 2016;pii: S1871-4021(16)30226-0.

34. Pratipanawatr T, Cusi K, Ngo P, Pratipanawatr W, Mandarino LJ, DeFronzo RA. Normalization of plasma glucose concentration by insulin therapy improves insulin stimulated glycogen synthesis in type 2 diabetes. *Diabetes.* 2002;51:462-468.
35. Ghosh S, Unnikrishnanb AG, Sabooc B, Kesavadevd J, Aravinde SR et al. Evidence-based recommendations for insulin intensification strategies after basal insulin in type 2 diabetes. *Diabetes Metab Syndr.* 2017;pii: S1871-4021(17)30057-7.
36. Owens D, Bolli G, Charbonnel B, Haak T, Landgraf W, Porcellati F, Traylor L, Kautzky-Willer A. Effects of age, gender, and body mass index on efficacy and hypoglycaemia outcomes across treat-to-target trials with insulin glargine 100 U/ml added to oral antidiabetes agents in type 2 diabetes. *Diabetes Obes Metab.* 2017; doi: 10.1111/dom.12966.
37. Jensen MV, Joseph JW, Ronnebaum SM, Burgess SC, Sherry AD, Newgard CB. Metabolic cycling in control of glucose-stimulated insulin secretion. *Am J Physiol Endocrinol Metab.* 2008;295:E1287-1297.
38. Henquin JC. Regulation of insulin secretion: a matter of phase control and amplitude modulation. *Diabetologia.* 2009;52:739-751.
39. Huypens PR, Huang M, Joseph JW. Overcoming the spatial barriers of the stimulus secretion cascade in pancreatic β-cells. *Islets.* 2011;4(1):1-9.
40. Huang M, Joseph JW. Assessment of the metabolic pathways associated with glucose-stimulated biphasic insulin secretion. *Endocrinol.* 2014;155:1653-1666.
41. Hatlapatka K, Willenborg M, Rustenbeck I. Plasma membrane depolarization as a determinant of the first phase of insulin secretion. *Am J Physiol Endocrinol Metab.* 2009;297:E315-322.
42. Misler S. Unifying concepts in stimulus-secretion coupling in endocrine cells and implications for therapeutics. *Adv Physiol Educ.* 2009;33:175-186.
43. MacDonald MJ, Longacre ML, Stoker SW, et al. Differences between human and rodent pancreatic islets: low pyruvate carboxylase, ATP citrate lyase, and pyruvate carboxylation and high glucose-stimulated acetoacetate in human pancreatic islets. *J Biol Chem.* 2011;286(21):18383-18396.
44. Newgard CB, Lu D, Jensen MV, et al. Stimulus/secretion coupling factors in glucose-stimulated insulin secretion: insights gained from a multidisciplinary approach. *Diabetes.* 2002;51(3):S389-393.
45. Pillai R, Huypens P, Huang M, et al. Aryl hydrocarbon receptor nuclear translocator/hypoxia-inducible factor-1β plays a critical role in maintaining glucose-stimulated anaplerosis and insulin release from pancreatic β-cells. *J Biol Chem.* 2011;286(2):1014-1024.
46. Huypens P, Pillai R, Sheinin T, Schaefer S, Huang M, Odegaard ML, Ronnenbaum SM, Wettig SD, Joseph JW. The dicarboxylate carrier plays a role in mitochondrial malate transport and in the regulation of glucose-stimulated insulin secretion from rat pancreatic beta cells. *Diabetologia.* 2011;54(1):135-145.
47. Huang M, Paglialunga S, Wong JM, Hoang M, Pillai R, Joseph JW. Role of prolyl hydroxylase domain proteins in the regulation of insulin secretion. *Physiol Rep.* 2016;4(5):e12722.
48. Fallon MJ, MacDonald MJ. Beta cell α-ketoglutarate hydroxylases may acutely participate in insulin secretion. *Metabolism.* 2008;57(8):1148-1154.

49. Myllyharju J, Kolvunen P. Hypoxia-inducible factor prolyl 4-hydroxylases: common and specific roles. *Biol Chem.* 2013;394(4):435-448.
50. Rishi MT, Selvaraju V, Thirunavukkarasu M, et al. Deletion of prolyl hydroxylase domain proteins (PHD1, PHD3) stabilizes hypoxia inducible factor-1 alpha, promotes neovascularization, and improves perfusion in a murine model of hind-limb ischemia. *Microvasc Res.* 2015;97:181-188.
51. Appelhoff RJ, Tian Y, Raval RR, et al. Differential function of the prolyl hydroxylases PHD1, PHD2, and PHD3 in the regulation of hypoxia-inducible factor. *J Biol Chem.* 2004;279(37):83458-83465.
52. Fong GH, Takeda K. Role and regulation of prolyl hydroxylase domain proteins. *Cell Death Differ.* 2008;15:635-641.
53. Kaelin WG Jr., Ratcliffe PJ. Oxygen sensing by metazoans: the central role of the HIF hydroxylase pathway. *Mol Cell.* 2008;30(4):393-402.
54. Bruick RK, McKnight SL. A conserved family of prolyl-4-hydroxylases that modify HIF. *Science.* 2001;294:1337-1340.
55. Ivan M, Kondo K, Yang H, et al. HIFα targeted for VHL-mediated destruction by proline hydroxylation: implications for O_2 sensing. *Science.* 2001;292:464-468.
56. Metzen E, Berchner-Pfannschmidt U, Stengel P, Marxsen JH, Stolze I, Klinger M, Huang WQ, Wotzlaw C, Hellwig-Bürgel T, Jelkmann W, Acker H, Fandrey J. Intracellular localisation of human HIF-1α hydroxylases: implications for oxygen sensing. *J Cell Science.* 2003;116(7):1319-1326.
57. Soilleux EJ, Turley H, Tian YM, Pugh CW, Gatter KC, Harris AL. Use of novel monoclonal antibodies to determine the expression and distribution of the hypoxia regulatory factors PHD-1, PHD-2, PHD-3 and FIH in normal and neoplastic human tissues. *Histopathol.* 2005;47:602-610.
58. Koivunen P, Tiainen P, Hyvärinen J, Williams KE, Sormunen R, Klaus SJ, Kivirikko KI, Myllyharju J. An endoplasmic reticulum transmembrane prolyl 4-hydroxylase is induced by hypoxia and acts on hypoxia-inducible factor α. *J Biol Chem.* 2007;282(42):30544-30552.
59. Boulahbel H, Durán RV, Gottlieb E. Prolyl hydroxylases as regulators of cell metabolism. *Biochem Soc Trans.* 2009;37(1):291-294.
60. Koivunen P, Hirsila M, Remes AM, Hassinen IE, Kivirikko KI, Myllyharju J. Inhibition of hypoxia-inducible factor (HIF) hydroxylases by citric acid cycle intermediates. *J Biol Chem.* 2007;282(7):4524-4532.
61. Bento CF, Pereira P. Regulation of hypoxia-inducible factor 1 and the loss of cellular response to hypoxia in diabetes. *Diabetologia.* 2011;54:1946-1956.
62. Takeda K, Ho VC, Takeda H, Duan LJ, Nagy A, Fong GH. Placental but not heart defects are associated with elevated hypoxia-inducible factor α levels in mice lacking prolyl hydroxylase domain protein 2. *Mol Cell Biol.* 2006;26(22):8336-8346.
63. Puri S, Cano DA, Herok M, A role for von Hippel-Lindau protein in pancreatic β-cell function. *Diabetes.* 2009;58:433-441.
64. Minamishima YA, Moslehi J, Bardeesy N, Cullen D, Bronson RT, Kaelin WG Jr. Somatic inactivation of the PHD2 prolyl hydroxylase causes polycythemia and congestive heart failure. *Blood.* 2008;111(6):3236-3244.
65. Köditz J, Nesper J, Wottawa M, et al. Oxygen-dependent ATF-4 stability is mediated by the PHD3 oxygen sensor. *Blood.* 2007;110(10):3610-3617.

66. Majmundar AJ, Wong WJ, Simon MC. Hypoxia inducible factors and the response to hypoxic stress. *Mol Cell.* 2010;40(2):294-309.
67. Takeda K, Aquila HL, Parikh NS, et al. Regulation of adult erythropoiesis by prolyl hydroxylase domain proteins. *Blood.* 2008;111(6):3229-3235.
68. Wang L, Fan J, Ling R, Yun J. Activation of hypoxia-inducible factor-1α by prolonged in vivo hyperinsulinemia treatment potentiates cancerous progression in estrogen receptor-positive breast cancer cells. *Biochem Biophys Res Commun.* 2017;pii: S0006-291X(17)30604-6.
69. Heinis M, Simon MT, Ilc K, et al. Oxygen tension regulates pancreatic β-cell differentiation through hypoxia-inducible factor 1α. *Diabetes.* 2010;59:662-669.
70. Heinis M, Soggia A, Bechetoille C, et al. HIF1α and pancreatic β-cell development. *FASEB J.* 2012;26:2734-2742.
71. Sato Y, Endo H, Okuyama H, et al. Cellular hypoxia of pancreatic β-cells due to high levels of oxygen consumption for insulin secretion *in vitro. J Biol Chem.* 2011;286(14):12524-12532.
72. Ma Z, Moruzzi N, Sergiu-Bogdan C, Grill V, Björklund A. Hyperoxia inhibits glucose-induced insulin secretion and mitochondrial metabolism in rat pancreatic islets. *Biochem Biophys Res Commun.* 2014;443:223-228.
73. Spégel P, Malmgrev M, Sharoyko VV, Newsholme P, Koeck T, Mulder H. Metabolomic analyses reveal profound differences in glycolytic and tricarboxylic acid cycle metabolism in glucose-responsive and –unresponsive clonal β-cell lines. *Biochem J.* 2011;435:277-284.
74. Ma Z, Moruzzi N, Sergiu-Bogdan C, et al. Preconditioning with associated blocking of Ca^{2+} inflow alleviates hypoxia-induced damage to pancreatic β-cells. *PLoS One.* 2013;8(7):e67498.
75. Cheng K, Ho K, Stokes R, et al. Hypoxia-inducible factor-1α regulates β-cell function in mouse and human islets. *J Clin Invest.* 2010;120(6):2171-2183.
76. Sergiu-Bogdan C, Okamoto K, Pereira T, Brismar K, Poellinger L. Hyperglycemia regulates hypoxia-inducible factor-1α protein stability and function. *Diabetes.* 2004;53:3226-3232.
77. Hyvärinen J, Hassinen IE, Sormunen R, Ma JM, Kivirikko KI, Koivunen P, Myllyharju J. Hearts of hypoxia-inducible factor prolyl 4-hydroxylase-2 hyomorphic mice show protection against acute ischemia-reperfusion injury. *J Biol Chem.* 2010;285(18):13646-13657.
78. Rahtu-Korpela L, Karsikas S, Hörkkö S, et al. HIF prolyl 4-hydroxylase-2 inhibition improves glucose and lipid metabolism and protects against obesity and metabolic dysfunction. *Diabetes.* 2014;63:3324-3333.
79. Taniguchi CM, Finger EC, Krieg AJ, et al. Cross-talk between hypoxia and insulin signaling through Phd3 regulates hepatic glucose and lipid metabolism and ameliorates diabetes. *Nat Med.* 2013;19(10):1325-1330.
80. Jaakola PM, Rantanen K. The regulation, localization, and functions of oxygen-sensing prolyl hydroxylase PHD3. *Biol Chem.* 2013;394(4):449-457.
81. Tennant D, Gottlieb E. HIF prolyl hydroxylase-3 mediates α-ketoglutarate-induced apoptosis and tumor suppression. *J Mol Med.* 2010;88:839-849.
82. Luo W, Lin B, Wang Y, et al. PHD3-mediated prolyl hydroxylation of nonmuscle actin impairs polymerization and cell motility. *Mol Biol Cell*. 2014;25:2788-2796.

83. Andersen S, Donnem T, Stenvold H, Al-Saad S, Al-Shibli K, Busund LT, Bremnes RM. Overexpression of the HIF hydroxylases PHD1, PHD2, PHD3 and FIH are individually and collectively unfavorable prognosticators for NSCLC survival. *PLoS One.* 2011;6(8):e23847.
84. Yan B, Jiao S, Zhang HS, Lv DD, Xue J, Fan L, Wu GH, Fang J. Prolyl hydroxylase domain protein 3 targets Pax2 for destruction. *Biochem Biophys Res Commun.* 2011;409(2):315-320.
85. Feng ZC, Popell A, Li J, Silverstein J, Oakie A, Yee SP, Wang R. c-kit receptor signaling regulates islet vasculature, β-cell survival, and function *in vivo. Diabetes.* 2015;64(11):3852-3866.
86. Yamaguchi S, Ishihara H, Yamada T, Tamura A, Usui M, Tominaga R, Munakata Y, Satake C, Katagiri H, Tashiro F, Aburatani H, Tsukiyama-Kohara K, Miyazaki J, Sonenberg N, Oka Y. ATF4-mediated induction of 4E-BP1 contributes to pancreatic beta cell survival under endoplasmic reticulum stress. *Cell Metab.* 2008;7(3):269-276.
87. Hiwatashi Y, Kanno K, Takasaki C, Goryo K, Sato T, Torii S, Sogawa K, Yasumoto K. PHD1 interacts with ATF4 and negatively regulates its transcriptional activity without prolyl hydroxylation. *Exp Cell Res.* 2011;317(20):2789-2799.
88. Xie L, Xiao K, Whalen EJ, Forrester MT, Freeman RS, Fong G, Gygi SP, Lefkowitz RJ, Stamler JS. Oxygen-regulated beta(2)-adrenergic receptor hydroxylation by EGLN3 and ubiquitylation by pVHL. *Sci Signal.* 2009;2(78):ra33.
89. Puri S, Cano DA, Hebrok M. A role for von Hippel-Lindau protein in pancreatic beta-cell function. *Diabetes.* 2009;58(2):433-441.
90. Kikuchi D, Minamishima YA, Nakayama K. Prolyl-hydroxylase PHD3 interacts with pyruvate dehydrogenase (PDH)-E1β and regulates the cellular PDH activity. *Biochem Biophys Res Commun.* 2014;451(2):288-294.
91. Luo W, Hu H, Chang R, Zhong J, Knabel M, O'Meally R, Cole RN, Pandey A, Semenza GL. Pryuvate kinase M2 is a PHD3-stimulated co-activator for hypoxia-inducible factor 1. *Cell.* 2011;145(5):732-744.
92. German NJ, Yoon H, Yusuf RZ, et al. PHD3 loss in cancer enables metabolic reliance on fatty acid oxidation via deactivation of ACC2. *Mol Cell.* 2016;63(6):1006-1020.
93. Zhdanov AV, Okkelman IA, Collins FWJ, Melgar S, Papkovsky DB. A novel effect of DMOG on cell metabolism: direct inhibition of mitochondrial function precedes HIF target gene expression. *Biochim Biophys Acta.* 2015;1847(10):1254-1266.
94. Chan MC, Ilott NE, Schödel J, et al. Tuning the transcriptional response to hypoxia inhibiting hypoxia-inducible factor (HIF) prolyl and asparaginyl hydroxylases. *J Biol Chem.* 2016;291(39):20661-20673.
95. Rodriguez J, Pilkington R, Garcia Munoz A, Herrero A, Taylor CT, von Kriegsheim A. Substrate-trapped interactors of PHD3 and FIH cluster in distinct signaling pathways. *Cell Rep.* 2016;14(11):2745-2760.
96. Sears JE, Hoppe G, Ebrahem Q, Anand-Apte B. Prolyl hydroxylase inhibition during hyperoxia prevents oxygen-induced retinopathy. *Proc Natl Acad Sci USA.* 2008;105(50):19898-19903.
97. Trichonas G, Lee TJ, Hoppe G, Au J, Sears JE. Prolyl hydroxylase inhibition during hyperoxia prevents oxygen-induced retinopathy in the rat 50/10 model. *Invest Opthalmol Vis Sci.* 2013;54(7):4919-4926.

98. Wang J, Buss JL, Chen G, Ponka P, Pantopoulos K. The prolyl 4-hydroxylase inhibitor ethyl-3,4-dihydroxybenzoate generates effective iron deficiency in cultured cells. *FEBS Lett.* 2002;529(2-3):309-312.
99. Jain IH, Zezzeron L, Goli R, et al. Hypoxia as a therapy for mitochondrial disease. *Science.* 2016;352(6281):54-61.
100. Koivunen P, Serpi R, Dimova EY. Hypoxia-inducible factor prolyl 4-hydroxylase inhibition in cardiometabolic diseases. *Pharmacol Res.* 2016;114:265-273.
101. Olson E, Demopoulos L, Haws TF, Hu E, Fang Z, Mahar KM, Qin P, Lepore J, Bauer TA, Hiatt WR. Short-term treatment with a novel HIF-prolyl hydroxylase (GSK1278863) failed to improve measures of performance in subjects with claudication-limited peripheral artery disease. *Vasc Med.* 2014;19(6):473-482.
102. Bernhardt WM, Wiesener MS, Sciqalla P, Chou J, Schmieder RE, Günzler V, Eckardt KU. Inhibition of prolyl hydroxylases increases erythropoietin production in ESRD. *J Am Soc Nephrol.* 2010;21(12):2151-2156.
103. Chan MC, Atasoylu O, Hodson E. Potent and selective triazole-based inhibitors of the hypoxia-inducible factor prolyl-hydroxylases with activity in the murine brain. *PLoS One.* 2015;10(7):e0132004.
104. Thorens B, Tarussio D, Maestro MA, Rovira M, Heikkilä E, Ferrer J. Ins1Cre knock-in mice for beta cell-specific gene recombination. *Diabetologia.* 2015;58:558-565.
105. Xu J, Han J, Long YS, Epstein PN, Liu YQ. The role of pyruvate carboxylase in insulin secretion and proliferation in rat pancreatic beta cells. *Diabetologia.* 2008;51(11):2022-2030.
106. Muoio, DM Newgard CB. Molecular and metabolic mechanisms of insulin resistance and β-cell failure in type 2 diabetes. *Nat Rev Mol Cell Biol.* 3236-3244.
107. Jitrapakdee S, Wutthisathapornchai A, Wallace JC, MacDonald MJ. Regulation of insulin secretion: role of mitochondrial signaling. *Diabetologia.* 2010;53:1019-1032.
108. Maechler P, Carobbio S, Rubi B. In beta-cells, mitochondria integrate and generate metabolic signals controlling insulin secretion. *Int J Biochem Cell Biol.* 2006;38:696-709.
109. Joseph JW, Jensen MV, Ilkayeva O, Palmieri F, Alárcon C, Rhodes CJ, Newgard CB. The mitochondrial citrate/isocitrate carrier plays a regulatory role in glucose-stimulated insulin secretion. *J Biol Chem.* 2006;281(47):35624-35632.
110. Odegaard ML, Joseph JW, Jensen MV, et al. The mitochondrial 2-oxoglutarate carrier is part of a metabolic pathway that mediates glucose- and glutamine-stimulated insulin secretion. *J Biol Chem.* 2010;285(22):16530-16537.
111. Ronnebaum SM, Ilkayeva O, Burgess SC, Joseph JW, Lu D, Stevens RD, Becker TC, Sherry AD, Newgard CB, Jensen MV. A Pyruvate Cycling Pathway Involving Cytosolic NADP-dependent Isocitrate Dehydrogenase Regulates Glucose-stimulated Insulin Secretion. *J Biol Chem.* 2006;281(41):30593-30602.
112. Lorenz MA, El Azzouny MA, Kennedy RT, Burant CF. Metabolome response to glucose in the β-cell line INS-1 832/13. *J Biol Chem.* 2013;288(15):10923-10935.
113. Dolenšek J, Rupnik MS, Stožer. Structural similarities and differences between the human and the mouse pancreas. *Islets.* 2015;7(1): e1024405.
114. Steiner DJ, Kim A, Miller K, Hara M. Pancreatic islet plasticity: Interspecies comparison of islet architecture and composition. *Islets.* 2010;2(3):135-145.

115. Kim A, Miller K, Jo J, Kilimnik G, Wojcik P, Hara M. Islet architecture: A comparative study. *Islets.* 2009;1(2):129-136.
116. Komatsu M, Takei M, Ishii H, Sato Y. Glucose-stimulate insulin secretion: a newer perspective. *J Diabetes Investig.* 2013;4(6):511-516.
117. Leung E, Caims RA, Chaudary N, Vellanki RN, Kalliomaki T, Moriyama EH, Mujcic H, Wilson BC, Wouters BG, Hill R, Milosevic M. Metabolic targeting of HIF-dependent glycolysis reduces lactate, increases oxygen consumption and enhances response to high-dose single-fraction radiotherapy in hypoxic solid tumors. *BMC Cancer.* 2017;17(1):418-430.
118. Gerenscer AA, Mookerjee SA, Jastroch M, Brand MD. Positive feedback amplifies the response of mitochondrial membrane potential to glucose concentration in clonal pancreatic beta cells. *Biochim Biophys Acta.* 2017;1863(5):1054-1065.
119. Hu M, Lin H, Yang L, Cheng Y, Zhang H. Interleukin-22 restored mitochondrial damage and impaired glucose-stimulated insulin secretion through down-regulation of uncoupling protein-2 in INS-1 cells. *J Biochem.* 2017;161(5):433-439.
120. Brereton MF, Rohm M, Shimomura K, Holland C, Tornovsky-Babeay S, Dadon D, Iberl M, Chibalina MV, Lee S, Glaser B, Dor Y, Rorsman P, Clark A, Ashcroft FM. Hyperglycaemia induces metabolic dysfunction and glycogen accumulation in pancreatic β-cells. *Nat Commun.* 2016;7:13496.
121. Mugabo Y, Zhao S, Lamontagne J, Al-Mass A, Peyot ML, Corkey BE, Joly E, Madiraju SRM, Prentki M. Metabolic fate of glucose and candidate signaling and excess-fuel detoxification pathways in pancreatic β-cells. *J Biol Chem.* 2017;292(18):7407-7422.
122. Alarcon C, Boland BB, Uchizono Y, Moore PC, Peterson B, Rajan S, Rhodes OS, Noske AB, Haataja L, Arvan P, Marsh BJ, Austin J, Rhodes CJ. Pancreatic β-cell adaptive plasticity in obesity increases insulin production but adversely affects secretory function. *Diabetes.* 2016;65:438-450.
123. Pizarro-Delgado J, Deeneyl JT, Corkey BE, Tamarit-Rodriguez J. Direct stimulation of islet insulin secretion by glycolytic and mitochondrial metabolites in KCl-depolarized islets. *PLoS One.* 2016;11(11): e0166111.
124. Patel DP, Krausz KW, Xie C, Beyoğlu D, Gonzalez FJ, Idle JR. Metabolic profiling by gas chromatography-mass spectrometry of energy metabolism in high-fat diet-fed obese mice. *PLoS One.* 2017;16(12):e0177953.
125. Guay C, Joly É, Pepin É, Barbeau A, Hentsch L, Pinedal M, Madirajul SRM, Brunengraber H, Prentki M. A role for cytosolic isocitrate dehydrogenase as a negative regulator of glucose signaling for insulin secretion in pancreatic β-cells. *PLoS One.* 2013;8(10): e77097.
126. Williams SJ, Huang HH, Kover K, Moore W, Berkland C, Singh M, Smirnova IV, MacGregor R, Stehno-Bittel. Reduction of diffusion barriers in isolated rat islets improves survival, but not insulin secretion or transplantation outcome. *Organogenesis.* 2010;6(2):115-124.
127. Paneni F, Lüscher TF. Cardiovascular protection in the treatment of type 2 diabetes: a review of clinical trial results across drug classes. *Am J Cardiol.* 2017;120(1S):S17-S27.
128. Bonnet F, Scheen AJ. Impact of glucose-lowering therapies on risk of stroke in type 2 diabetes. *Diabetes Metab.* 2017;pii: S1262-3636(17)30075-7.

Appendix

A.1 Assessing the role of PHD in PHD123*fl/fl* primary mouse islets using a RIPCre adenovirus

After islet isolation, approximately 120-150 islets per treatment from PHD123*fl/fl* male mice were picked into 6-well plates containing 2mL of islet growth media. Islets were infected with 2µL of shGFP control virus or RIPCre adenovirus compared to NT. 20mM of glucose was added to each well and islets were incubated for 18 hours overnight (37˚C, 5% CO_2). Islets were analyzed for GFP and RFP and 60-72 hours after infection, an insulin secretion assay was performed. After GSIS, islets were either snap frozen where protein extraction was performed for western blot analysis or insulin secretion was measured by RIA.

PHD knockdown was measured by western blot analysis using primary antibodies for PHD1, PHD2, PHD3, HIF1α and tubulin as a control. A significant PHD knockdown for all isoenzymes was not detected, which may be due to experimental methods. This may be due to inaccurate concentrations of viruses, incubation time of viral infection or the quality of the RIPCre adenovirus, as islets treated with shGFP were 100% infected and islets treated with the RIPCre adenovirus were approximately 30-40% infected.

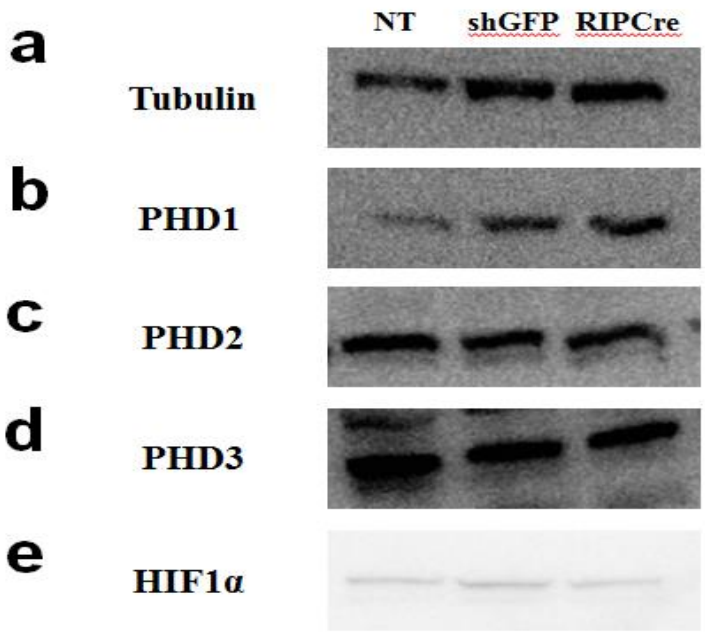

Figure A.1: PHD knockdown using a RIPCre adenovirus by western blot.

Total protein was isolated from PHD123*fl/fl* primary islets. Protein samples were analyzed by western blot for PHD knockdown of all three PHD isoenzymes and HIF1α. Tubulin was used as a control. Protein samples contained 120-150 islets and protein intensity was measured by Imagej. PHD1 was approximately 44kDa, PHD2 50 kDa, PHD3 47 kDa, HIF1α 132 kDa and tubulin 50 kDa.

To assess whether PHD plays a role in insulin secretion, a GSIS was performed using primary islets from PHD123*fl/fl* male mice treated with a shGFP virus, a RIPCre adenovirus or NT. Islets were treated with LG (2mM) KRB, HG (16.7mM) KRB, LG (2mM) KRB + KCl (30mM) + diazoxide (200μM), HG (16.7mM) KRB + KCl (30mM) + diazoxide (200 M) and HG (16.7 M) KRB + DMM (10mM) + DMαKG (10mM) in KRB for one hour (37˚C, 5% CO_2). Insulin secretion was measured by RIA. A significant difference in insulin secretion in the RIPCre treated islets compared to shGFP and NT was not detected, possibly due to experimental

methods, as a measurable difference in protein knockdown by western blot analysis was unable to be measured. It is thought that the RIPCre adenovirus containing Cre recombinase would be able to target *loxP* sites in PHD123*fl/fl* male mice to induce a knockdown. PHD knockdown via viral infection would be able to determine if PHD plays a role in insulin secretion.

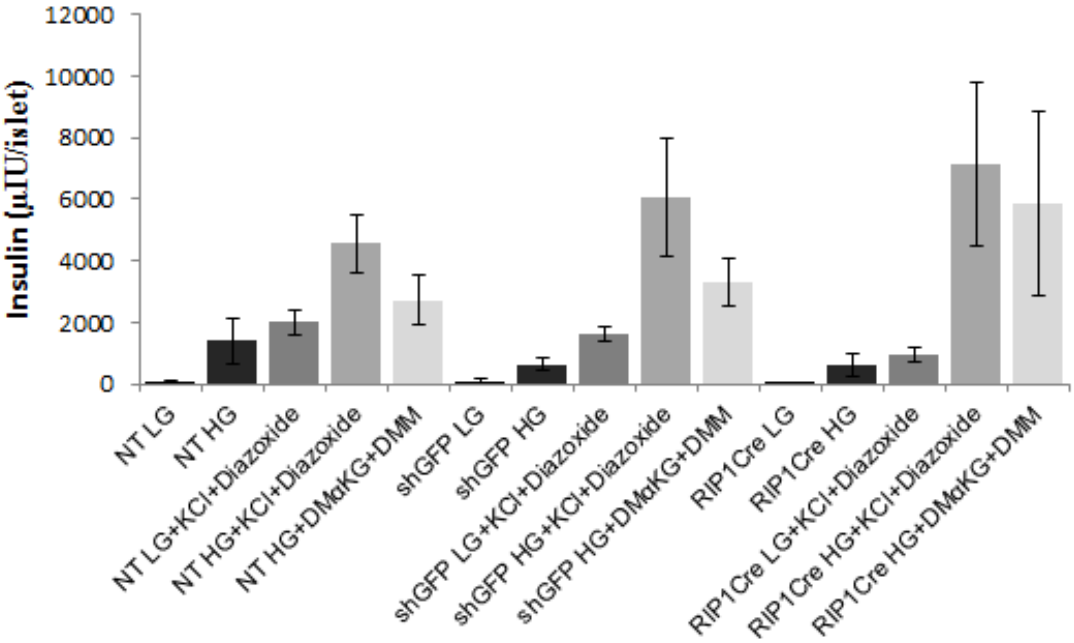

Figure A.2: Islet GSIS in PHD123*fl/fl* male mice using viral infection.

shGFP, RIPCre, and NT islets treated with LG (2mM) KRB, HG (16.7mM) KRB, LG (2mM) KRB+ KCl (30mM) + diazoxide (200µM), HG (16.7mM) KRB+ KCl (30mM) + diazoxide (200µM) and HG (16.7mM) KRB + DMM (10mM) + DMαKG (30mM) for one hour. (n=6-9). Data are mean ± SEM.

A.2 Antibody information

Table A.1: Primary and secondary antibodies

Target	Clonality	Host Species	Application	Manufacturer
PHD1	EPR2745	Rabbit	Western blot/immunofluorescence	Abcam
PHD2	D31E11	Rabbit	Western blot/immunofluorescence	Cell Signalling
PHD3	Polyclonal #196344	Rabbit	Western blot/immunofluorescence	Abcam
HIF1α	Sc-10790	Rabbit	Western blot	Santa Cruz
Tubulin	Monoclonal T8328	Mouse	Western blot	Sigma
Insulin	Polyclonal A0564	Guinea pig	Immunofluorescence	Dako
Alexa Fluor® 488	Polyclonal	Rabbit	Immunofluorescence	Jackson ImmunoResearch
Alexa Fluor® 647	Polyclonal A-21246	Rabbit	Immunofluorescence	ThermoFisher Scientific
Hydroxyproline	Polyclonal #37067	Rabbit	Co-immunoprecipitation	Abcam

A.3 Primer information

Table A.2: Primers for genotyping

Gene	Orientation	Sequence (5' to 3')	Primer length (nt)	Amplicon length (nt)	Reference
PHD1	Forward	TGAGACCAGGCAGAGGGAGTT	21	WT 500, f/f 600	Takeda K, 8337, 2006
	Reverse	GGAGCTGGAGTTCTAGGTCAGGTT	24		
PHD2	Forward	GTGTACCTCAACCTCCGCTC	20	WT 1900, f/f 1400	Designed by SJ
	Reverse	AGGGGATTTGTAGTTGGCCG	20		
PHD3	Forward	GCTCGGAGAACTTGACACGA	20	WT 1070, f/f 1550	Designed by SJ
	Reverse	TGACCTCGTAGGGCTCAGAT	20		
INS-1^{Cre}	Common	GGAAGCAGAATTCCAGATACTTG	23		Jackson Laboratories
	WT	GTCAAACAGCATCTTTGTGGTC	22	488	Jackson Laboratories
	Mutant	GCTGGAAGATGGCGATTAGC	20	675	Jackson Laboratories